The Pennsylvania State University

The Graduate School

SIMULATION OF NEEDLE INSERTION PROCEDURES

A Dissertation in

Mechanical Engineering

by

David F. Pepley

Submitted in Partial Fulfillment
of the Requirements
for the Degree of

Doctor of Philosophy

May 2019

The dissertation of David F. Pepley was reviewed and approved* by the following:

Jason Z. Moore
Associate Professor of Mechanical Engineering
Dissertation Advisor
Chair of Committee

Scarlett R. Miller
Associate Professor School of Engineering Design, Technology, and Professional Programs

Bo Cheng
Assistant Professor of Mechanical Engineering

Daniel Cortes
Assistant Professor of Mechanical Engineering

Karen Thole
Distinguished Professor of Mechanical Engineering
Head of the Department of Mechanical and Nuclear Engineering

*Signatures are on file in the Graduate School

Abstract

This dissertation contributes to the simulation of needle insertion procedures through the development of new simulation methods and devices. Experiments are conducted to understand the mechanics of needle insertion which leads to the development of both low cost training devices and high cost computer controlled simulators. The training potential of these simulators is then experimentally validated through studies conducted with novice and expert medical professionals. Using the knowledge gained from these studies, advanced needle insertion simulators can be developed, leading to improved training for medical professionals.

Ultrasound manikins are commonly used training devices for ultrasound guided needle insertion procedures, however they are often very expensive and limited to representing idealized patient anatomy. The first set of experiments involves the building of low cost ultrasound manikins using modified PVC plastisol. Needle insertion force and ultrasound image comparison experiments show that modified PVC plastisol is more similar to cadaver tissue than many commonly used manikin materials. This leads to a method of building low cost manikins that can be customized to represent a variety of patient types.

Computer-based surgical simulators have significant advantages in medical training including real time user feedback and the ability to simulate a variety of patients. This research developed a computer controlled haptic patient simulator for central venous catheterization. Experiments were conducted to create models for both ultrasound and haptic needle insertion simulation. The simulator was then developed and implemented into a resident training program and multiple research studies were conducted to compare traditional central venous catheterization training to computer simulation training. The research showed that the computer simulator was able to effectively train a variety central venous catheterization scenarios.

Finally, a new method of creating haptic feedback was explored for use in needle insertion training. Experiments were conducted to measure the puncture forces of a variety of

materials. This information was then implemented into a new haptic simulation device that uses the needle puncture of materials in a cartridge to simulate needle forces. Experiments showed the haptic device is able to accurately mimic the forces of a needle inserted into human tissue.

TABLE OF CONTENTS

LIST OF FIGURES

LIST OF TABLES

NOMENCLATURE

A_n	Parameterization factor for piecewise haptic force characterization
A_x	Y component of vector field vortex matrix for zone 2, px
A_y	X component of vector field vortex matrix for zone 2, px
a_i	Amplitude of Gaussian distribution peak, px
$a_{x,y,z}$	Measured accelerations
B_n	Parameterization factor for piecewise haptic force characterization
B_x	X component of vector field vortex matrix for zone 3, px
B_y	Y component of vector field vortex matrix for zone 3, px
b_i	Centroid of Gaussian distribution, px
C_n	Parameterization factor for piecewise haptic force characterization
c_i	Gaussian distribution peak width factor, px
D	matrix where each element corresponds to perpendicular pixel distance from needle
D_n	Parameterization factor for piecewise haptic force characterization
f	pixel color, 0 to 255
G	Gaussian distribution matrix, px
I	3D location of a needle plane intersection
i	Gaussian distribution index, 1 or 2
$\hat{I}$	x direction unit vector
$\hat{j}$	y direction unit vector
M_x	x coordinate grid matrix
M_y	y coordinate grid matrix
n	Gaussian distribution parameters, 2
P_n	Critical depths for piecewise intervals a haptic force characterization
p	pixel color reference location, (x, y)
Q_{ij}	known pixel location, (x_i, y_j)
S	stiffness factor matrix, 0 to 1
T	Transformation matrix
T^{-1}	inverse mapping transformation matrix

U	simulation horizontal pixel movement matrix, px
U_1	zone 1 horizontal pixel movement matrix, px
U_2	zone 2 horizontal pixel movement matrix, px
U_3	zone 3 horizontal pixel movement matrix, px
u	3D location of the ultrasound probe
V	simulation vertical pixel movement matrix, px
V_1	zone 1 vertical pixel movement matrix, px
V_2	zone 2 vertical pixel movement matrix, px
V_3	zone 3 vertical pixel movement matrix, px
x	image pixel column location in original image
x'	image pixel column location in new image
x_i	pixel reference location (i = 1 or 2)
y	image pixel row location in original image
y'	image pixel column location in new image
y_j	pixel reference vertical location (j = 1 or 2)
θ	Mock ultrasound probe angle
v_1	zone 2 vortex center location, px
v_2	zone 3 vortex center location, px
φ	Inertial measurement unit angles
CVC	Central Venous Catheterization
DHRT	Dynamic Haptic Robotic Trainer
IJ	Internal Jugular Vein
LCNIS	Low Cost Haptic Needle Insertion Simulator
PNB	Peripheral Nerve Block
px	pixels

ACKNOWLEDGEMENTS

To begin, I would like to thank my research advisor Dr. Jason Moore for guiding me through the long process of graduate school. It would not have been possible without all of his help designing experiments, writing papers, and mentoring. Next, I would like to thank Dr. Scarlett Miller for serving as a mentor on many of my projects. Her input on the design of the devices and user interfaces was vital to the success of these projects. I would also like to acknowledge Dr. Bo Cheng and Dr. Daniel Cortes for serving on my committee.

Additionally, I would like to thank Hong-En Chen, Mary Yovanoff, and Yichun Tang for all of their hard work with the DHRT and LCNIS projects. These projects were truly team efforts, and their work was invaluable to its success. From the Penn State Hershey Medical Center, I would like to thank Dr. Cassie Sonntag, Dr. Katelin Mirkin, Dr. David Han and Dr. Sanjib Adhikary. They were vital to organizing all of the studies performed at Hershey Medical Center and provided incredible amounts of important feedback for all of the simulation devices.

I would like to thank the National Heart, Lung, and Blood Institute of the National Science Foundation. This dissertation is based on work funded through the National Institute of Health award no. R01HL127316.

I would like to thank my parents and family for all of their love and support. They were always there for me with love, advice, and prayer during the difficult times, and I could not have done without them. Finally, I would like to thank my fiancée Sarah. The amount of love and patience she has shown me over the past four years has been incredible, especially considering at the same time she has been working her way painstakingly through medical school. It’s been a long time coming, but I am excited to finally begin the rest of our lives together,

Chapter 1
Introduction

1.1 Background

Andrew J. Walter describes the four main factors that make a competent surgeon as being knowledge, leadership, decision making, and technical skills [1]. A strong surgical education program will look to reinforce all of these factors, however the way in which these skills have been taught has varied widely over the past century. Historically, the most popular of these training methods has been the Halsted apprenticeship model which takes a "see one, do one, teach one" approach to learning [2-4]. This method of learning is still seen by many today as the gold standard of surgical training [5]. However, one of the biggest drawbacks of the apprenticeship model is that it requires a large time investment to gain the necessary experience to become proficient in a procedures. This is problematic when considering the twenty-first century challenges such as regulated resident work hours and overstressed operating rooms and places significant pressure on residency programs to not only train residents effectively, but more efficiently as well [6-9].

To address this problem, new methods of education are being added to residency training programs including competency-based education and patient simulation. Competency-based medical education allows for advancement in learning based on clinician skills training and the reaching of milestones as opposed to purely time based experience. Proponents of competency based medical education espouse its increased focus on outcomes and flexibility of training time [10, 11]. Critics of competency-based education believe that it overemphasizes easily measurable skills, is logistically difficult, and claim that doctors need skills that are not easily measured using competencies [12, 13].

Patient simulation is being integrated into both apprenticeship and competency based medical education. Simulation offers a safe training environment where training can be focused on key skills. They also provide the ability for students and residents to practice procedures when a patient is not available [14]. Surgical training simulators are often categorized as either low-fidelity or high-fidelity [15]. The fidelity of the simulator can be defined as how well the simulator replicates the physical characteristics of the task and how well the simulator captures the skills used in the task. Some examples of low fidelity trainers are static devices such as box-trainers for laparoscopic skills, tissue models for suturing, knot-tying boards, and upper torso manikins (Figure 1-1) [16-18].

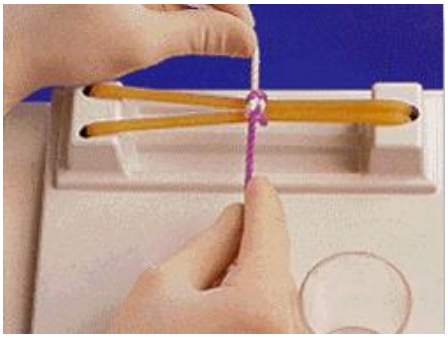

(B)

(C)

Figure 1-1 Images of surgical training devices: (A) laparoscopic surgery box trainer, (B) surgical knot tying board, (C) central venous catheterization upper torso manikin [19, 20].

While simple in form, these kind of simulators work well as “partial-task trainers” to teach specific skills associated with a wide variety of procedures. They also require feedback from an instructor to evaluate skill. High fidelity simulators can vary from full body training manikins with life like breathing, sounds, and fluid circulation to computer based virtual reality simulations [21, 22]. An example of this is the CAE Healthcare (Sarasota, FL) *iStan* which features a pulse, patient sounds, reactive eyes, mechanical ventilation, flail chest, and fully articulated wrist, elbows, knees, and ankles [23]. Simulators such as these can be used to practice the entirety of a surgical procedures and provide real time feedback to the user [24].

Figure 1-2 CAE Healthcare (Sarasota, FL) *iStan* fully body training manikin [23].

In recent years, the rapid increase in computer processing power has enabled the disruptive potential of computer based surgical simulators [25, 26]. Computer simulators have the ability to create a wide variety of patient anatomies, provide realistic haptic feedback, and provide performance feedback to the users. For example, the *LAPSIM* laparoscopic simulator by Surgical Science (Göteborg, Sweden) creates a high fidelity virtual environment that can be manipulated using realistic mock laparoscopic tools. This system then provides feedback to the user on their

performance in the simulated task [27]. Another example is the CAE Healthcare *Vimedix 2.0* combines manikins with augmented or mixed reality glasses to visually project internal patient anatomy and ultrasound images onto physical manikins [28]. While the number of computer based simulators is growing, each type of simulator comes with its own design challenges. Currently, a category of procedures that is still lacking a variety of high fidelity computer simulation is percutaneous procedures.

Figure 1-3 Surgical Science (Göteborg, Sweden) *LapSim* haptic laparoscopic training simulator [29].

The ability to control a needle during a percutaneous procedure is one of the most basic skills required by a doctor. A percutaneous procedure is any type of medical procedure that requires a needle puncturing through the skin. Some common percutaneous procedures include the insertion of stents into blood vessels, the introduction of drainage catheters, and the insertion of needles for nerve blocks. Ultrasound guided central venous catheterization (CVC) is another percutaneous procedure performed over 8 million times per year in the United States and is used to create an access port into vessels in the body [30]. Despite the fact that CVCs are performed frequently, dangerous mechanical complications including hematoma, hemothorax,

pneumothorax, thrombosis, and accidental atrial punctures occur in up to 19 percent of patients. Rates of infection are even greater being reported as high as 26 percent.

In summary, there is an increasing need for new surgical procedure training methods in residency programs. Due to factors such as reduced resident work hours, the old apprenticeship model must be adapted to fit the needs of the twenty-first century. The increased use of simulation is one way in which residency programs are adapting, and more new high and low fidelity simulators are needed to meet the needs of modern residency programs. Despite this increase in the use of simulation, there are still few advanced needle insertion based simulators despite them being some of the most commonly conducted procedures.

1.2 Research Purpose and Organization

The intended contributions of this dissertation are as follows. First, this research intends to develop new, more affordable and effective materials for manikin style simulators. Next, this research looks to determine the effectiveness of computer simulation for the training of needle insertion procedures. Finally, this research aims to develop new methods for simulating ultrasound tissue-needle interactions and generating haptic feedback. These contributions have the potential to make needle insertion simulation more effective and affordable. This in turn will lead to improved surgical training, resulting in improved patient outcomes, more efficient training, and reduced costs for hospitals.

The intended contributions of this work are achieved through the following research studies. First, a new method for creating affordable, yet high fidelity ultrasound manikins is developed. This new method is then evaluated through experimental needle force testing and ultrasound comparison studies with trained experts. Second, to address the need for high fidelity computer simulation, the Dynamic Haptic Robotic Trainer (DHRT) for CVC is designed and implemented into a surgical training program. Third, to improve ultrasound guided needle

insertion simulation devices such as the DHRT, a new method of simulating ultrasound and needle interactions with ultrasound imaged tissue is explored. Finally, a novel alternate method of simulating haptic needle forces using low-cost material fracture as opposed to computer control is detailed.

To address these research goals, this dissertation is organized as follows. Chapter 2 will address the development of a PVC plastisol based ultrasound manikin material. The current methods of creating ultrasound manikins is discussed, followed by the methodology of building the PVC plastisol manikin, and a series of force and image comparison experiments to evaluate the manikin material. Chapter 3 is a detailed description of the development of the DHRT for CVC simulator. The need for the DHRT will be discussed followed by an explanation of the hardware and software developed for the system. The chapter will then detail studies used to evaluate and improve the DHRT. Chapter 4 involves improvements made to the DHRT and the details of the implementation and evaluation of the DHRT in a surgical resident program. Chapter 5 explores a new method for simulating ultrasound and needle tissue ultrasound interactions using vector fields and inverse image mapping. Chapter 6 explores a new method for creating needle insertion haptic feedback a new Low-Cost Needle Insertion Simulator (LCNIS). The design of the LCNIS, and the method for creating haptic feedback using material fracture is explained. Finally, Chapter 7 concludes the dissertation and summarize the important contributions of this work.

Chapter 2
Using Modified PVC Plastisol to Create Low Cost Training Manikins

2.1 Introduction

The first intended contribution of this dissertation is to improve the simulation of needle insertion procedures through the creation of more affordable and effective training manikins. The use of ultrasound manikins are among the most commonly used methods for training needle insertion procedures. Ultrasound manikins, or phantoms, are either full or partial physical recreations of the human body. These manikins allow for a safe introduction to a variety of clinical skills and are associated with improved in-hospital performance [30, 31]. However, ultrasound manikins are also expensive with many costing well over $1000, making them a difficult purchase for residency programs with tight budgets or in less affluent nations [32, 33]. As a result, many simulation centers build their own low cost manikins from a wide variety of materials including gelatin, agar, and chicken breast [32, 34, 35]. The following chapter presents the development and testing of a novel modified PVC Plastisol material for use in ultrasound manikins. The chapter begins with a review of commonly used ultrasound manikin materials, as well as the advantages and disadvantages of these materials. Next, a novel method of creating manikins using modified polyvinyl chloride (PVC) Plastisol is detailed. This is followed by the experimental testing of the force and ultrasound properties of the PVC material and a variety of commonly used manikin materials. Finally, the results and discussion compares the modified PVC plastisol and evaluate its qualities as an ultrasound manikin material against the tested alternatives.

This chapter is based on the paper "Building Ultrasound Phantoms with Modified Polyvinyl Chloride: A Comparison of Needle Insertion Forces and Sonographic Appearance with Commercial and Traditional Simulation Materials" from the journal Simulation in Healthcare [36].

2.2 Ultrasound Manikin Materials

According to a review of upper torso manikin simulators by Sultan et al., an ideal manikin should reproduced the texture and resistance of human tissue, have sufficient ultrasound penetration, be easily reproducible, be easily transportable, have clearly distinguished targets, and be affordable [37]. In an attempt to fulfill these needs, a wide variety of ultrasound manikins have been developed, but all have some disadvantages. Commercial simulators such as the CAE Healthcare (Sarasota, FL) Blue Phantom and the Kyoto Kagaku (Kyoto, Japan) CVC Insertion Simulator are widely used in training. These are durable and can withstand dozens of needle insertions but cost between $1,000 and $6,000 a unit and are not easily repairable. Low cost homemade manikins are often made from materials such as gelatin, algae-based agar, and meat. While very low cost, agar and gelatin must be refrigerated, have short shelf lives, and provide very weak resistance to needle insertion [32, 34, 38, 39]. Animal-based manikins have been created by implanting tubing and other structures into meat such as chicken breast. Using actual muscle creates very realistic ultrasound images and needle forces, however this is messy, poses infection risks, cannot be easily shaped, must be refrigerated, and has a short shelf life [37, 40]. Another low cost solution is using Clear Ballistics (Fort Smith, AR) Ballistics Gel. This does not decompose like the animal and agar based solutions and provides better needle resistance. However, Ballistics Gel has a very low echogenicity, or ability to bounce ultrasound signals. This results in very dark, or even black ultrasound images [41, 42].

With the recommendation on what constitutes a good ultrasound manikin in mind, a method of creating ultrasound manikin using PVC plastisol has been developed. The use of PVC plastisol for ultrasound manikins was first proposed by Li et al. [43, 44], however these papers only conducted basic compression testing on the material and performed limited needle insertion force testing. They also used glass beads to increase the material's echogenicity. This dissertation

details a new formulation of the PVC plastisol manikins and compares its material properties against a variety of commonly used ultrasound materials.

2.3 Building a Modified PVC Plastisol Manikins

Four ingredients are used to create the novel modified PVC plastisol manikin: M-F Manufacturing (Fort Worth, TX) regular liquid plastic PVC plastisol polymer, diethyl hexyl adipate plasticizer softener, mineral oil, and chalk powder. Different ratios of PVC to softener to mineral oil are used to create manikins with varying echogenicity and needle force characteristics. Three different ratios were used in testing. Mixture 1 used a volume ratio of 9:1:2 of PVC plastisol, to softener, to mineral oil. Mixture 2 had a ratio of 11:0:1, and Mixture 3 had a ratio of 3:0:1. All 3 mixtures added 1 g of chalk powder for every 150 mL of total mixture volume. Doping agents, such as chalk powder, are used to increase the echogenicity of a material. The PVC, softener, and mineral oil are mixed thoroughly under a fume hood in a pot and slowly heated to approximately 175°C, stirring frequently to ensure even heating and homogeneous mixing. When the material begins to thicken and turn from a milky white color to translucent, chalk powder is slowly added while stirring, taking care to minimize clumping of the powder. Once the material has turned translucent, it is removed from heat and quickly poured into a manikin mold. Any required internal structures (such as silicone tubing to act as vessels) must be positioned in the manikin material before the material solidifies. The mold is then left to cool to room temperature. If multiple layers of modified PVC plastisol are desired, it is best to wait to pour the additional layer until after the previous layer has hardened but while it is still warm. This improves adhesion between layers and prevents them from mixing. Finally, extract the solidified and cooled material to complete the manikin. A summary of these instructions is shown in Table 2-1.

Table 2-1 Instruction summary for the creation of a 600 mL modified PVC plastisol polymer manikin with PVC to softener to mineral oil ratio of 9:1:2.

Materials	M-F Manufacturing regular liquid plastic PVC polymer (450 mL) M-F Manufacturing Plastic Softener (50 mL) Mineral Oil (100 mL) Chalk Powder (4 g)
Instructions	1. Thoroughly mix the PVC polymer, softener, and mineral oil in a cooking pot. 2. Slowly heat the mixture to a temperature of 175°C, stirring frequently to ensure even heating and homogenous mixing. 3. When the material begins to thicken and change from a milky white color to translucent, slowly add chalk powder while stirring. Take care to minimize clumping of the powder. 4. Once the material has turned clear, remove the material from heat and pour into the desired mold. 5. While the material is still hot and liquefied, add desired internal structures such as heat resistant silicon tubing for vessels. 6. Allow to cool to room temperature. A refrigerator may be used to speed the cooling process.
Variations	Alternate ratios of PVC polymer to softener to mineral oil may be used to increase or decrease material softness. More mineral oil and softener will produce a softer material. If multiple layers of different softness tissues are desired, pour additional layers after the previous layer has solidified but is still warm to maximize layer adhesion. For larger or smaller manikins, maintain the ratio of PVC polymer to softener to mineral oil and increase or decrease the total volume of ingredients used accordingly. Use 1 g of chalk powder for every 150 mL of total material volume.

2.4 Experimental Procedure

Two different experiments were conducted to compare the properties of the new PVC plastisol ultrasound manikin against a variety of commonly used manikin materials. The first

experiment used an 18-gauge introducer needle (Teleflex, Wayne, PA) mounted to a linear actuator (Dunkermotoren, Bonndorf, Germany) to measure the axial force of a needle being inserted into manikin tissue. An ATI industrial automation (Apex, NC) Nano17 force transducer was placed in line with the needle to measure the axial needle force of insertion. The needle was inserted four times into samples of each testing material at a steady rate of 10 mm/s and to a depth of 50 mm using a controlled velocity provided by the linear actuator. For the duration of each experimental insertion, the position of the needle and axial needle force was recorded at a rate of 1000 Hz. The following materials were tested: a Blue Phantom Ultrasound Training Model, Kyoto Kagaku CVC simulator, Ballistics Gel, agar, gelatin, and three different mixtures of PVC proposed in section 2.3 and shown in Table 2-2. Statistical analysis involved calculating the mean and standard deviation of the needle forces at depths of 5, 10, 16.6, 20, 30, 40, and 50 mm. Insertions into the Kyoto Kagaku CVC simulator were limited to a depth of 40 mm due to the shape of the manikin. Methods for creating manikins from Ballistics Gel, agar and gelatin were acquired from articles by Amini et al., Bude and Alder, and Earle et al. respectively [34, 36, 42]. The reference depth of 16.6 mm was included due to this being the depth of maximum needle insertion force during a previously conducted 17 mm needle insertion into cadaver neck tissue. The cadaver needle insertion force at this depth was recorded as 1.41 N [45].

Table 2-2 The three different mixtures used for the PVC CVC manikin experiments.

	PVC [mL]	Softener [mL]	Mineral Oil [mL]	Chalk [g]
Mixture 1	225	25	50	2
Mixture 2	275	0	25	2
Mixture 3	225	0	75	2

The second experiment evaluated the ultrasound image quality and realism of seven manikin materials. Materials were evaluated using a pairwise image comparison survey administered to 15 experts in ultrasound-guided CVC insertion. An expert in ultrasound-guided

CVC is defined as someone who has conducted more than 50 ultrasound-guided CVC insertions [46, 47]. All of the materials from the linear actuator experiment were tested except PVC Mixture 3 and the Kyoto Kagaku. These two materials were not surveyed to prevent the survey from being excessively long and fatiguing to the participants, leading to poor results. It is assumed that they are similar to the other PVC mixtures and commercially available simulators such as the Blue Phantom. The images of each material had the same dimension with the simulated vein centered in the image and identical ultrasound machine settings as shown in Figure 2-1. The ultrasound machine used was a GE Healthcare Logiq e with gain set to 70, frequency of 10.0 MHz, and depth ranging from 3.0 cm to 4.5 cm. Focal zone was set to the center of the image. A GE 8L-rs linear vascular ultrasound transducer was used to scan the material. Silicone rubber tubing with a 50 Shore A hardness, inside diameter of 0.25 in, and thickness of 0.0625 in was placed in the Ballistic Gel, agar, gelatin, and PVC samples to simulate a right internal jugular vein. Tubing was filled with water to simulate blood.

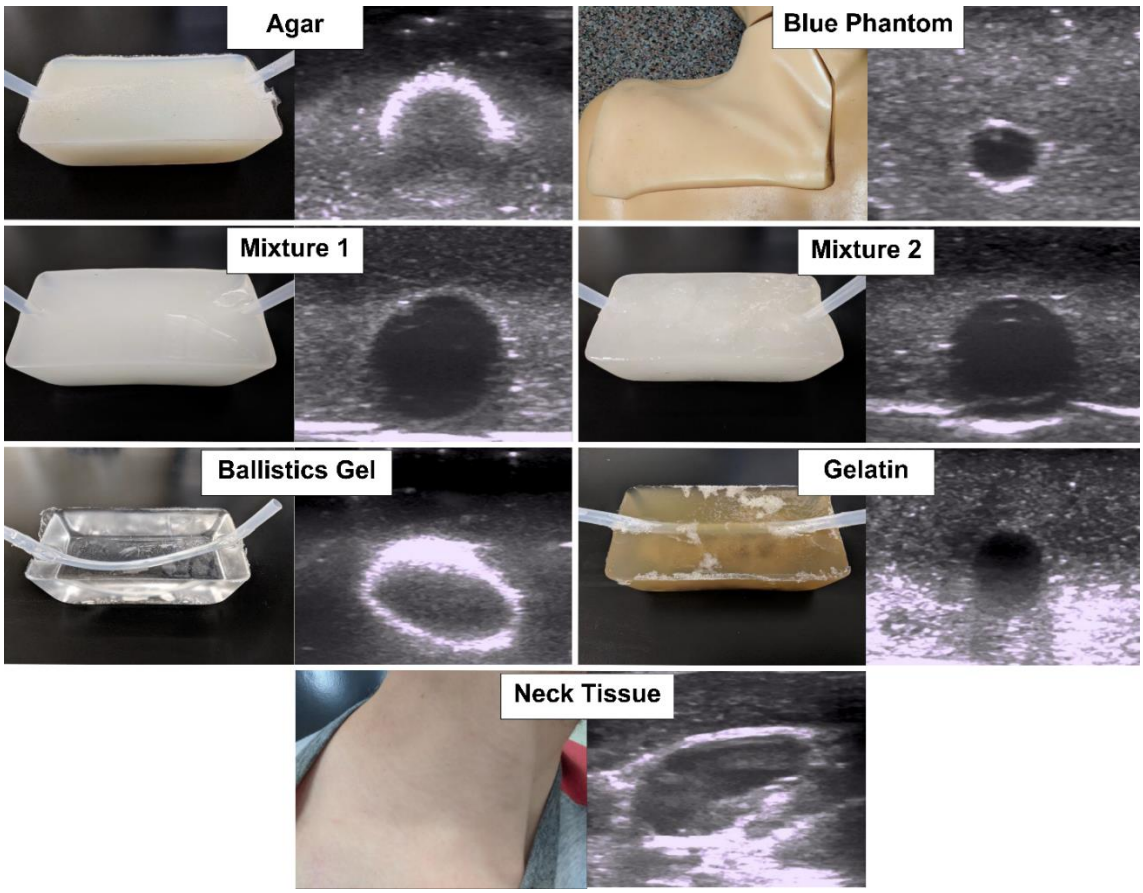

Figure 2-1 Materials used for ultrasound pairwise comparison testing. One of the two ultrasound images used for each material is shown. The ultrasound machine used was a GE Healthcare Logiq e with a gain set to 70, frequency of 10.0 MHz, and depth ranging from 3.0 cm to 4.5 cm. Focal zone was set to the center of the image. A GE 8L-rs linear vascular transducer was used to scan the material.

Experts in ultrasound-guided CVC were presented with an identical set of 84 paired ultrasound images presented in a randomized order. Images were displayed side by side on a computer screen. And participants were asked to select which of the two images more closely resembled an ultrasound image of a right internal jugular vein or “no difference”. For each image pair, the image selected would receive a score of 1, whereas the other image would receive a 0. If “no difference” was selected, both images received a score of 0.5. The seven manikin materials tested were the Blue Phantom Ultrasound Training Model, Ballistics Gel, agar, gelatin, PVC mixtures 1 and 2, and an ultrasound image of living neck tissue from a volunteer patient. For statistical analysis, scored results of the pairwise image comparison were fit to a Bradley-Terry

logit model with a 95% confidence interval to compare the results relative to the living tissue [48].

2.5 Results and Discussion

As shown in Figure 2-2, Ballistics Gel, Blue Phantom, and PVC mixture 2 tissues provided the greatest needle resistance and most closely resembled the resistance provided by cadaver tissue at a depth of 16.6 mm. Gelatin and agar tissue manikins showed the least resistance throughout the insertions. Increasing the amount of mineral oil in the PVC mixtures decreases the resisting needle force in the PVC mixtures. Adding softener to the PVC also decreases the needle resistance.

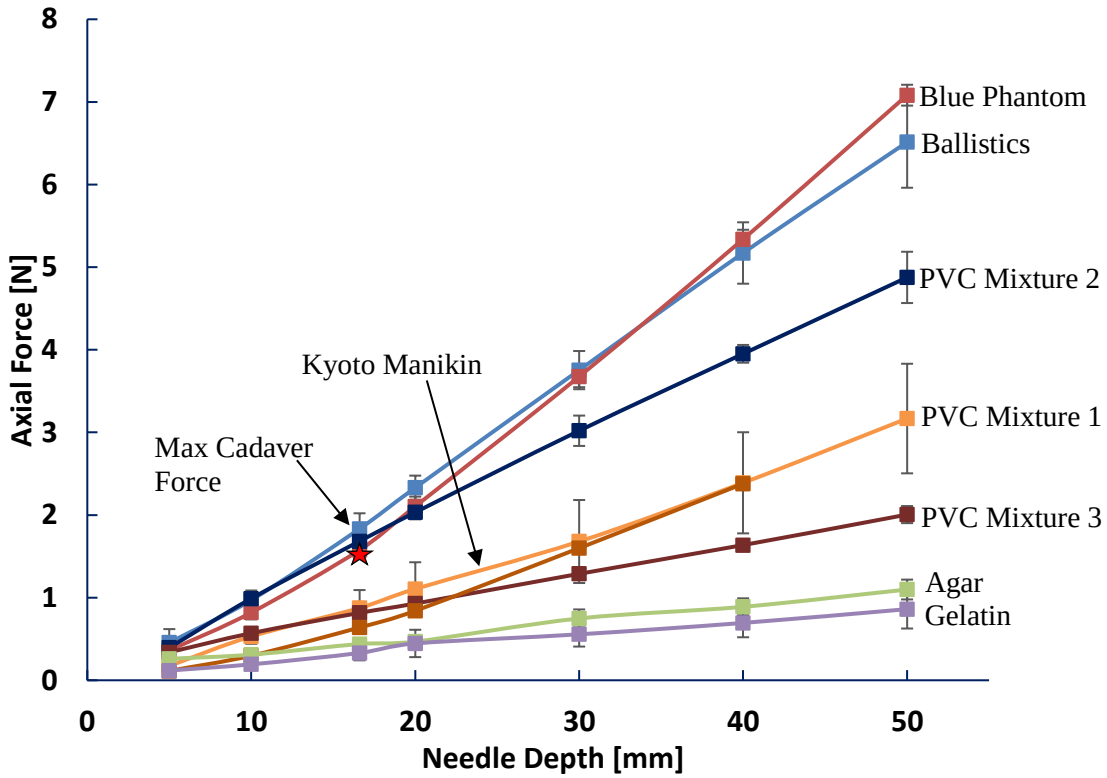

Figure 2-2 Average axial needle insertion force for seven ultrasound guided manikin materials. Star indicates maximum needle force during a 17 mm cadaver needle insertion. Error bars indicate standard deviation (figure data is not continuous, lines are sued to increase visual clarity).

The results of the pairwise comparison survey are shown in Figure 2-3 along with the maximum likelihood estimates of the fitting parameters of a Bradley-Terry Logit model (λ). A baseline fit of $\lambda = 0$ is applied to the living neck tissue for comparison. Images with a positive λ are less likely to be selected when viewed against the living tissue. The best performing material was the PVC plastisol Mixture 1, which used a combination of both softener and mineral oil additives. No statistically significant difference was found between PVC plastisol Mixture 2 and living tissue. The images produced by gelatin, Blue Phantom, Ballistics Gel, and agar were all statistically less likely to be chosen than the images of the living tissue. The worst performing materials were that agar and Ballistics Gel.

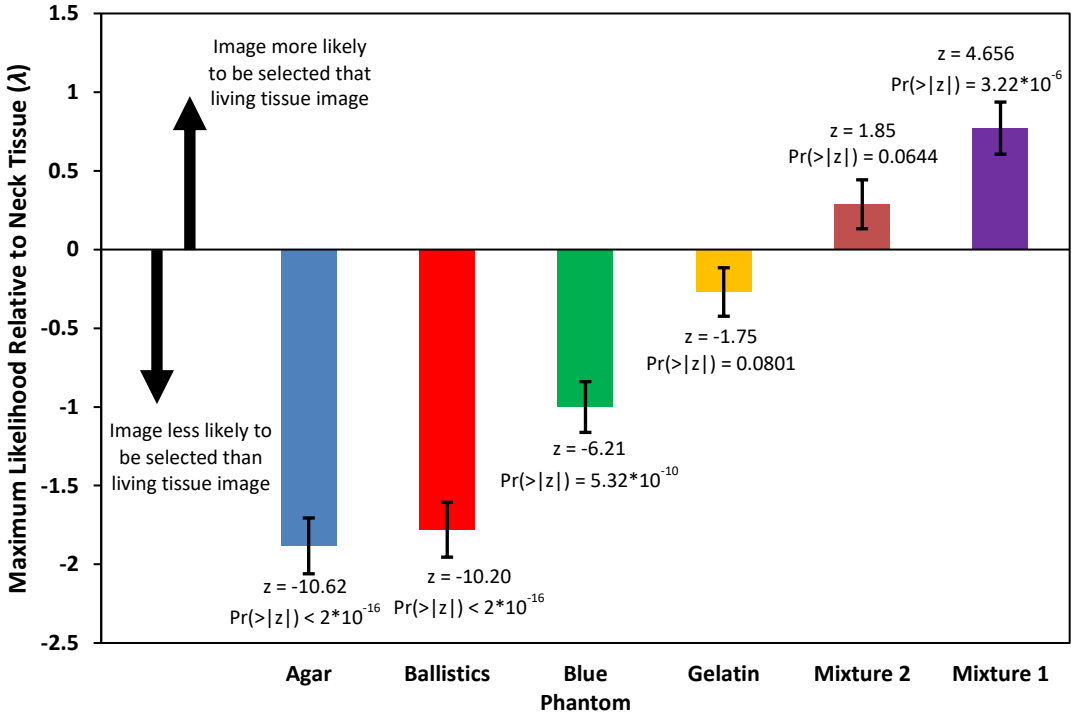

Figure 2-3 Final ranking results of the pairwise image comparison with the Bradley-Terry fitting parameters (λ) compared against a baseline fit parameter of 0 for living tissue.

The results of the needle force and pairwise image comparison show the variety of strength and weaknesses of the different commonly used manikin materials. For example, gelatin was viewed by experts to have significant similarities in ultrasound image to living tissue,

however it also had much lower axial needle insertion force. Inversely, Ballistics Gel and the Blue Phantom both had similar force properties to the cadaver but produced unrealistic ultrasound images. The worst performing material overall was the agar which had both low needle forces and unrealistic ultrasound images. Surprisingly, both PVC plastisol Mixtures 1 and 2 scored higher in ultrasound image realism than the living tissue. The ultrasound images of the two mixtures were more uniform, with lower contrast between the higher echogenic (whiter) and lower echogenic (blacker), than the images taken from the volunteer patients. It is possible that the experts surveyed were expecting the living tissue to have less contrast compared to the artificial images. Further research could explore why the images of the artificial tissue were observed to be more realistic that the images from the volunteer patient and what features in ultrasound are experts expecting to find. When comparing all 14 ultrasound images individually, there was consistency among the results. The two highest scoring images overall were from PVC plastisol Mixture 1, followed by Mixture 2. The two images of the living tissue came next, followed by two from gelatin, two from Blue Phantom, two form Ballistics Gel, and two form agar. This consistency implies that the images captured were equally representative of the ultrasound visualization of the different samples.

The PVC plastisol material was found to be easily adaptable. By changing the ratio of PVC to softener to mineral oil, needle insertion force can be adjusted. These adjustments allow for the easy creation of realistic PVC plastisol multilayered phantoms as shown in Figure 2-4. Multilayered manikins can be customized to represent different patient types such as obese or muscular patients. This is done by using different PVC plastisol mixture ratios to simulate tissue such as skin, muscle, and fat. The ability to offer diverse patient scenarios is a significant strength of the modified PVC plastisol mixtures that cannot be offered by the other materials tested. The PVC plastisol was also found to be durable and easily repairable. Through repeated testing, it was found that the multilayered PVC plastisol CVC manikin insert pictured in Figure 2-4 was able to withstand at least 10 needle insertions before needle to replace the tubing. Tubing replacement

was also as simple as sliding the old tubing out of the material and sliding new material in. Finally, although the modified PVC plastisol mixtures do develop a thin oil surface over time, the quality of the needle force resistance and ultrasound imaging does not degrade based on continued experience with the material.

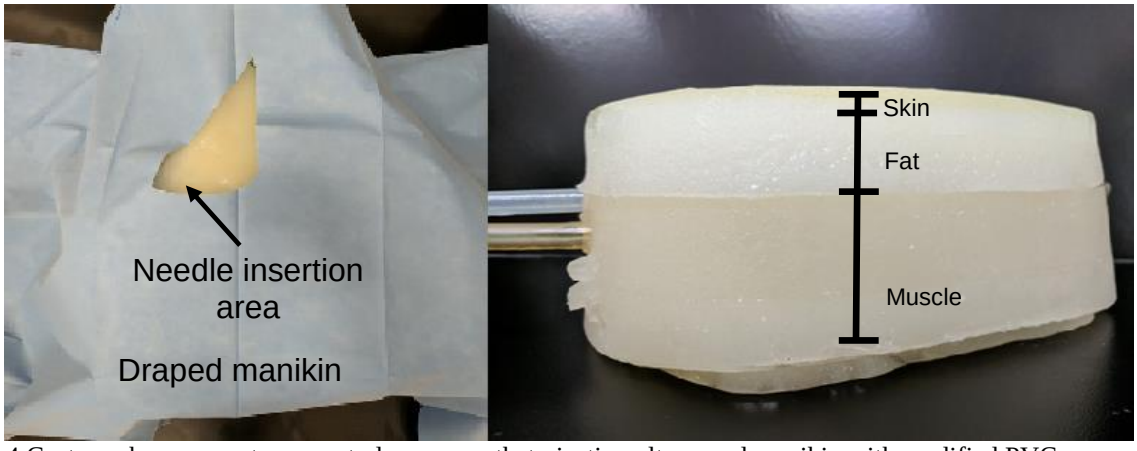

Figure 2-4 Custom obese upper torso central venous catheterization ultrasound manikin with modified PVC plastisol insert (left) and side view of the insert (right).

2.6 Conclusions

A method of creating a novel modified PVC plastisol manikin has been developed. Testing showed that this material outperformed tradition phantom materials. Force testing showed how the modified PVC mixtures can be altered to vary needle forces to be similar to cadaver neck tissue or softer tissues. The modified PVC plastisol mixtures also provide more realistic ultrasound images than the four other manikin materials tested and were viewed as similar to living tissue. In addition, the modified PVC plastisol mixtures are low cost. The cost of a 2000 mL phantom insert made from modified PVC plastisol is approximately $15 compared to thousands of dollars for a commercial phantom. Modified PVC plastisol has great future potential for surgical training manikins due to its customizability, human tissue-like needle resistance and echogenicity, and affordability.

Chapter 3
Design of the Dynamic Haptic Robotic Trainer for Central Venous Catheterization

3.1 Introduction

The second stated contribution of this dissertation is to determine the effectiveness of computer simulation for use in needle insertion training. Advances in computing power are leading to a revolution in the ways in which medical students and residents are trained in surgical procedures. Where previously training involved manikins, cadavers, or live patients, computer simulators are starting to change the way in which future doctors are educated. This chapter describes work that has been conducted developing a computer simulator called the Dynamic Haptic Robotic Trainer (DHRT) for Central Venous Catheterization. The chapter begins by describing ultrasound guided central venous catheterization and how haptic computer simulation is being utilized to surgical training. Next, the chapter describes the original design of the DHRT. Finally, the first preliminary study conducted with third year medical students is detailed followed by concluding remarks.

This chapter is based on the papers "Design of a Virtual Reality Haptic Robotic Central Venous Catheterization Simulator" from the Proceedings of the ASME 2016 International Design Engineering Technical Conferences and "A Virtual Reality Haptic Robotic Simulator for Central Venous Catheterization Training" from the ASME Journal of Medical Devices [49, 50].

3.2 Central Venous Catheterization Procedure and Training

Ultrasound guided CVC is a common surgical procedure performed over 5 million times per year in the United States. This procedure provides an access point for surgery and allows doctors to provide nutrition, medication, and administer testing not possible through less invasive means [30]. When performing a CVC, the doctor has the option to cannulate several different sites including the right internal jugular vein (IJ), the right subclavian vein, and the femoral vein. The most commonly chosen site is the right IJ vein because of a decreased risk of infection compared to femoral insertions and the right IJ vein's more superficial nature and decreased risk of pneumothorax compared to the subclavian vein [51, 52]. Because right IJ vein insertion is most common, it has been chosen as the focus of this simulation training research.

The procedure for CVC of the right IJ vein is as follows: the doctor begins by finding the triangle formed by the heads of the sternocleidomastoid muscle in the neck and the clavicle bone. Once found, the area is sterilized and local anesthesia is administered. Next, an ultrasound probe is used to scan the insertion area and identify the right IJ vein and the carotid artery. The two vessels can be distinguished by the compressible nature of the IJ and the slight pulsatility of the artery. Typical patient anatomy also places the IJ vein lateral to the more medial carotid artery, however patients with atypical vessel positioning do exist. Now the doctor will attempt to insertion the tip of their catheterization needle into the triangle towards the ipsilateral nipple at a 30 to 45 degree angle and into the right IJ vein. The ultrasound probe is used as guidance for the insertion, and it is important for the doctor to identify the needle on the ultrasound display using its echogenic reflection and local tissue deformation. During insertion, the doctor must also pull on the syringe plunger in an action known as aspiration. This ensures that blood will fill the syringe, known as flash, whenever they enter a vessel. It is also important for the doctor to note the color of the blood to ensure that it is dark deoxygenated venous blood as opposed to bright oxygenated arterial blood. Once the vein has been accessed by the needle, the doctor will

carefully remove the syringe from the needle and insert a guide wire through the needle and into the vein. The needle is then removed and a dilator is inserted over the wire to dilate the tract. The dilator is then removed and the catheter is finally inserted over the guided wire until the tip is positioned in the superior vena cava just outside of the entrance to the right atrium of the heart. To finish, the catheter is sutured in place, and a sterile dressing is applied [53].

Extensive training and experience is necessary for surgical procedures such as CVC, and it has been shown the CVCs administered by doctors who have completed over 50 CVC insertions are at a significantly lower risk of complications [46, 47, 54]. Training methods for CVC vary by residency program, however modern training typically involves the use of upper torso surgical training manikins. Manikin simulators such as this allow residents to practice their insertion techniques more frequently and without placing patients at risk [15, 55]. While training manikins have benefits, there are several drawbacks to training with these static simulators. First research has shown that there is a rapid decay in the skills trained by upper torso central line manikins during the first few months after training has been completed [56]. Another issue is the anatomy presented in manikin simulators is often idealized and does not accurately represent the anatomy of a wide variety of patients including those who are obese or difficult relative positioning of the IJ vein and carotid artery. Furthermore, manikin training relies on observation based qualitative feedback and assessment from an instructor which is vulnerable to biases such as “examiner burnout” due to busy work schedules and the instructor’s personal opinions of the resident being trained [57]. More effective training solutions that combine both quantitative and qualitative feedback need to be developed to fulfill the training needs of residents. Computer simulation presents a solution.

3.3 Computer and Haptic Simulation for Surgical Training

Modern computing power has made possible the creation of sophisticated haptic feedback systems and virtual reality (VR) based surgical simulators with extensive training capabilities [58]. A 2007 study by Morris et al. suggested that haptic feedback training in combination with visual feedback may be an effective training tool for skills where force sensitivity and fine motor skills are a crucial component. It also suggested that combined visual and haptic feedback training provides a better education than separate visual and haptic training [59]. A 2016 study indicated that the ability to better understand haptic sensations felt during a CVC could affect performance [60]. In response, both high and low fidelity computer based patient simulators have been developed for surgical training.

Advanced haptic simulators such as the *PalpSim* palpitation simulator developed by Coles et al. are able to provide extremely realistic haptic feedback to the user [61]. The *LAPSIM* laparoscopic surgical simulator combines haptic feedback, VR, and user feedback to create an immersive high fidelity laparoscopic simulation and is able to distinguish between expert and novice performance for procedures such as simulated suturing and clip applying [27]. The *Sonosim* (Sonosim Inc. Santa Monica, CA) ultrasound training device is used to practice ultrasound scanning of different parts of the body using high fidelity ultrasound images and can be used on any surface for training. One study found that it can serve as an adequate replacement to live model training, but does not provide superior training results to live model training [62]. Finally, the *Mediseus* (Medic Vision, Tirat Carmel, Israel) epidural simulator is designed to be mobile, easily deployable, and give instant feedback to the user. However, this comes at the cost of it being less effective at distinguishing performance between experts and novices [63, 64]. This is a small sample of the many computer based VR and haptic simulators that have been developed for surgical training. The DHRT for CVC has been developed to explore the potential of haptic and VR training for percutaneous procedures.

3.4 Design of the DHRT 1.0

The design of the DHRT version 1.0 is pictured in Figure 3-1. The DHRT 1.0 system was programmed in *MATLAB* and *Simulink* (MathWorks, Natick, Massachusetts). A computer was custom built for the simulator running the Microsoft Windows 8.1 operating system with an Intel *Core i7-5930* 3.5 GHz processor to ensure that the system processed fast enough for real time simulation. Also included was 32 GB of DDR4 RAM, and 250 GB of solid state drive storage to ensure fast read and write times. The DHRT 1.0 can be divided into two main components: the haptic robotic arm and the virtual ultrasound device. A subsection has been dedicated to each of these components. The DHRT system also focuses exclusively on the needle insertion portion of the CVC procedure due to the fact that this is the sources of the majority of CVC complications.

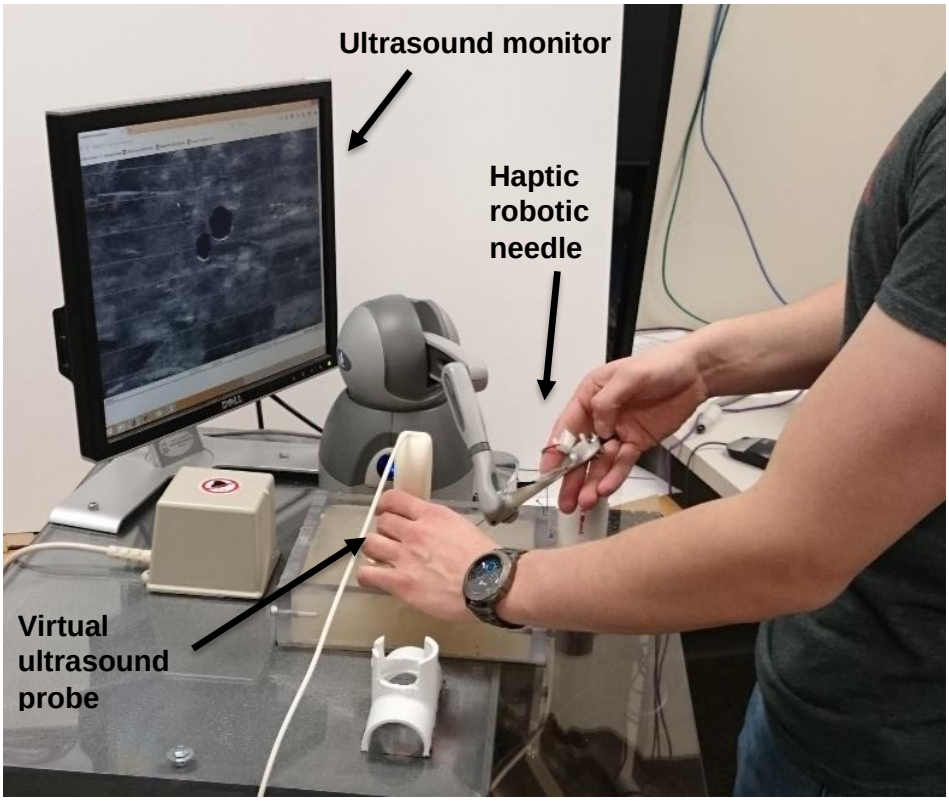

Figure 3-1 Picture of the DHRT for CVC 1.0 system.

3.4.1 Haptic Robotic Arm

The haptic robotic arm is used to simulate needle insertion forces and track needle position for the DHRT. The DHRT 1.0 used a *Geomagic Touch* (3D Systems, Rock Hill, SC) robotic arm as seen in Figure 3-2. The *Geomagic Touch* provides three degrees of force feedback up to 3.3 N of force and six degrees of position tracking with a resolution of 0.055 mm. To interface the robotic arm with *Simulink*, the Quanser *Quarc* (Markham, ON, Canada) software package was utilized.

Figure 3-2 Geomagic Touch haptic robotic arm [65].

A program was written in *Simulink* to determine robotic arm position and used a position feedback loop to determine the magnitude and direction of force to be applied by the robotic arm. The direction of the force was calculated using a unit vector where the direction of the vector is pointed in the axial direction of the robotic end effector. The magnitude of the force feedback was based on the vertical depth of a projected needle tip relative to a virtual tissue surface. The depth

was entered into a piecewise force characterization, as shown in Equation 3-1, developed using a method by Gorden et al., and the output force was calculated [66].

$$F(x) = \begin{cases} A_1 e^{B_1(x-D_1)} + C_1 & if\ 0 \le x < P_1 \\ A_2 e^{B_2(x-D_2)} + C_2 & if\ P_1 \le x < P_2 \\ \vdots & \\ A_n e^{B_n(x-D_n)} + C_n & if\ P_{n-1} \le x < P_n \end{cases} \quad (3\text{-}1)$$

F and *x* are the needle insertion haptic feedback force and the depth of the needle respectively. A_n, B_n, C_n, and D_n are used to parameterized the needle force. P_n are the critical depths for each of the piecewise intervals. For the DHRT 1.0, force characterizations were developed using bovine and manikin needle insertion force profiles as reference [66].

Originally, a virtual needle tip was projected 8 cm from the gimbal end of the robotic end effector. However, through feedback with experts and surgical residents, it was soon determined that this virtual needle tip was problematic. Not being able to visually reference the tip of the needle made it very difficult for those evaluating the device to know where their needle tip was located and when it was entering the simulated tissue surface. To solve this problem, a new syringe-like end effector was developed.

For the development of the custom syringe end effector, there were four main design requirements: the attachment needed to be similar in size to a real syringe, it needed a retractable needle, it must have an extendable plunder for aspiration, and it must attach to the end of the *Geomagic Touch*. Following these guidelines, the end effector in Figure 3-3 was created. The retractable needle was necessary so that all forces felt by the user came from the robotic arm, not from the needle entering the mock tissue surface. The extendable plunger was including and linked to an electric switch so that trainees could train their aspiration skills and so that aspiration could be detected by the robot. This was achieved using a 3 shell design. The inner shell contained a series of low force compression springs attached to the needle. This allowed for needle retraction and extension with minimal force. The middle shell was the plunger, which

attached to an extension spring fixed to the front of the outer shell. The outer shell was syringe shaped and formed to fit onto the gimbal of the *Geomagic Touch*. The attached syringe is shown in Figure 3-4. An artificial tissue surface made from PVC plastisol was sued for the practice insertions. The material provided a soft surface to mimic the feel of human tissue. A thin plastic sheet was planted 0.5 cm below the tissue surface. This allows the needle to only penetrate the surface to a depth of 0.5 cm, yet give the illusion of a needle entering deep into tissue.

Figure 3-3 Custom syringe end effector for *Geomagic Touch.*

Figure 3-4 *Geomagic Touch* haptic robotic arm with custom syringe end effector.

3.4.2 Virtual Ultrasound Device

The second major component of the DHRT 1.0 was the virtual ultrasound device. This device used a Northern Digital Inc. (Waterloo, Ontario, Canada) *3D Guidance TrakSTAR* electromagnetic position tracking sensor as the foundation for controlling the ultrasound. This tracking probe has six degrees of position tracking with an accuracy of 1.4 mm RMS and 0.5 mm RMS. The probe was outfitted with a custom 3D printed ultrasound probe casing to familiarize users with the feel of an actual ultrasound probe as shown in Figures 3-5 and 3-6.

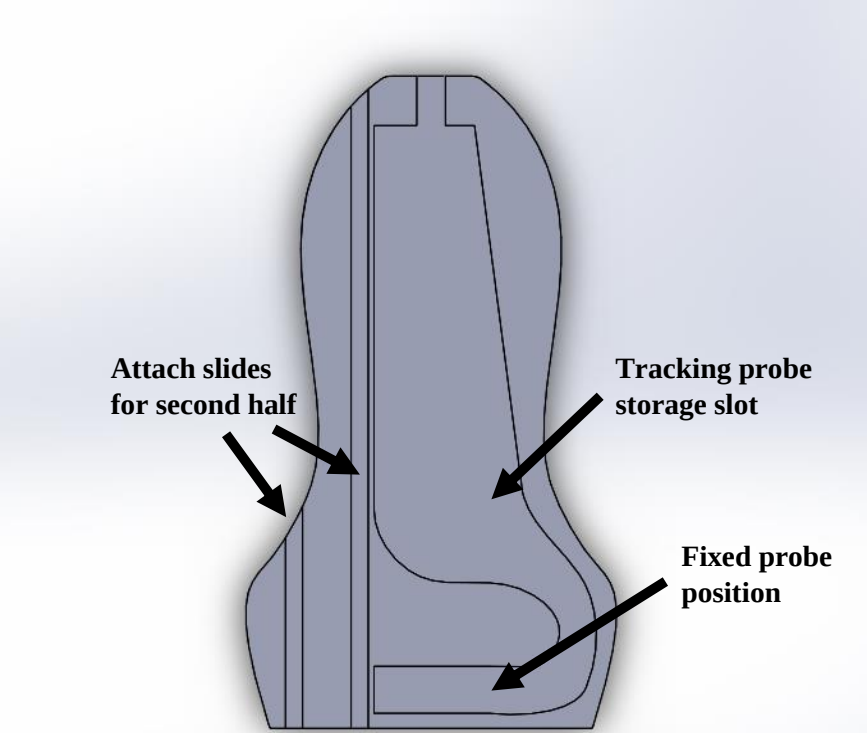

Figure 3-5 One half of the mock ultrasound probe showing how the tracking probe is stored.

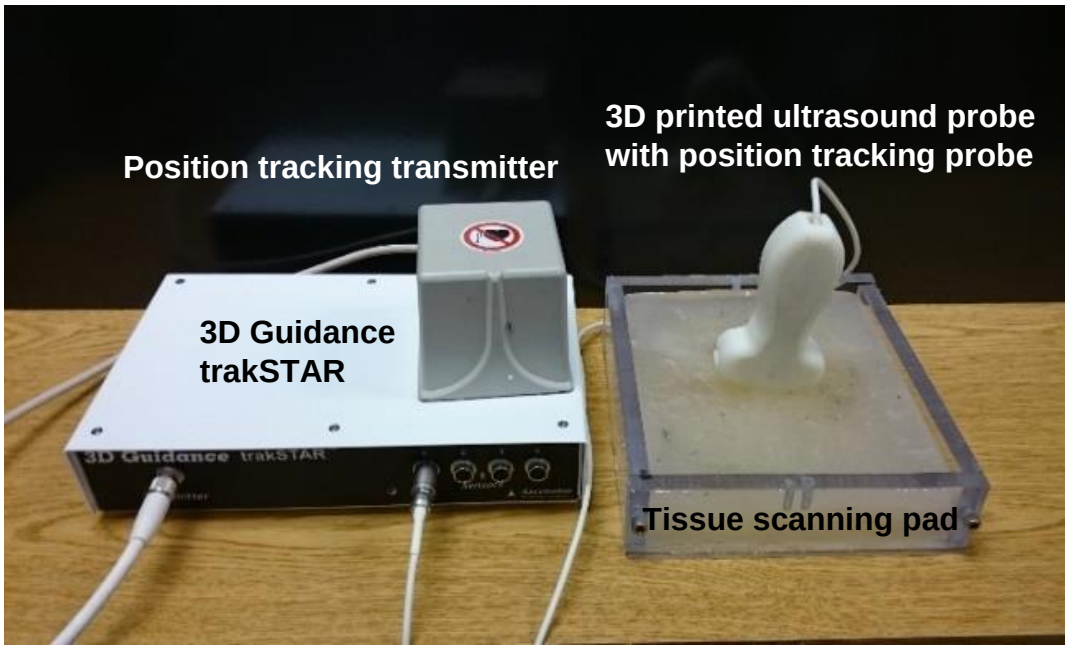

Figure 3-6 *3D Guidance TrakSTAR* with 3D printed mock ultrasound probe and PVC plastisol simulated tissue scanning surface.

Testing was conducted in order to evaluate the rotational accuracy of the mock probe. A protractor was attached to a testing surface and the probe was rotated through a series of angles. When measuring the rotations of the robe, the average error in probe angle θ of rotation around the z-axis was measured to be 1.7 degrees. The error in the probe with the trend line equation in Equation 3-2 with a R^2 value of 0.88 is shown in Figure 3-7.

$$Absolute\ Error = 0.0252 * \theta + 1.685 \quad (3\text{-}2)$$

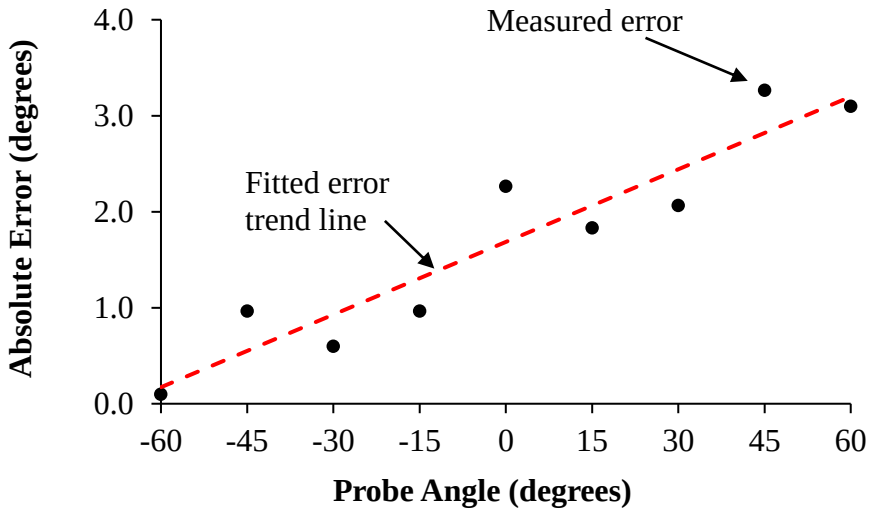

Figure 3-7 Absolute error between the actual probe angle and the measured angle.

Through testing, the importance of minimizing the amount of magnetic material near the mock ultrasound probe was learned. It was found that small amounts of magnetic metal attached to the bottom of the testing table had an effect on probe accuracy. By changing to a new test bench, the probe angle error was greatly reduced.

After completing the mock ultrasound probe, a virtual ultrasound simulation for CVC needed to be created. This simulation was created in *Simulink* and the *3D Guidance TrakSTAR* was interfaced with the software using a C++ API, *Quarc* interfacing software, and a server client relationship. When the simulation begins, a C++ program is activated that sends out a client data signal from the tracking probe. The *Simulink* code contains a server block which reads the input from the C++ client. The simulate ultrasound visual was created using the Virtual Reality Modeling Language due to its compatibility with *Simulink*. The visualization was designed to mimic the 2D cross section created by an ultrasound beam plane. The DHRT 1.0 ultrasound simulation contained five main objects: a vein, an artery, a rectangle representing the location where the needle crosses the ultrasound plane, tissue deformation lines, and a background which was a still ultrasound image.

The simulated ultrasound's vein and artery were represented by two ellipses, created by a series of points along the edges of the shapes. The points of the vein were then designed to move vertically with respect to the location of the tip of the robotic arm needle. When approached by the needle, the circle points move away from the needle tip vertically, simulating tissue deflection. The points also moved whenever the mock ultrasound probe was pressed into the testing surface to simulate vein compressibility. The artery also deformed slightly by pulsing to simulate a heartbeat. This can be seen in Figure 3-8.

Whenever the robotic needle crossed the ultrasound beam plane, the location of this crossing was represented in the simulator by a small rectangle at this crossing location. The mock ultrasound probe and the robotic arm were able to interact through the use of known relative starting locations of the devices. The location of needle beam crossing was calculated using a line-plane intersection equation and a 2x3 transformation matrix as shown in Equation 3-3. *T* is the transformation matrix, *I* represents the 3D location of the needle plane intersection and *u* is the 3D location of the ultrasound probe. Being able to determine the location of the needle tip using the ultrasound guidance is a key CVC skill, so it was essential that this was included in the simulator.

$$\begin{bmatrix} x_{new} \\ y_{new} \end{bmatrix} = T * \begin{bmatrix} I_x - u_x \\ I_y - u_y \\ I_z - u_z \end{bmatrix} + \begin{bmatrix} u_x \\ u_y \end{bmatrix} \quad (3\text{-}3)$$

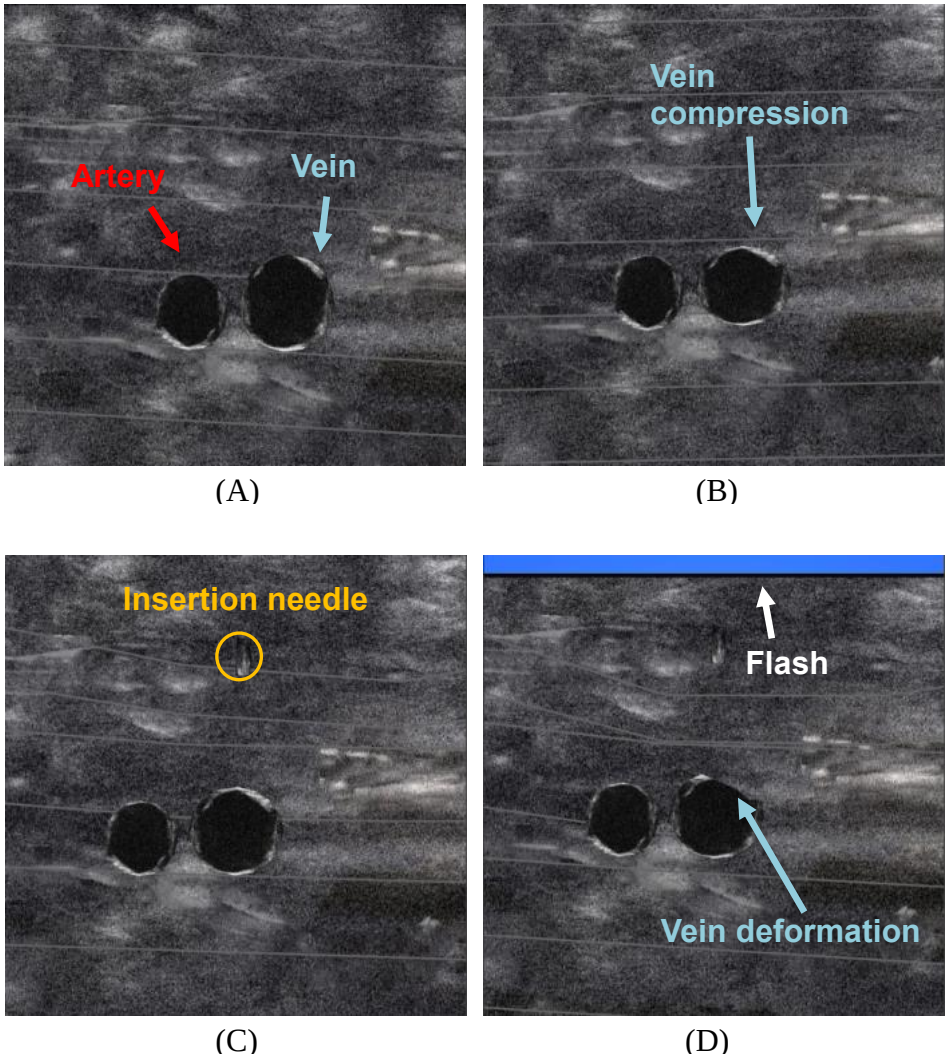

Figure 3-8 Virtual ultrasound during different stages of needle insertion: (A) finding vessels, (B) determine vein by checking for compressibility, (C) identify where needle crosses the ultrasound plane, (D) vein deformation and needle flash appears during successful insertion.

Because of some limitations of the Virtual Reality Modeling Language, the background of the simulated ultrasound was not able to deform with respect to the location of the robotic needle tip. Through consultation with CVC experts, it was determined that finding a way to convey this background tissue deformation was important to include in the simulation since it helps a surgeon properly identify needle position. This was achieved through the use of tissue

deformation lines shown in Figure 3-9. These lines are created by a series of points which deform with respect to the needle position in the same way as the virtual vein.

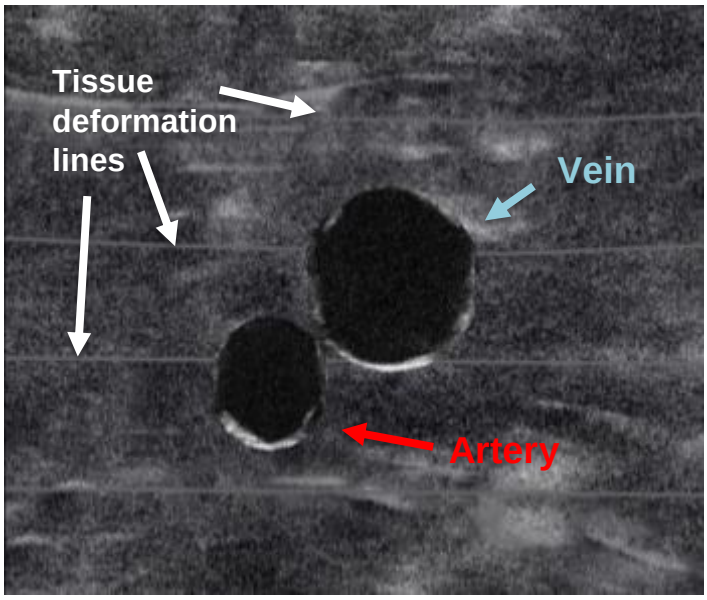

Figure 3-9 Simulated ultrasound image of an IJ vein, carotid artery and tissue deformation lines.

The textures used on the background and the objects in the simulation were based on several actual ultrasound images of the region around the right IJ vein and the carotid artery. The images were then blended together into a realistic mock ultrasound image. As mentioned in section 3.2, if the syringe enters a vessel while the surgeon is pulling on the plunger, blood will fill the syringe. This is known as flash and is used to confirm venous access. To emulate this, a flash indicator was added to the screen. If the needle entered the vein while the plunger was being aspirated, a blue bar would appear. If the vessel entered was the artery, a red bar would appear. . If the vessel entered in the artery, a red bar would appear. This feature can be seen in Figure 3-8 (D). Through the use of this virtual ultrasound image and control using the mock ultrasound probe, a strong simulation of the ultrasound aspect of CVC was created.

Once the two main components of the first DHRT was completed, it was determined that a mobile testing station was necessary to ensure consistent calibration of the system and easy transportation. The system was built on a large plastic push cart. Plastic was chosen to avoid any

possible interference with the electromagnetic position tracker. A large acrylic glass surface was mounted on top of the cart. Affixed to this surface is a computer monitor used for navigating the computer program and the ultrasound image, the motion tracking receiver, the haptic robot, position calibration holsters for the robotic syringe and the ultrasound probe, and the artificial CVC testing surface. By affixing these parts to the cart, a consistent position based calibration of the devices could be achieved. The testing surface is placed in the middle of the acrylic glass surface. The lower portion of the cart holds the computer running the simulation and the position tracking unit.

3.5 Third Year Medical Student Study Methods

Both qualitative and quantitative testing of DHRT CVC simulator were conducted. During development, a surgeon and a trained medical resident who teaches first year medical residents CVC were consulted to ensure realism in our simulation scenarios, haptic forces, and ultrasound images. Eight different testing scenarios were developed varying vessel size, location, and force characterizations as seen in Table 3-1.

Table 3-1 List of DHRT scenarios for the third year medical student study.

Scenario	Vein Depth (cm)	X Distance between Vessels (cm)
1	2.60	0.050
2	1.90	0.750
3	2.90	0.00
4	2.10	1.50
5	2.20	-0.250
6	1.95	0.850
7	3.15	0.150
8	2.50	0.150

A study was conducted with 12 third year medical students with no CVC experience to evaluate effectiveness of the simulator and difference between training scenarios. All 12 students were given an introduction to the CVC procedure and shown an example of the procedure on a training manikin by a trained medical resident. The students then each took a pretest where they attempted to properly insert a needle into the right IJ of a standard CVC training manikin. The 12 students were then split into three groups as seen in Table 3-2.

Table 3-2 Training groups for third year medical students DHRT study. All robotic tests used randomized scenario orders

	Number of Students	Training Session 1	Training Session 2
Group 1	6	8 Robotic	None
Group 2	3	4 Robotic	4 Manikin
Group 3	3	4 Manikin	4 Robotic

Group 1 had six students who practiced on each of the 8 different patient scenarios on the robotic simulator. Group 2 had three students who practiced on 4 random patient scenarios on the robotic simulator followed by four practice attempts on a CAE Healthcare *Blue-Phantom Gen II Ultrasound Central Line Training Model* (Model #BPH660) manikin. Group 3 had three students who took four practice attempts on the training manikin followed by four random patient scenarios on the robotic simulator. Before each DHRT training scenario, the medical students were given a sheet of paper with the patient details in which the scenario was based on. After each attempt, they were asked if the anatomy they found during the simulation matched what they expected from the patient details and given feedback on their performance. The simulator is able to output a wide variety of data for further analysis including: test time, 3D needle tip position, 3D ultrasound probe position, needle insertion angle, artery puncture, vein and artery positions, vein and artery size, needle aspiration, and full video and audio of the simulation.

During training, an assistant was present to give performance feedback to the medical students and answer any questions they may have had. Finally, after completing their practice

session, each medical student completed a posttest on a modified version of the CVC training manikin. After completion of their posttest, a brief exit survey was conducted for feedback on their experience with the robotic simulator.

For the purpose of this study, a successful insertion using the DHRT simulator was defined as follows. First, when the trainee verbally declared that their virtual needle tip was in the vein, the needle tip must have been that vein. Second, if the trainee inserted their virtual needle into the artery at any time during the test, it was deemed a failed test. Special note was taken if the trainee managed to successfully insert their needle during their first attempt at a patient scenario because this reduces the possibility of adverse effects.

3.6 Study Results

During their practice sessions with DHRT, the medical students were able to successfully insert the needle into the vein 69% of the time into the virtual vein. Their success rate during their first insertion attempt during a scenario was 50%.

Group 3 was 22.2% more successful on their first four robotic insertion attempts than the groups 1 & 2 (Figure 3-10). For comparisons between groups 1, 2, and 3, the only first four scenarios attempted by group 1 participants were analyzed because groups 2 and 3 only attempted four robotic insertions. If multiple insertion attempts are taken into account, groups 1 and 2 slightly outperformed group 3, but the results were similar (Figure 3-11).

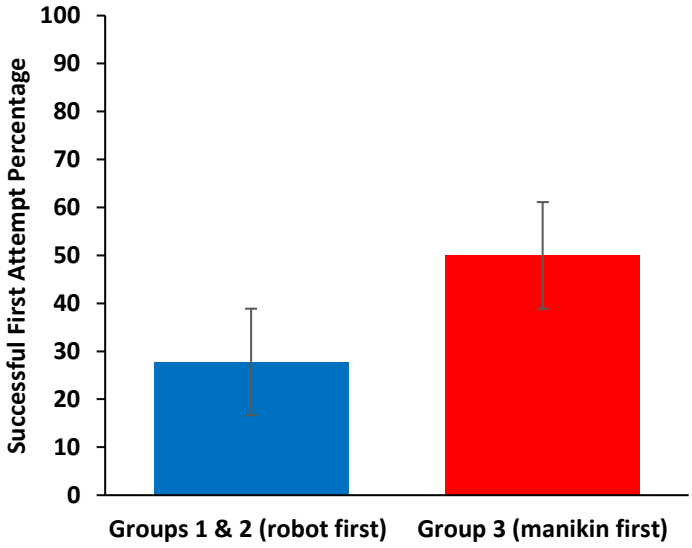

Figure 3-10 Comparison of successful first attempts at needle insertion between groups who received robotic training first (groups 1 & 2) and the group who received manikin training first (group 3).

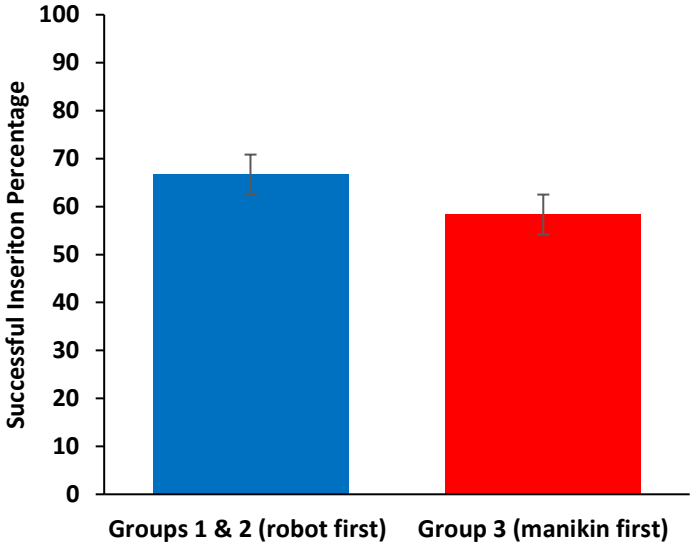

Figure 3-11 Comparison of successful attempts over multiple attempts at needle insertion between groups who received robotic training first (groups 1 & 2) and the group who received manikin training first (group 3).

When analyzing the running average of the success rate of the eight practice scenarios of group 1, there was an overall average increase in first attempt success percentage of 4.2% after each practice insertion attempt using the robotic simulator (Figure 3-12).

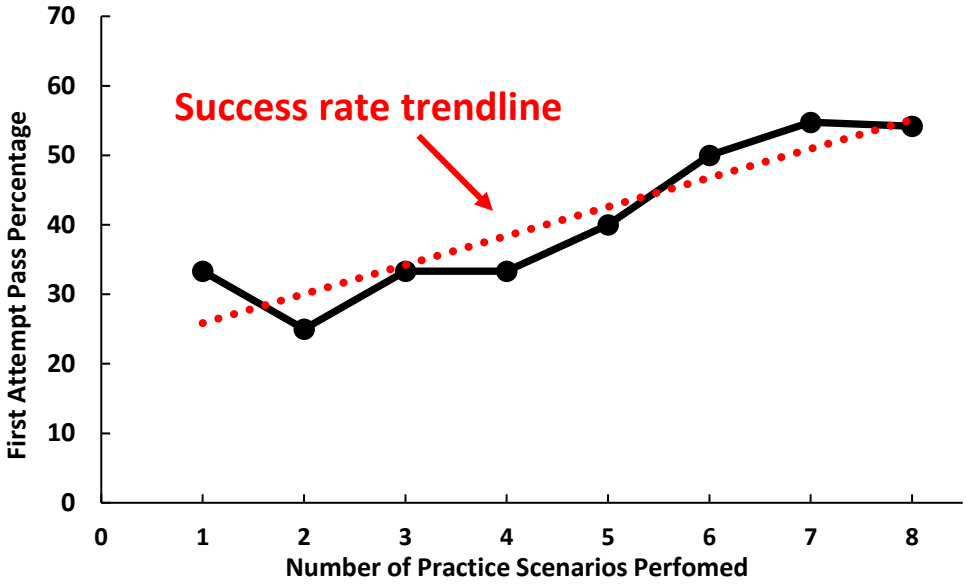

Figure 3-12 Percentage of successful practice insertions on first attempt versus the number of practice scenarios performed.

The difficulty of each scenario was assessed by the overall successful insertion rate for each scenario. The scenario with the overall highest success rate was scenario 4, with 88.9%. Scenario 4 had the greatest distance between the vein and artery of the 8 scenarios. The scenario with the lowest pass rate was scenario 2, with 44.4% (Figure 3-13). Scenario 2 had the shallowest vein depth of the scenarios.

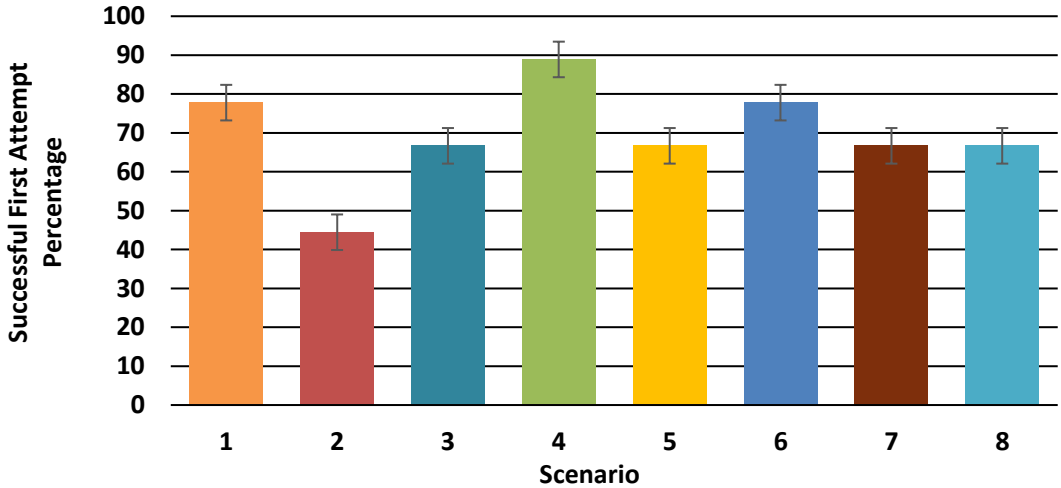

Figure 3-13 Successful robotic training needle insertion percentage for each training scenario.

The length of time it took for the students to insert the needle during the simulation showed a slight linear relationship with the depth of the vein (Figure 2-14). As the target vessel deepened, the time it took to access the vessel with the needle increased.

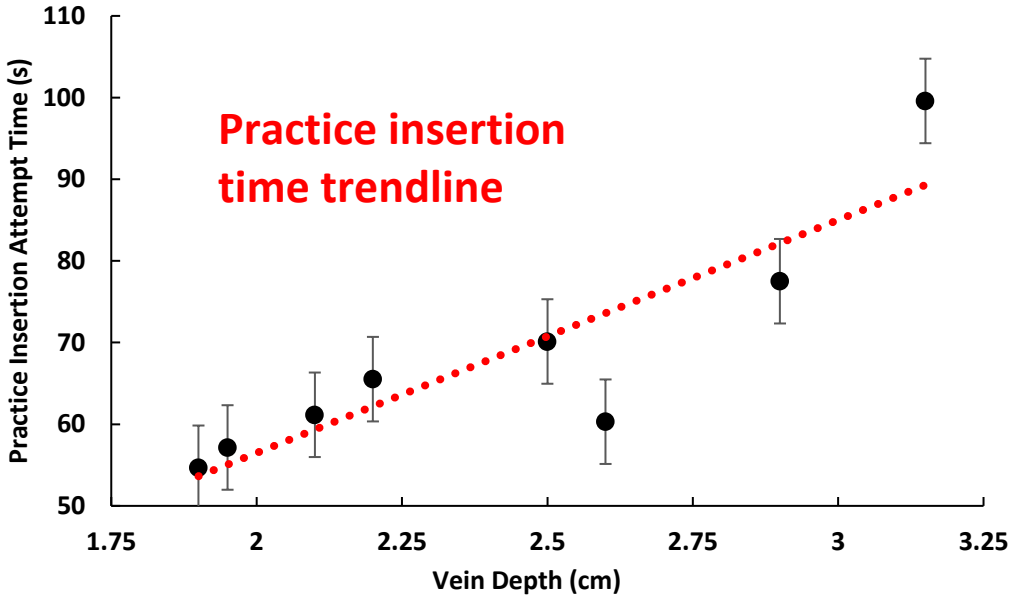

Figure 3-14 Length of time of the practice insertion attempts vs the depth of the target vein.

When the medical students were asked to rate if the DHRT CVC simulator was an effective method of learning the CVC procedure, with 1 being completely disagree and 5 being completely agree a Wilcoxson Rank Sum test indicated that the trainees who used the robot (Median = 4) did not a have significantly better opinion of the DHRT that the group who used mixed training (Median = 3), $U = 7$, $p < 0.05$.

3.7 Discussion of Results

The results showed that group 3, who received manikin training prior to training on the DHRT simulator, performed better during their first insertion attempts than groups 1 and 2 who received no prior training. This implies that the skills acquired during manikin training apply to

training with the DHRT. From this, it can be inferred that skills useful for CVC apply to the DHRT and vice versa.

The results of group 1 show a gradual improvement in their first insertion attempts over 8 practice insertions, but an overall slight decrease or no change in performance during the first 4 practice insertions. A sudden increase in successful first insertion occurs after the fourth practice scenario. This may reflect the initial learning curve of the device. An important aspect of training with a new device such as the DHRT is becoming comfortable with using the device. Minimizing the initial learning period is important to creating a successful training device.

There was a distinctly low success rate for the robotic practice scenario with the shallowest vein. It was noted by the robotic practice attendant during testing that the students seemed to be surprised by how shallow the vein was and had a tendency to quickly overshoot the vein. This could be a very useful scenario to help trainees to not begin their insertions too quickly and be more controlled in their movement. The highest success rates came from medium to shallow vein depth but with the artery and vessel further apart from each other. This could be because students felt less of a risk of hitting the artery and were more comfortable with the scenario. A larger sample size would be help to confirm this.

The length of time of the robotic insertions relating linearly to vein depth was an expected result. If the vein is deeper into the tissue, the needle has further to travel, thus will take longer to complete. It may also take longer to be confident that the needle is following the intended path through the tissue. This information and the varying success rate of the different scenarios show how it is possible to vary the difficulty of CVC scenarios using the VR haptic robotic CVC simulator. This is a distinct advantage that the robotic training has over the CVC training manikin.

The results of the exit survey show an overall positive attitude towards the haptic simulation by the medical students, however there is a notable difference between the group trained only on the robot and the groups trained on both the manikin and the robot. One student

commented that they “felt much more confident going back to practical application on the manikin after multiple patient scenarios on the robot.”

Groups 2 and 3 (both manikin and robotic training) had a very wide variety of opinions about the robotic simulator. One dissatisfied student who was trained first on the manikin and then on the robot wrote “I think the ultrasound image was not representative of an actual US image in that the needle visualization was different. I also felt that the needle was difficult to maneuver in aspirating and applying a constant force to insert the needle.” A different student was very satisfied and wrote that the robot was “very fun” and provided “precise feedback on final location and angle [and] great visual feedback for aiming needle”. These two very different opinions may result from individual feelings towards VR simulation versus training on manikins which more readily give the illusion of working on a patient.

Overall, the results of this study show the potential of the DHRT system as a tool for training individuals to learn how to insert a needle for central venous catheterization. After an initial learning curve, there seems to be a gradual improvement in performance. It also appears possible to vary the difficulty of the practice sessions by altering the scenarios. Students mostly seem comfortable learning on this robotic system, yet more work needs to be done to improve the overall user experience.

3.8 Concluding Remarks

Upon completion of this study several areas in need of improvement were identified for the DHRT system. First, it was decided that in order improve the quality of the haptic feedback, needle force data for human tissue would be needed. Next, a higher quality haptic arm needed to be acquired to allow for a finer level of haptic feedback, more accurate position sensing, and an improved syringe end effector. Finally, a user friendly GUI needed to be developed. This would give improved feedback to the user, and allow a trainee to use the DHRT without an instructor.

This chapter presented the design of the DHRT 1.0 system, as well as two experiments involving the development of the system. First, the process of performing a CVC was detailed as well as the potential risks of the procedure. Next, the different training methods for CVC were explained along with the current state-of-the-art regarding haptic and computer based medical simulation. The chapter continued by explaining in detail the hardware and software used in the DHRT as well as the design and implementation of the haptic robotic arm and virtual ultrasound device. Finally, the chapter presented a research study involving the training of medical student using the DHRT system. Interesting results of this study included improved CVC performance using the DHRT by student who were first exposed to a training manikin, an approximate DHRT learning curve of four practice insertions, and how very shallow vessels were found to be more difficult by the students than deeper vessels. Overall, the results of this research was promising and was the driving force behind the changes made to the DHRT system and research that will be detailed in the next chapter.

Chapter 4
Modifications and Residency Program Implementation of the Dynamic Haptic Robot Trainer

4.1 Introduction

As chapter 3 brought to light, many insights were gained through the development process for the DHRT 1.0 system. The virtual ultrasound device was found to be an effective simulation of ultrasound for the CVC procedure. The system was able to effectively capture the behaviors of the medical students training with the device in a way that could be effectively analyzed for notable trends in their performance. Factors such as these drove further work to improve the DHRT that is explained in the following chapter. The chapter begins by presenting a cadaver study conducted to improve our understanding of the axial needle forces involved in insertions into human neck tissue. Next, improvements to the haptic needle force model and haptic robotic arm are detailed. The chapter presents the development of a GUI for the DHRT and the factors used to score the performance of trainees. Then, a major study involving training first year surgical residents is described. Last, a final series of improvements to the DHRT are detailed.

The following chapter details the development of the DHRT system and uses content from the following first author papers: "Measurement of Syringe Needle Forces for a Haptic Robotic Training Device" in the ASME Journal of Medical Devices September 2017 and "Training Surgical Residents with a Haptic Robotic Central Venous Catheterization Simulator" to be published in the Journal of Surgical Education [67, 68].

4.2 Cadaver Haptic Force Characterization for Central Venous Catheterization

As mentioned in the section 3.4 “Design of the DHRT 1.0” in Chapter 3, previous work completed by Gordon et al. found that axial needle insertion force of a needle insertion can be characterized through the use of a piecewise exponential equation. This equation (3-1) is capable of capturing the “saw tooth” shape commonly seen in plots of needle force versus needle depth [69]. This work also resulted in *MATLAB* (MathWorks, Natick, MA) code that is capable of determining an approximate piecewise equation of needle force versus needle depth for a given data set. To utilize these equations, accurate needle force data during a CVC insertion was needed. To acquire this data, a human cadaver research study was performed.

4.2.1 Force Sensing Syringe Design

Needle insertion force data was captured by designing and implementing a force sensing syringe. The design of this syringe utilized an ATI Industrial Automation (Apex, NC) *Nano17* 6-axis force transducer which has a resolution of 0.00625 N for forces under 17 N. The transducer was placed between two custom machined fixtures. The front fixture was designed to attach to a standard locking needle attachment point from a syringe. The rear fixture was designed to slide into the body of a 5 mL syringe. A Northern Digital Inc. (Waterloo, Ontario, Canada) *Guidance TrakSTAR Model 55* was attached to the syringe to provide 3D position tracking and determine the depth of the needle in the cadaver tissue. A National Instruments (Austin, TX) *PXIe-5351* data acquisition unit and *LABVIEW* software collected data from the force transducer at a rate of 180 Hz.

4.2.2 Cadaver Study

The force sensing syringe was employed in an experiment to gather cadaver tissue needle insertion force data for use in a haptic based CVC simulator. A middle aged, male, fresh frozen, unembalmed cadaver was acquired for this experiment. Five needle insertions into the cadaver's neck by an expert vascular surgeon were captured using the force sensing syringe. The goal of these insertions was to better understand the axial needle forces that occur during CVC insertion into the right jugular vein.

Three insertion types were captured. First, one standard ultrasound guided CVC of the jugular vein with no extra instruction. Next, two needle insertions were performed at the CVC rate site where the surgeon attempted to insert at a steady velocity. Finally, two needle insertions were inserted into the middle of the sternocleidomastoid muscle of the neck, again attempting to insert at a steady rate. For the purposes of this study, only axial forces were recorded.

4.2.3 Cadaver Study Results

Table 4-1 shows the maximum axial needle force and the accompanying needle depth for each of the five insertions. The highest maximum needle force occurred during the standard CVC insertion while the lowest maximum force occurred during the second of the neck muscle insertions. For the two neck muscle insertions, the highest forces were found near the middle of the insertion. For the other three insertions, the maximum force occurred 0.31 mm of the maximum insertion depth.

Table 4-1 Needle insertion forces during different types of insertions

	Max Axial Force (N)	Depth at Max Force (cm)	Max Depth (cm)
CVC Insertion	2.021	1.440	1.452
Steady 1	1.348	1.275	1.306
Steady 2	1.413	1.661	1.675
Neck Muscle 1	1.527	0.9064	1.450
Neck Muscle 2	1.196	0.7105	1.598

There are a few distinct features when observing the axial needle force during the standard CVC insertion as shown in Figure 4-1. The first is a noticeable saw tooth shape that occurs when force increases. This shape is typical when inserting a needle into soft tissue. It can also be attributed to slight hesitations during the insertion. This predictable shape implies that the surgeon was most steady in the initial stages of insertion. Another notable component is the large fluctuation in force between 1.00 cm and 1.25 cm. This is the approximate depth of the cadaver's right IJ vein. Due to some blood clotting, it was difficult for the surgeon to determine if the syringe was in the vein, so many adjustments were made at this location. The device captured these adjustments.

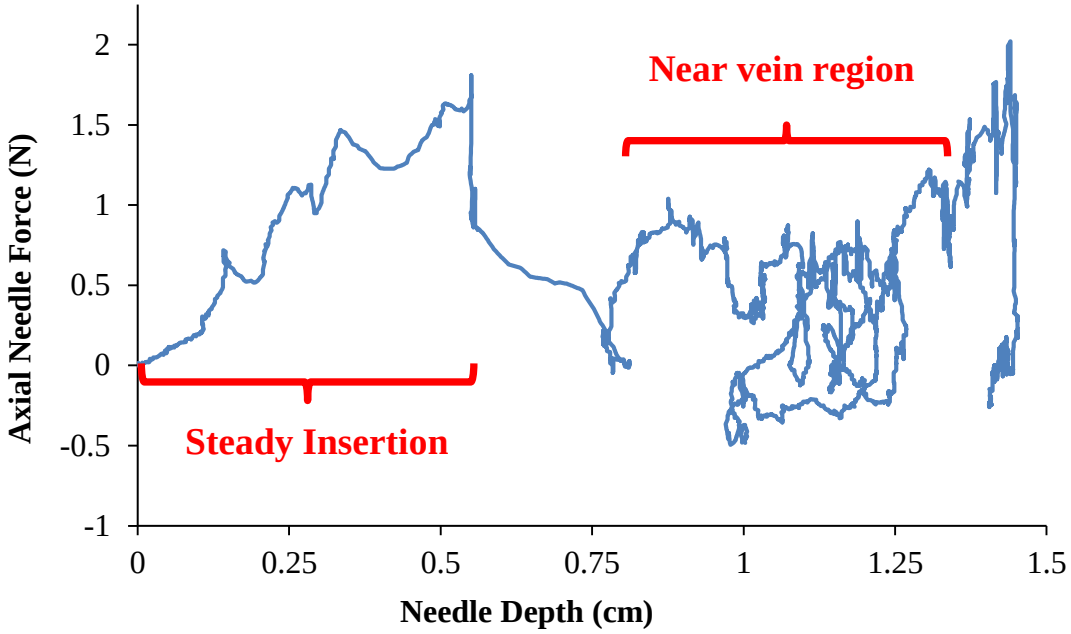

Figure 4-1 Needle insertion force during a CVC procedure on a fresh frozen unembalmed cadaver.

The steady state insertion shows similar saw tooth shape like the CVC insertion, as shown in Figure 4-2. However, the force peaks and drops are more noticeable in this situation. Also, no negative forces are recorded indicating that the surgeon never withdrew the needle. The insertions directly into the middle of the neck muscle had similar results to the previous steady CVC insertion, except the maximum force occurs at a shallower depth. The force appears to stabilize slightly in the middle region, as shown by Figure 4-3. This behavior is seen in both of the neck muscle insertions. This could indicate either a lack of consistent insertion rate by the surgeon or that the tissue in the region is softer and small anatomical are greatly effecting the forces.

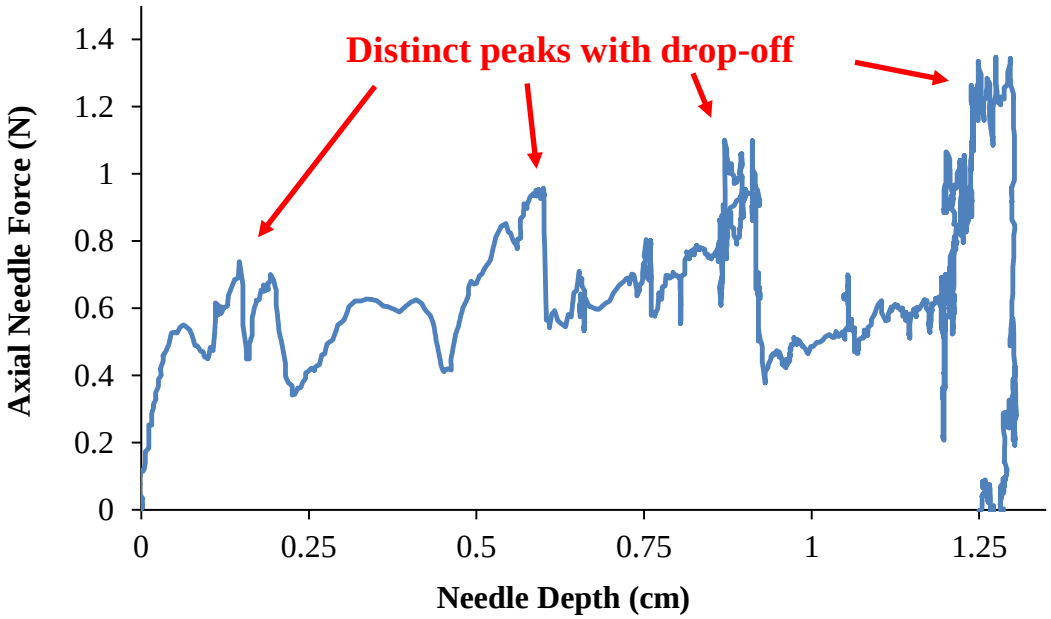

Figure 4-2 Needle insertion force during a steady insertion into the apex of the sternal head and clavicle of a fresh frozen unembalmed cadaver.

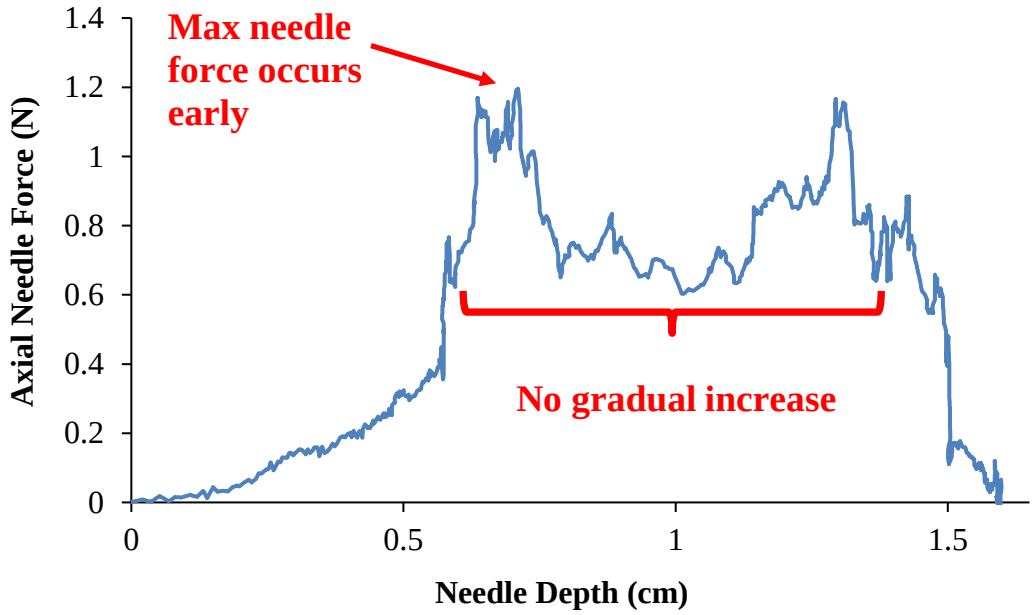

Figure 4-3 Needle insertion force during a steady insertion into the sternocleidomastoid of a fresh frozen unembalmed cadaver.

4.2.4 Interpretation of Results

The force sensing syringe was able to successfully capture needle force and depth data. The final device is the size of a standard 5 mL syringe, and the surgeon was able to complete the insertions with minimal interference from the device. This ensured that the force data being collected was from a realistic scenario and was minimally affected by the device's form factor.

The needle insertion force profiles for these hand insertions show similar results to previous animal tissue insertions implying that it is capable of taking reliable data. It was also able to capture certain behaviors of the surgeon such as his fine adjustments near the vein. This opens up possibilities for future studies measuring the needle forces during different types of insertion and using these measurements to detect common trends. This data also proved to be extremely useful in the creation of haptic force characterizations for use in the DHRT.

4.3 Improvements to the DHRT Haptic Robot and Syringe End Effector

Through feedback from the third year medical student training study, it was determined that the *Geomagic Touch* did not have the force resolution necessary to fully capture the feel of a needle insertion. The design of the haptic arm also made it very difficult to calibrate with the syringe end effector. The *Geomagic Touch* arm was designed to be calibrated by placing the pen end effector into a holster on the device. By replacing the end effector, workarounds had to be devised that caused some inconsistencies in calibration. To fix these issues, the decision was made to upgrade the Geomagic Touch to a Geomagic Touch X haptic robotic arm as shown in Figure 4-4.

Figure 4-4 Geomagic Touch X haptic robotic arm [70].

The Geomagic Touch X can provide a maximum force of 7.9 N with three degrees of freedom which is more than double the force of the Geomagic Touch. It also has a nominal resolution of 0.023 mm of six degrees of freedom position sensing (double the resolution of the Geomagic Touch). The device has dramatically less joint friction than the Geomagic Touch. However, these benefits came at an increased cost of $8,720. The Geomagic Touch X uses the same software as the Geomagic Touch, so it was able to be immediately implemented into the DHRT system with minimal changes to the simulation code.

The new haptic robotic arm required a new syringe end effector to be developed. Drawing inspiration from the first syringe end effector, the new end-effector used the same three shell design with minor changes. The shape of the middle shell was altered to use a compression spring as opposed to an extension spring for needle aspiration. This made the new syringe dramatically more reliable than the previous design. The attach point was also altered to allow for attachment to the Geomagic Touch X's arm. Finally, the new design uses a cap on the front of the syringe. This allows for the syringe to be easily disassembled for maintenance purposes. The

improved syringe end effector can be seen attached to the robotic arm in Figure 4-5 and a cross section in Figure 4-6.

Figure 4-5 Geomagic Touch X haptic robotic arm with attached syringe end effector.

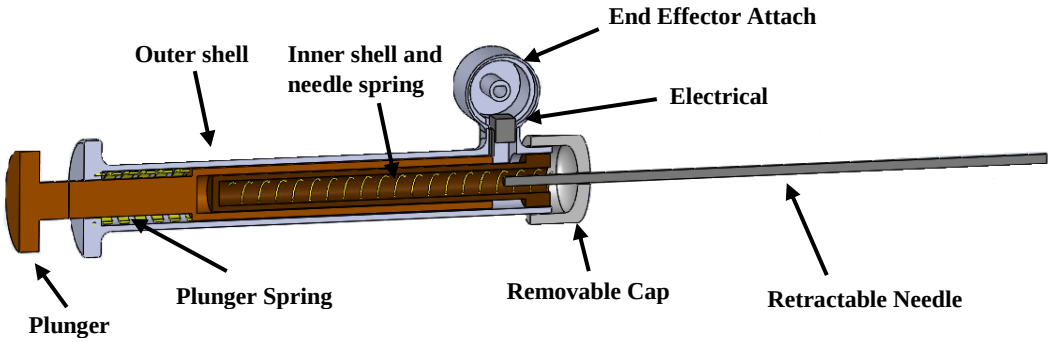

Figure 4-6 A cross-section view of the syringe end effector for the Geomagic Touch X.

4.4 Design and Implementation of the DHRT Graphical User Interface

A major component that needed to be added to the DHRT was a GUI. A GUI would allow people to train with the DHRT without the need of a teacher or attendant. Creating a GUI could also set the groundwork for the creation of a system that dynamically adjusts training to the individual needs of a user. The look and design of the GUI for the DHRT was developed in the

publication “Personalized Learning in Medical Education: Designing a User Interface for a Dynamic Haptic Robotic Trainer for Central Venous Catheterization” [71]. Using subject transcripts and feedback from the third year medical resident study, content analysis was conducted to determine the most common CVC feedback given to trainees by teachers. This combined with focus testing was used to design the following GUI for the DHRT.

Upon starting the DHRT, the user is presented with a login screen. This login screen allows the program to identify the current user and access their personal CVC training information from a central database. After logging in, the user is presented with a home screen with several key features including: a plot of their previous performance scores using the simulator, tips for CVC, a high score board, a list of things to remember for CVC, and a drop down selector for choosing training (Figure 4-7). The performance plot allows a user to track their improvement over time using the simulator. The high score board was included to foster a feeling of competition between trainees as motivation to improve.

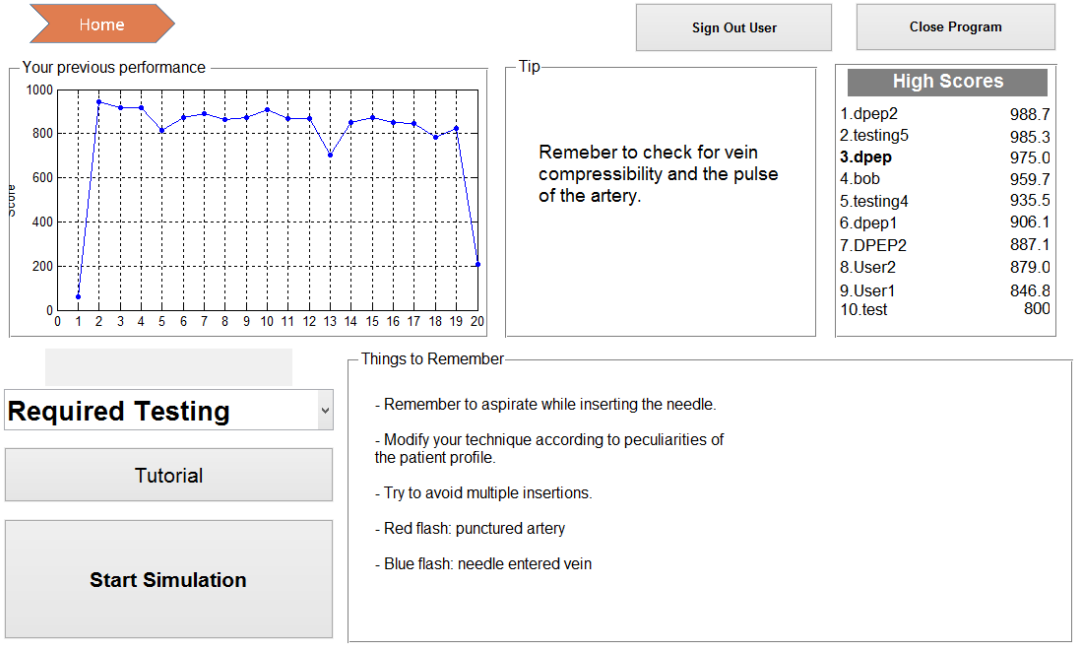

Figure 4-7 DHRT home screen.

When the user presses “start simulation” on the home screen, they are then sent to the patient profile screen. The patient profile screen serves two important purposes. It presents the trainee with virtual patient information for their upcoming training scenario. These patient profiles are representative of profiles a surgeon would receive before performing a real CVC insertion. This screen also presents the user with the steps needed to successfully complete the needle insertion of a CVC procedure (Figure 4-8).

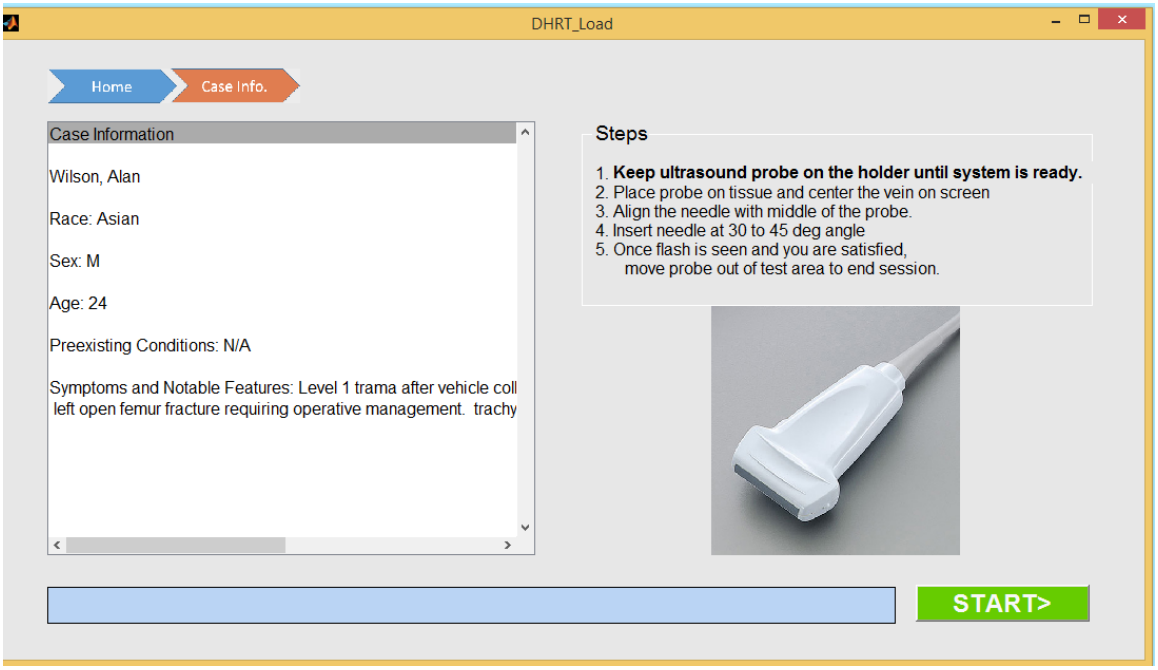

Figure 4-8 DHRT patient profile screen.

After the patient profile screen, the user is presented with one more screen reminding the user to place the mock probe and syringe in their holsters before the practice procedure beings and to place the mock ultrasound probe in the indicated area when they are satisfied with their final needle insertion position at the end of the procedure. The user will then proceed with the simulated CVC procedure. Upon completing the procedure, the user will rate themselves on how well they believed they performed before being sent to the results screen. The results screen pictured in Figure 4-9 contains several boxes with important user feedback.

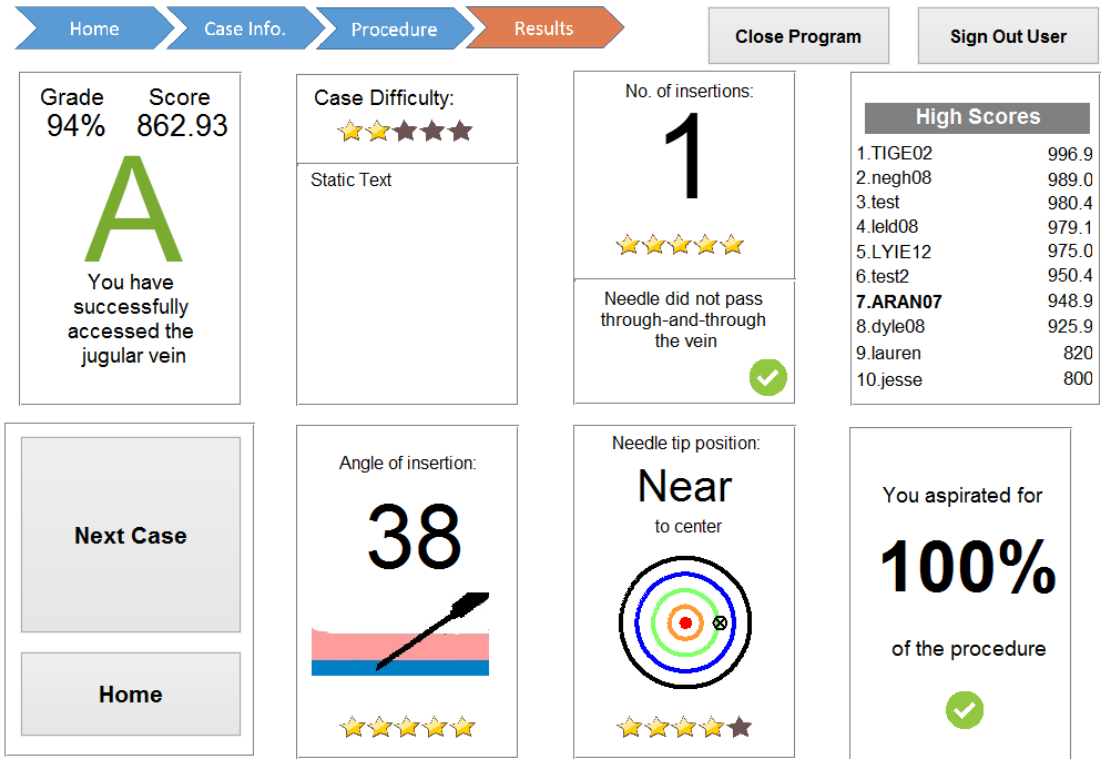

Figure 4-9 DHRT results screen

The first box contains a letter grade, score, and percentage indicating their training performance. The score is calculated using Equation 4-1 and the factors indicated in Table 4-2. The next box presents important information regarding the patient and the difficulty of the case. Box three informs the user on the number of insertions attempted and if they passed through the back wall of the vein. Box four is the high score board from the home screen. Box five shows the average angle of insertion by the user. Box six indicates how close the user's needle tip was to the center of the target vessel. Finally, the last box informs the user how often they aspirated during the procedure. Each of the feedback boxes also provides a score out of five stars. Star ratings are based on the criteria given for a successful CVC procedure. All scores and star ratings can be improved by more accurately following the procedure instructions given before the beginning of the simulation. All test information is then saved to a central databased for future analysis. At this point, the user can chose to move on to another scenario, return to the home screen, or log out.

$$Score = I_s * (161.3 * (\theta_s * C_s * a_s) - B_s - A_s) \quad (4\text{-}1)$$

Table 4-2 Description of DHRT simulator performance scoring variables.

Variables	Description
I_s	0 if needle ends in artery 0.5 if needle in neither vessel 1 if needle ends in vein
Θ_s	Average needle angle factor
C_s	Needle centering factor
a_s	Needle aspiration factor
B_s	Vein back wall puncture penalty
A_s	Multiple attempts penalty

4.5 First Year Surgical Residency Study

Upon completion of the GUI and the other additions to what will now be called the DHRT 2.0 simulator shown in Figure 3-10, a research study was conducted to train first year surgical residents with the DHRT 2.0 system. The surgical resident training study looked to answer three main research questions: how does resident performance using the simulator change over time, what factors most impact this change in performance, and what patient anatomical factors make a simulation scenario more or less challenging? To answer these questions, the DHRT was integrated into the curriculum of 13 first year surgical residents over three months. The participants were chosen randomly and began training during their first week of residency. They had no previous clinical experience in CVC. Institutional review board approval was obtained and identities of residents were made anonymous.

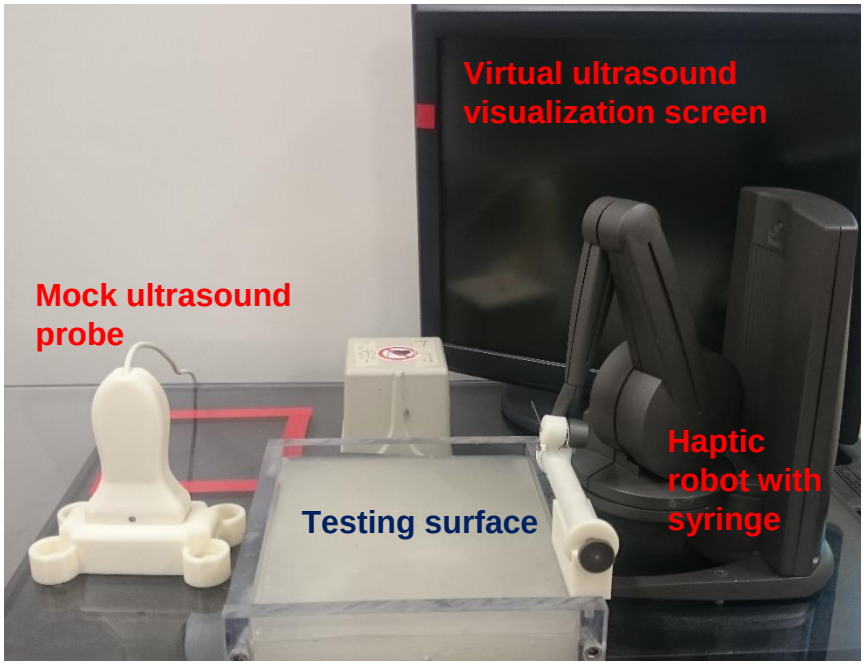

Figure 4-10 Updated DHRT 2.0 system for the residency training study.

All 13 participants received identical training. The training regimen was as follows. During the introduction session, the residents were presented with the CVC procedure through a short lecture and video commonly used to teach CVC. The residents then performed a needle insertion into a traditional CVC training manikin to familiarize themselves with CVC patient anatomy and anatomical landmarks. A month later, the first training session introduced the residents to the VR haptic robotic CVC simulator and two needle insertions were attempted on the baseline training scenario. This baseline training scenario would be repeated to monitor the residents' progress throughout the training program. The following month, training session two was conducted. This was a more extended session where residents were given the baseline training scenario on the simulator, followed by eight practice scenarios, and ending with the baseline training scenario. The final training session took place a month later and was identical to the second, but with different practice scenarios. By the end of testing, the residents completed 22 practice insertions on 17 different scenarios. For comparison, the 22 simulated insertions were also completed by an expert vascular surgeon with 20 years of experience and a third year

surgical resident with approximately 25 clinical CVC insertions. This information allows a greater understanding about how clinical experience translates to haptic robot performance.

The 17 different patient scenarios were developed with the assistance of an experienced surgical resident who is responsible for teaching the CVC procedure. These scenarios were designed to test a wide variety of patient types including those who are morbidly obese, extremely thin, edematous, hypovolemic, hypotensive, hemodynamically unstable, and dehydrated. Simulator vessel depth's range from 13 mm to 35 mm. Relative vessel position was based on known typical anatomical position of the right IJ vein and carotid artery and placed in positions that are typically considered more or less challenging for surgeons based on desired scenario difficulty (i.e. a more posterior artery in relation to the vein increases chance of arterial puncture). The sizes of the vessels ranged from 7 mm to 15 mm based on patient scenario and typical vessel size [72-75]. One of these scenarios was designated as the baseline training scenario. This represented a patient with average vessel depth, and vessel orientation. Over the course of training, the residents would repeat this baseline training scenario so their overall skill changes could be monitored. To create the most accurate haptic force feedback characterization possible, data from the cadaver study was used to create a realistic force characterization [67].

4.6 Results

4.6.1 Baseline Training Scenario

Figure 4-11 shows the average resident performance for the baseline training scenario as a percentage of the maximum possible score. The average user scores increased from 52% to 96% of the maximum possible score between the first overall and final overall test. The expert surgeon and experience surgical resident performed at a high level throughout the training with average scores of 98% and 96%, respectively. This indicates that the new surgical residents were able to

achieve near expert proficiency with the robotic training after three training day sessions. These scores were based on the factors previously discussed in Table 4-2.

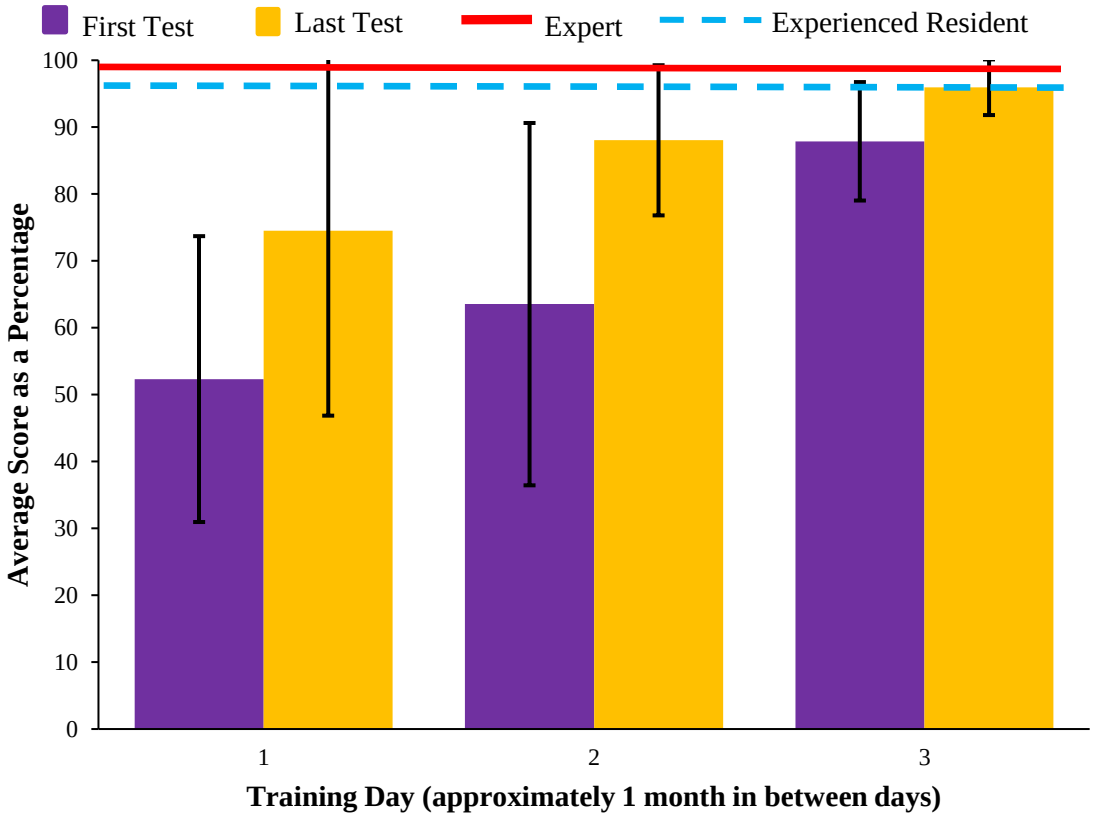

Figure 4-11 DHRT performance of the surgical residents on the baseline training scenario across the three training days. The average scores of an expert vascular surgeon and a third year surgical resident are shown for reference.

A two-way analysis of variance (ANOVA) test revealed statistically significant improvement ($F(1,76) = 8.45$, $p < 0.005$) between the first and last test of each training day and a statistically significant improvement in performance ($F(1,50) = 11.8$, $p < 0.005$) between the second and third training days. A decrease in performance is seen between baseline training scenario two and three. This decrease is typical of a learning curve when there is a large gap in time between learning sessions, which in this case was a month between baseline training scenario two and three. A Bartlett's Test revealed there to be significant difference between the variance in scores between the six baseline training scenario insertions ($\chi 2(5) = 42.4$, $p < 0.005$).

Using a Levene's Test, the major statistical differences were found to be between the first and last baseline training scenarios on day two ($F(1,22) = 4.30$, $p < 0.005$) and the first and last baseline training scenarios on day three ($F(1,24) = 8.60$ $p = 0.007$).

On the final training day, all participants successfully inserted the needle into the vein when presented with the baseline training scenario: an improvement of 64%. Proper centering of the catheterization needle tip in the target vessel also is an important factor in CVC that leads to easier insertion of a guide wire. The mean distance between the needle tip and vein center decreased by 61% between the first and last baseline training scenario insertion. A Levene's Test showed a significant decrease in the variance in distance between the needle tip and vein center across the baseline training scenarios ($F(5,72) = 4.53$, $p < 0.005$).

In addition, throughout the course of training, the mean number of insertion attempts decreased from 1.92 to 1.23 attempts over the course of testing. Importantly, a Levene's Test found an overall decrease ($F(5,72) = 3.90$, $p < 0.005$) in the variance of the number of attempts over the six tests. Participants also aspirated their syringe 12% longer during insertion between the first and last baseline training scenarios. The fact that the residents are increasing their aspiration time shows that they are both improving their chosen grip and remembering to aspirate more often. Finally, while other data factors such as the number of artery punctures and number of times the rear wall of the vein was punctured were recorded, no meaningful trends in this data was found. Specifically, only one of the overall 78 baseline training scenario needle insertions resulted in an accidental artery puncture.

4.6.2 Results Comparing Simulated Anatomical Factors

The different types of patient anatomy in which the surgical residents practiced could be divided into five groups: average, shallow vessels, deep vessels, contracted vessels, and abnormal

(rare vessel positioning). The practice scores are plotted in Figure 4-12 and the mean scores of the different groups are listed in Table 4-3.

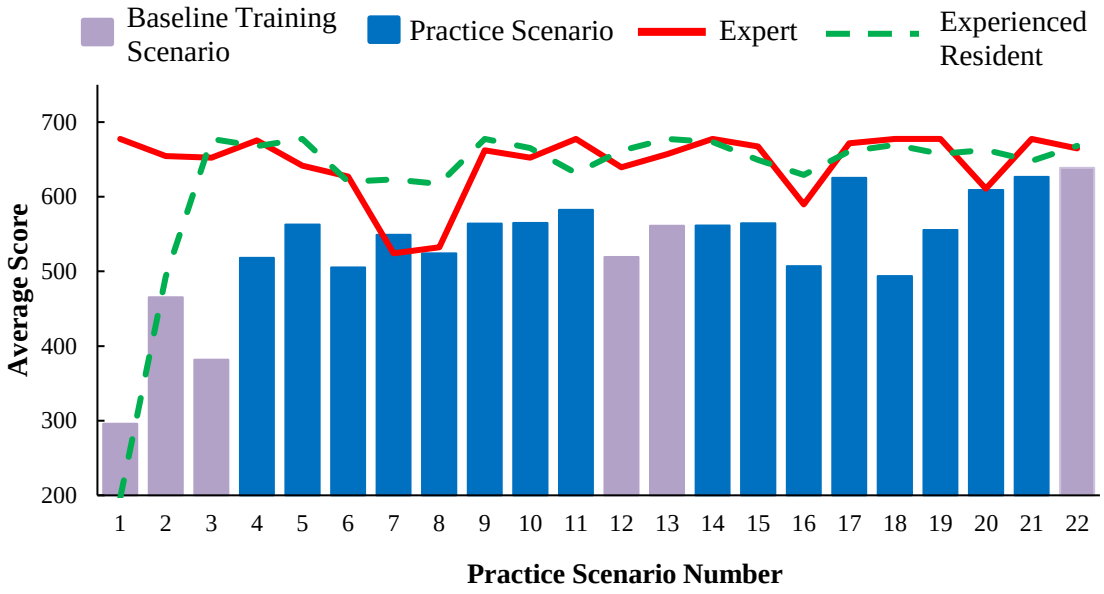

Figure 4-12 The average user, expert, and experienced resident scores for across each of the 22 simulated CVC insertions using the DHRT 2.0. The repeated baseline training scenario is highlighted against the 16 unique practice scenarios.

Table 4-3 Mean scores and values of scoring factors by anatomy type for the 16 practice scenarios (excluding the baseline training scenario). Shallow vessels depth ≤ 2.0 cm. Deep vessel depth ≥ 3.2 cm. Contracted vessels diameter ≤ 1.0 cm. Abnormal anatomy included scenarios such as the vein being located medial to the artery and the vein being than the artery.

	Anatomy Types				
	Average	**Shallow Vessel**	**Deep Vessels**	**Contracted**	**Abnormal**
Mean score	529	561	580	519	568
Variance of Score	19900	16500	12700	33200	16000
Mean distance to vein center	0.386	0.277	0.264	0.242	0.278
Mean attempt	1.49	1.67	1.28	1.40	1.35
Mean angle (deg)	40.9	39.9	41.2	41.1	42.3
Mean in vessel	87%	94%	96%	85%	96%
Mean in artery puncture rate	0.0%	1.9%	1.3%	5.8%	3.9%
Mean back wall puncture rate	0.0%	5.8%	0.0%	7.7%	0.0%

Notably, the contracted vessel scenarios had the lowest overall mean scores and the highest overall variance compared to other scenarios. Looking at the individual scoring factors in Table 4-2, the reason for the lower scores for the contracted vessel scenarios is the fact that the trainees punctured the back wall of the vein more often (7.7% back wall puncture rate), punctured the artery more often (5.8% arterial puncture rate), and successfully inserted into the vein at a less often (85% successful insertion rate) when compared to the other scenarios. It is also notable that the average anatomy scenarios also a lower overall mean score of 529, but these scenarios as a whole took place earlier in the training, possibly biasing them towards lower scores.

Examining Table 4-3, the scenario type with the best overall scores was the deep vessel obese patients. There appears to be two main reasons. First, residents were able to successfully end the insertion with the needle in the vein 7.0% more often than the other scenarios combined. Second, the average number of insertion attempts during deep vessel patient scenarios was 1.29 compared to 1.51 for the other scenarios.

4.7 Discussion

The surgical resident training study resulted in findings for each of the three previously stated research questions. The first research question was how does resident performance using the simulator change over time? The results showed that resident performance on the simulator improves as more insertions are completed. The residents also increased their performance relative to an expert and experienced surgical resident. This suggests that they also are improving their CVC skills following the assumption that an expert performs well using the simulator because of their advanced CVC skills.

The second research question asked what factors most impact change in performance using the simulator. By far the greatest changes in performance occurred during the first four practice scenarios as seen in Figure 4-12. This suggests that it takes a surgical resident

approximately three to four practice scenarios to familiarize themselves with the training device. The patient anatomy for a training scenario also had an effect on user performance. Overall, a combination of experience and the type of training scenario had the greatest impact on performance.

The final research question asked what patient anatomical factors make a simulation scenario more or less challenging. The anatomical feature that had the greatest impact on user performance was vessel size. Small contracted vessels proved difficult for residents throughout testing. This is understandable because small vessels require a higher degree of needle insertion accuracy and greater skill using the ultrasound guidance. It is also easier to puncture through the back wall of these small veins.

The current cost to build the DHRT is approximately $18,000. While this is more expensive than ultrasound manikins, which cost between $1,000 and $6,000, this cost comes with several significant advantages. First, a user training with the DHRT can complete practice needle insertions faster than a user training with a traditional manikin. This is due to factors such as the need to reset an ultrasound manikin by refilling the fluid in the mock vessels. It was found over the course of testing, manikin users needed approximately 3.5 minutes per insertion compared to only 1.5 minutes per insertions with the DHRT. The improved time efficiency with the DHRT means that it would require at least 3 ultrasound manikins to train the same amount of residents in the same amount of time as the DHRT. Second, for manikin testing, each manikin requires a trained resident or attending to observe and evaluate the insertion. The DHRT does not need a trained observer because the system itself is capable of evaluating trainees. The need for a trained observer is a significant expense of manikin training over time. For example, if a single observer needs to train 75 residents practicing 15 manikin insertions each, this would take approximately 66 hrs to complete using the assumptions of 3.5 minutes per insertion. At Hershey Medical Center, during our testing, observers were paid $45/hr for their time. This would mean that there is an estimated additional $2,970 in labor costs associated with manikin training per training

season. Robotic systems such as the DHRT do not have this additional labor cost. Finally, the cost of the DHRT comes with the benefit of the system being able to simulate a wide variety of patients. This enables trainees to prepare for many different scenarios such as obese patients that they cannot train for using traditional manikins.

4.8 Third Set of Improvements to the DHRT

After completing the first year surgical resident study, further improvements were made to the DHRT increase the overall performance of the DHRT simulation and improve the overall reliability of the training system. The first improvement made the DHRT ambidextrous and is shown in Figure 4-13. The DHRT 1.0 and 2.0 both could only be used by right-handed users. By adding an adjustable arm to the monitor and centering the testing DHRT equipment, the DHRT was made ambidextrous. This also required a new interface screen prompt where the user would choose if they are left or right handed. Choosing left handed would reverse the direction of the robotic and ultrasound X-axis and use a separate device calibration designed for this axis reversal.

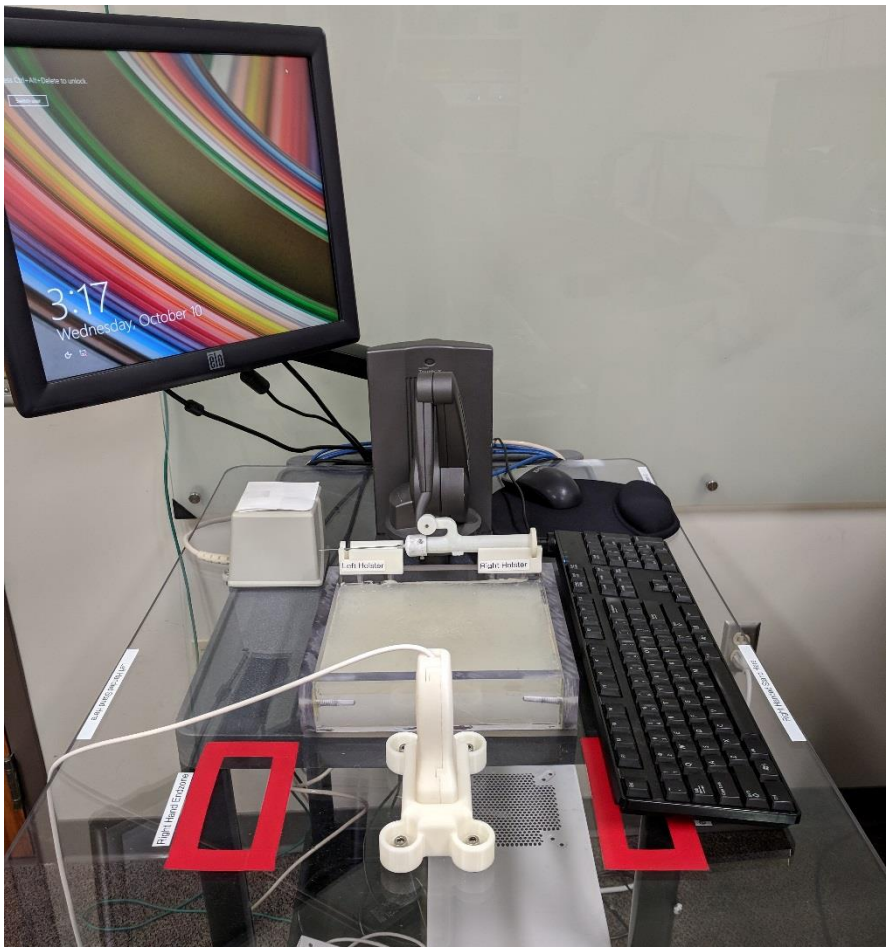

Figure 4-13 Ambidextrous configuration for DHRT with centered equipment and adjustable monitor.

To improve the reliability of the DHRT software and simulation, the entire program was rewritten to convert the program from *MATLAB* and *Simulink* to using *Python* and *Blender*. *Python* is an open source programming language with similarities to *MATLAB*, while *Blender* is open source 3D graphics software. Moving the simulation to *Python* has brought several benefits. The DHRT loads faster and is dramatically less prone to crashing than the *MATLAB* based program. The DHRT program is now run from a simple executable file from the desktop instead of from within the *MATLAB* interface, making the program much more accessible to average users. Finally, the ultrasound simulation now has improved tissue deformation due to the ability to alter the objects in the simulation using animations in *Blender*. This allows the background of the simulation to deform and the ability to fade between image textures to create different effects.

There is room for future improvement with the DHRT. First of all, a surgical resident broke the robotic arm by quickly and forcefully over-rotating the gimbal in a direction that it does not rotate while they were trying to set up the device for left handed operation. This could be corrected by better direction on how to swap to left handed mode in the video tutorial, as well as a visible warning on the device. Furthermore, the some specialties perform the CVC procedure using an in-plane approach where the ultrasound probe is place longitudinally along the target vessel and the needle is visible throughout the entirety of the procedure. This type of visualization in not currently possible with the DHRT. This would be important feature to implement into future iterations.

Future plans for the DHRT include distributing the device to several other institutions. By expanding to more hospitals, the system will be able to collect large amounts of training data and create models of training performance. These models can then be utilized to automatically build dynamic individualized training programs for each surgical resident based on their performance. This type of individualized instruction has the potential to make a strong positive impact on CVC training.

4.9 Conclusions

This chapter presented research involving further work done to improve the quality of resident training using the DHRT. It began by explaining the details of a cadaver study to better understand the needle forces involved during a CVC procedure. Using the data, new force characterizations were developed and implemented into the DHRT. Next, two major additions to the DHRT were discussed. The first was the implementation of a new, more accurate haptic robotic arm and the new haptic robotic syringe were detailed. Second, a GUI was developed and implemented into the DHRT. Through this new GUI, a user can train using the DHRT without the need of an instructor for feedback. It also gives more detailed quantitative and qualitative

feedback than could be given through traditional manikin training. Third, the chapter went into detail regarding a major research study involving implementing the DHRT into the CVC training curriculum of 13 surgical residents at Hershey Medical Center. The study found that user performance greatly increased over time and approached the levels of a trained CVC expert implying that the DHRT was indeed training the residents in the CVC procedure. This lead to a final set of improvements to the DHRT which involved rewriting the program in *Python* and *Blender* to create a more reliable and realistic simulation. Overall, the DHRT has been shown to be an effective device for the training of residents in the CVC procedure.

Chapter 5
Ultrasound Deformation Simulation Using Inverse Mapping

5.1 Introduction

The third stated contribution of this work is to determine a new method of simulating tissue-needle interactions for use in the computer simulation of needle insertion procedures. As computer simulation of surgical procedures continues to improve, the development of new visualization techniques is needed to provide accurate real-time simulation of different aspects of each procedure. The previously discussed CVC insertion is part of a category of procedures that are ultrasound guided. These procedures use ultrasound to help guide a tool, such as a needle, into a precise position. Advances in ultrasound simulation are necessary to further the simulation of ultrasound guided procedures. This chapter presents a new method of simulating tissue deformation in an ultrasound image using a method known as inverse mapping. This chapter begins with an overview of ultrasound guidance and a summary of the current methods of simulating ultrasound. Next, the details of a cadaver study conducted to obtain images of ultrasound guided needle insertions and the characterization of the captured tissue deformations are explained. Finally, a new method of simulating ultrasound is developed and evaluated.

This chapter is based on the paper "Simulating Ultrasound Tissue Deformation Using Inverse Mapping" currently under review.

5.2 Ultrasound Guidance

The implementation of ultrasound guidance into needle insertion medical procedures has resulted in improved patient outcomes across a wide variety of medical specialties. In anesthesia, studies have shown that applying ultrasonography to peripheral nerve blocks is associated with a lower rate of serious complication such as local anesthetic systemic toxicity [76]. It also results in

a higher rate of successful nerve blocks, improved patient safety, higher quality of pain relief, shorter procedure and onset times, and longer block durations [77-79]. In surgery and interventional radiology, the use of ultrasound has significantly decreased the rate of CVC failure and patient complications when compared to the traditional landmark CVC insertion technique [80-82]. Using ultrasound to visualize the needle insertion site for thoracentesis and paracentesis results in a decreased risk of serious bleeding complications and pneumothorax [83]. Because of these advantages, ultrasound guidance has become standard in many procedures [53, 78]. However, there is currently no standard method for the teaching of ultrasound skills [84-87].

Initial training for ultrasound guided needle insertion procedures typically uses specially designed manikins [15, 55]. Manikins provide a safe controlled environment for practicing, but often replicate ideal patients, failing to portray a less common patient such as one who is severely injured or obese. Cadavers have also been utilized in the training of ultrasound guided anesthesia procedures, but can be expensive and are not always available [88]. Both of these training methods also require the presence of a trained resident or attending to oversee progress and evaluate the trainees. Recently, improvements in computing power have resulted in the development of computer-based ultrasound simulators as an alternative to training with manikins and cadavers, which allow for diverse scenario training, quantitative feedback, and assessment [27, 58, 61, 68].

5.3 Ultrasound Simulation

Many methods for simulating ultrasound imaging have been developed that provide realistic imaging, but do not allow for instrument insertion. As previously discussed in Chapter 3, the *Sonosim* (Santa Monica, CA) Ultrasound Training Solution is a commercially available ultrasound simulator that uses a technique called 3D ultrasound reconstruction to generate a real time ultrasound image from pre-acquired ultrasound images [89, 90]. This device can only

simulate the rotations of an ultrasound probe around a fixed point, not full 3D motion. It also does not allow for the simulation of tissue interactions and movement caused by interventions such as needle insertion. Another common ultrasound simulation method uses computed tomography scans of living patients to generate 3D virtual anatomy. The anatomy is then built in a 3D graphical environment assigned physical properties such as ultrasound reflectivity. These simulations combine the physical ultrasound properties of tissues and organs with image filtering techniques that simulate features such as ultrasound shadowing artifacts, speckle noise, and radial blurring [91, 92]. While these simulation techniques provide realistic virtual ultrasound images, they do not account for the effects of tissue deformation due to instrument interactions. Simulating this type of interaction is critical to effectively training ultrasound guided needle insertion procedures since tissue deformation provides an indication of the location and orientation of the needle [93].

One method of simulating ultrasound image deformation caused by instrument interactions is by first simulating the mechanical deformation of soft tissue and using this information to update a tissue model. This updated model is then used in an ultrasound simulation. Mass-spring-dampers are commonly used to simulate mechanical deformation due to their low computational requirements, but these simulations are often only able to show tissue deformation in the path of the needle [93, 94]. This limits the model's ability to simulate how different layers of tissue interact outside of the direct needle path. During a needle insertion, varying tissue properties cause different tissue layers to deform at a differing rates. This causes additional tissue deformation outside of the direction of the needle insertion. Ultrasound tissue deformation has also been simulated using a fixed real ultrasound image or solid gray image as a background image and the manipulation of foreground objects representing anatomy such as veins and arteries. This is the method utilized by the DHRT in Chapters 3 and 4. While the DHRT has been shown to be an effective teaching tool CVC, this deformation model is simplistic and there is significant room for improvement in its ultrasound simulation.

With this in mind, a new method of simulating ultrasound images with tissue deformation has been developed. The new interactive ultrasound model is developed using a four step process. First, ultrasound video was captured from an ultrasound guided needle insertion into a cadaver. Second, tissue motion in this ultrasound video was measured using optical flow analysis and characterized into three zones of motion. Third, a method of emulating these three zones of tissue motion using vector fields was developed. Finally, inverse mapping using these vector fields and real ultrasound images is used to simulate tissue-needle interactions in an ultrasound image. Computational performance of the simulation is then evaluated through measuring the time it takes for the simulation to processes each image frame, and ways of optimizing this processing time are proposed. Overall, this unique simulation process can allow for accurate training of ultrasound guided procedures and provides deeper insight into needle-tissue interactions.

5.4 Ultrasound Cadaver Experiment

5.4.1 Methods

The cadaver experiment was conducted to obtain ultrasound video from an ultrasound guided peripheral nerve block so that tissue movement due to the needle insertion could be characterized. For the cadaver experiment, a needle insertion was conducted into an adult male fresh-frozen cadaver. The needle used was a 20 Gauge, 100 mm, 30 degree bevel, B. Braun Medical Inc. (Bethlehem, PA) *Stimuplex Ultra 360 Insulated Echogenic Needle*. This needle was chosen because it is often used in peripheral nerve block procedures, and it is echogenic making it clearly visible in ultrasound imaging. The needle insertion was conducted into the thigh near the sciatic nerve to emulate a sciatic peripheral nerve block. The insertion was conducted by an anesthesiologist with over 15 years of experience. The anesthesiologist was directed to insert the needle using a constant velocity so that the tissue movement could be clearly observed and

characterized. Ultrasound video was captured using a Sonosite (Bothell, WA) *L38xp* linear ultrasound probe at a frame rate of approximately 12 frames/sec and a resolution of 580 px by 600 px. For this experiment, the pixel scale is 15.2 px/mm.

Ultrasound video captured was analyzed using MathWorks's (Natick, MA) *MATLAB* and *MATLAB's* Farnebäck optical flow estimation algorithm with a local neighborhood size around each pixel of 9 and 3 pyramid levels. Farnebäck optical flow approximates the neighborhood around the pixels of two consecutive frames using a polynomial expansion transform [95]. The algorithm then generates an image pyramid to better estimate pixel movement greater than the size of the neighborhood. The result of this analysis is a vector field with the estimated relative motion of each pixel between frames of the video.

5.4.2 Results

The recorded ultrasound video contains minimal movement of the ultrasound probe and nearly horizontal needle orientation allowing for the accurate characterization of the tissue movement. Figure 5-1 shows the calculated optical flow for one of the ultrasound video frames. The optical flow vector field revealed a trend in the motion of the tissue. First, there are three distinct zones of deformation in the tissue. Zone 1 is near the needle where tissue is pulled in the direction of needle movement. This pulling in Zone 1 is caused by friction between the needle and the tissue. Zone 2 is above the needle and shows that the tissue rolls in a counterclockwise motion as the needle moves from left to right across the screen. Zone 3 is below the needle and shows that the tissue rolls in a clockwise motion as the needle moves from left to right. Zone 2 and 3 are caused by the friction in the needle pulling to the right, while connective tissue attempts to resist this pull. Rotations of Zones 2 and 3 were found on average to be centered 20.3 px (1.34 mm) above and below the needle respectively, and 68.8 px (4.53 mm) behind the needle tip.

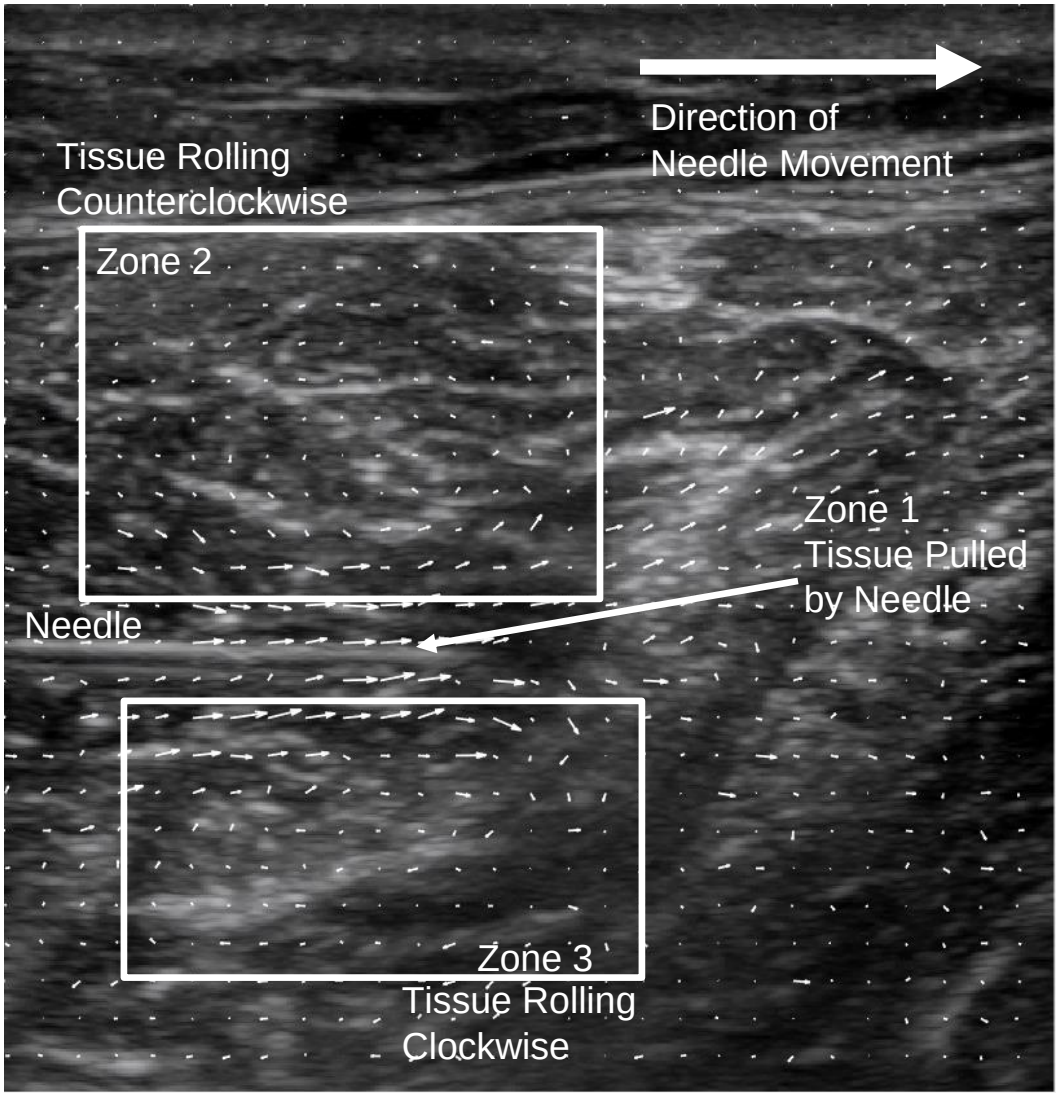

Figure 5-1 Ultrasound image from a needle insertion into the thigh of a cadaver with the vector field showing tissue movement for 2 video frames overlaid. Three distinct zones of tissue movement are highlighted.

A second trend was also found in the vector field. The magnitude of the optical flow vectors decreases in the direction perpendicular to the needle. To characterize this decrease in magnitude, the average magnitude of each vertical line of pixels in each of the analyzed ultrasound frames was calculated. Figure 5-2 shows these average magnitudes plotted and Equation 5-1 shows the Gaussian distribution fit to the plot for one of the image frames.

$$Tissue\ Movement = \sum_{i=1}^{n} a_i e^{\left[-\left(\frac{y-b_i}{c_i}\right)^2\right]} \quad (5\text{-}1)$$

The variable y is the row location in a given column. The parameters for the Gaussian distribution fit were a_i as the amplitude of the distribution peak, b_i as the centroid peak, and c_i as a value relating to the peak width. The number of parameters n was set to 2. For all frames, b_i was found to be equal to or very close to the vertical pixel location of the needle. An average overall Gaussian distribution was calculated by averaging the Gaussian distribution parameters for all of the optical flow plots calculated between ultrasound video frames. These parameters are shown in Table 1. Utilizing this Gaussian magnitude distribution and the three distinct zones of optical flow motion, an accurate simulation method to create realistic ultrasound image deformation is developed and discussed in the following section.

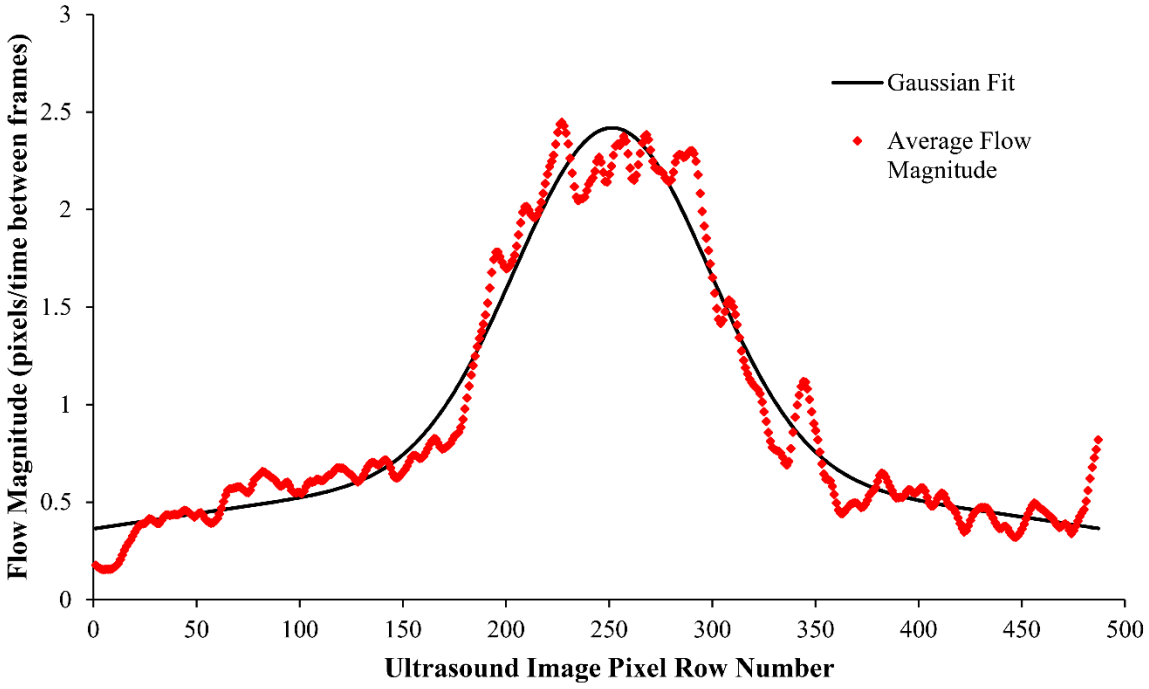

Figure 5-2 Average tissue optical flow magnitude for each row in an ultrasound image. A Gaussian distribution is fit to the data.

5.5 Simulating Ultrasound Tissue Deformation

The proposed method of simulating needle deformation in an ultrasound image uses inverse mapping and bilinear interpolation to transform an original ultrasound image. There are

three main parts to this process. First, three vector fields representing the three zones of tissue deflection are generated and merged. Second, the magnitude of the vector field is scaled using the Gaussian distribution measured in the cadaver study. Third, a base ultrasound image is transformed according to the vector field to simulate tissue deformation.

5.5.1 Building Vector Fields

A vector field representing the simulated motion of the pixels is generated by combining three vector fields. Each vector field represents one of the three zones of tissue motion described in the cadaver study. The flowchart in Figure 5-3, shows how the three different vector fields are combined with a Gaussian distribution and tissue stiffness factor matrix to make a single vector field that simulates the overall ultrasound tissue deformation. This method is applied to each generated frame in the ultrasound simulation. For each frame, the simulated needle position in the frame is known. For all of the following matrices, the rows and columns of the matrices correspond directly to a pixel location in the simulated ultrasound image.

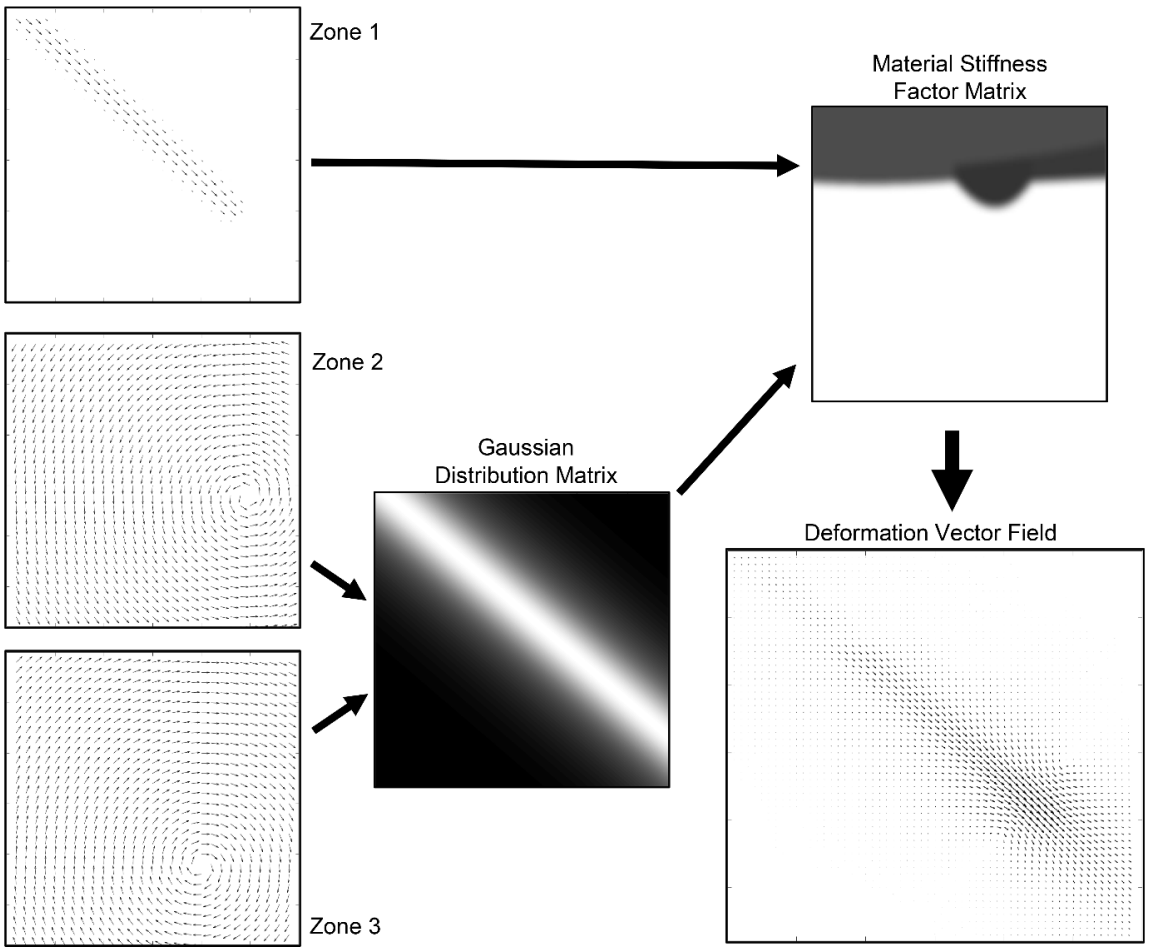

Figure 5-3 Flowchart showing the construction of a deformation vector field for use in ultrasound simulation. Zone 1 is pulling due to needle friction. Zone 2 and 3 are tissue rolling above and below the needle. The magnitude of Zones 2 and 3 is modified by the Gaussian distribution matrix. The Gaussian distribution matrix is visualized where darker colors represent numbers approaching 0, and lighter colors approach 1.8. The material stiffness matrix is visualized using color and is used to account for varying tissue densities. Blacker colors approach 0, while white colors approach 1.

First, a vector field representing tissue deformation Zone 1 described in Figure 5-1, tissue pulling due to needle friction, is created. A matrix, D, is generated where each element corresponds to the perpendicular distance from the simulated needle position to each pixel. Next, the x and y components of the unit vector, $\hat{\imath}$ and $\hat{\jmath}$, for the needle are calculated pointing in the direction of the needle tip. Finally, Equations 5-2 and 5-3 are used to calculate two matrices, U_1 and V_1, which represent horizontal and vertical pixel movement in the Zone 1 vector field. The symbol $\odot$ denotes the Hadamard product of two matrices.

$$U_1 = \left(\left(\frac{-1}{1000}\right) * D \odot D + 1\right) * \hat{\imath} \tag{5-2}$$

$$V_1 = \left(\left(\frac{-1}{1000}\right) * D \odot D + 1\right) * \hat{\jmath} \tag{5-3}$$

The vector field around the needle tip has a parabolic shape, with a maximum value of 1, to prevent a rapid decrease in vector magnitude between two pixels. This prevents a disjointed appearance or tearing effect at the edge of the vector field from appearing in the simulated image. A final operation is performed to prevent the vector field from reversing direction at locations far from the needle due to Equations 5-2 and 5-3. For insertions in positive directions, values lower than 0 are set to 0, while for insertions in negative directions, values greater than 0 are set to 0.

The next two components are vector fields with each vector being a unit vector simulating the tissue rolling found in deformation Zones 2 and 3. U_2 and V_2 are matrices that represent the horizontal and vertical components of the rolling pixel movement centered above the needle, while U_3 and V_3 represent the horizontal and vertical rolling components centered below the needle. First, the centers of the two vortices that represent the tissue rolling are found. Let P_1 be a vector that represents the x and y coordinates of the needle tip location and let $\hat{\imath}$ and $\hat{\jmath}$ represent the unit vector in the direction that the needle is pointing. As previously discussed, the cadaver study showed that the average center position of the tissue rolling is approximately 20.3 px away from the needle tip in the direction perpendicular to the needle and 68.8 px behind the needle tip. These two values are rounded to 20 and 69 for simplicity. Equations 5-4 and 5-5 determines the x and y location of the two vortex, v_1 and v_2, centers relative to the needle tip.

$$v_1 = P_1 + 20 * \begin{bmatrix} -\hat{\imath} \\ -\hat{\jmath} \end{bmatrix} + 69 * \begin{bmatrix} -\hat{\imath} \\ \hat{\jmath} \end{bmatrix} \tag{5-4}$$

$$v_2 = P_1 + 20 * \begin{bmatrix} -\hat{\imath} \\ -\hat{\jmath} \end{bmatrix} + 69 * \begin{bmatrix} \hat{\imath} \\ -\hat{\jmath} \end{bmatrix} \tag{5-5}$$

Two matrices, M_x and M_y representing the coordinate point grid of the simulated ultrasound image are needed. The form of the matrices is shown in Equations 5-6 and 5-7.

$$M_x = \begin{bmatrix} 1 & 2 & 3 & \\ 1 & 2 & 3 & \cdots \\ 1 & 2 & 3 & \\ & \vdots & & \end{bmatrix} \tag{5-6}$$

$$M_y = \begin{bmatrix} 1 & 1 & 1 & \\ 2 & 2 & 2 & \cdots \\ 3 & 3 & 3 & \\ & \vdots & & \end{bmatrix} \tag{5-7}$$

Four matrices, A_x, A_y, B_x, and B_y are formed in Equations 5-8 through 5-11. The elements of these matrices contain the x and y components of 2 vector fields, one centered above the needle tip, and one below. J is a matrix of ones with the same dimensions as M_x and M_y.

$$A_x = M_y - \nu_{11} * J \tag{5-8}$$

$$A_y = -(M_x - \nu_{21} * J) \tag{5-9}$$

$$B_x = -(M_y - \nu_{12} * J) \tag{5-10}$$

$$B_y = M_x - \nu_{22} * J \tag{5-11}$$

Finally, U_2, U_3 ,V_2 and V_3 are formed by finding the unit vector for each value in A_x, A_y, B_x, and B_y, respectively. An example for finding the unit vector at element (1,1) in U_2 is shown in Equation 5-12.

$$U_{2\ 1,1} = \frac{A_{x\ 1,1}}{\sqrt{{A_x}_{1,1}^{\ 2} + {A_y}_{1,1}^{\ 2}}} \tag{5-12}$$

Now that the unit vector fields for the tissue rolling have been formed, magnitudes are applied to these unit vectors. The magnitudes are determined using the Gaussian distribution found during the cadaver study, except that b_i, the location of distribution peak, is altered to equal the location of the needle in the y direction for each vertical column of pixels in the simulated image. This change in b_i causes the peak magnitude to occur at the location of the needle in every vertical line of pixels. Figure 5-4 shows a magnitude plot of the Gaussian matrix, *G*, values for a given needle position. Each vertical column in matrix *G* has a Gaussian distribution shape with a peak at the location the column crosses the needle. For the full matrix G, it can be see that the

magnitude is greatest along the direction of the needle and decreases in magnitude according to the Gaussian distribution further away in the direction perpendicular to the needle.

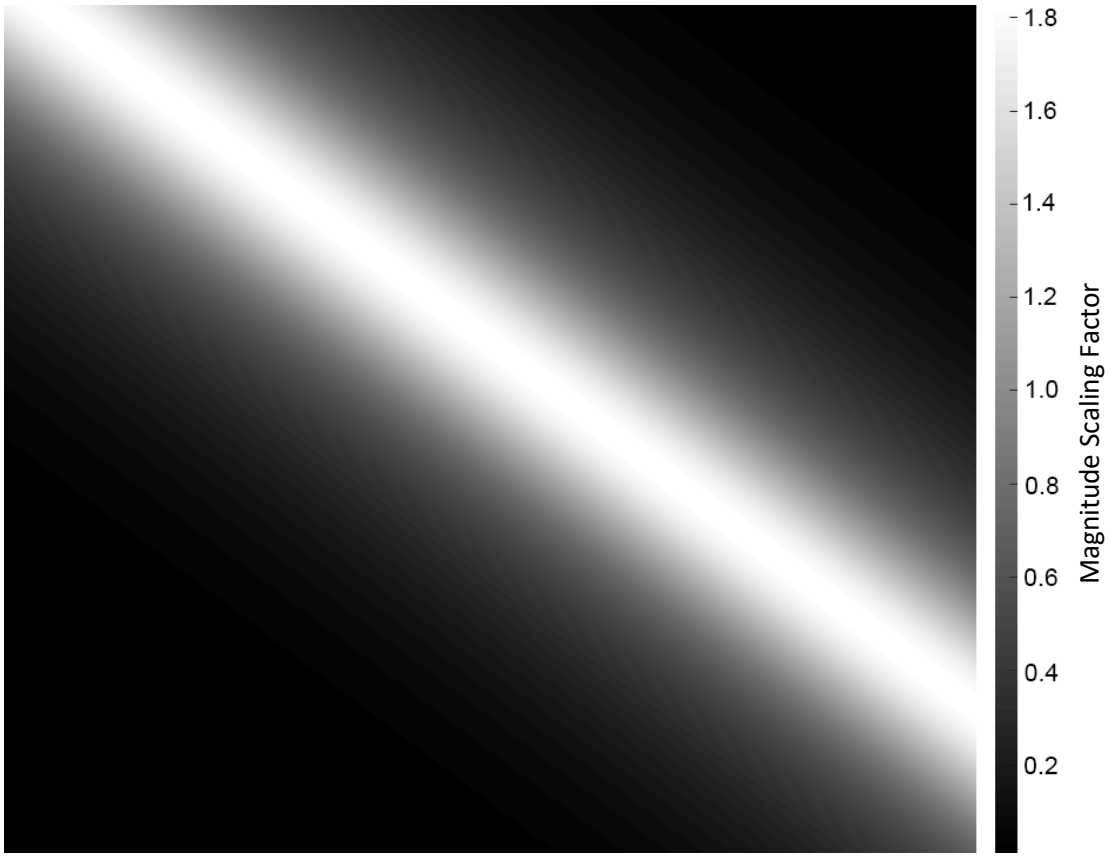

Units: pixels by time between video frames (1 px / 0.083 s)

Figure 5-4 Visualization of the Gaussian distribution matrix where white is the maximum value of 1.8 and black is 0.

The final factor in the simulation considers the stiffness of different layers of tissue in the ultrasound image. The stiffness factor matrix, *S*, creates a matrix where different zones are given a value between 1 and 0, where 1 is tissue that will be unaltered by the stiffness factor and 0 is tissue that will not move in the simulation. For example, Figure 5-5 shows a real ultrasound image and an ultrasound stiffness factor matrix used to estimate the stiffness of different tissues seen in the image. The ultrasound stiffness factor matrix is visualized as a grayscale image where white corresponds with matrix elements values of 1 and black corresponds with 0. The white region has no additional stiffness factor, while the region at the top has a stiffness factor of 0.3

which will reduce tissue defection in that region by 70%. A 2D Gaussian filter is applied *S* to smooth the edges between the different stiffness zones to prevent a disjoint image effect from appearing these transition zones in the simulation.

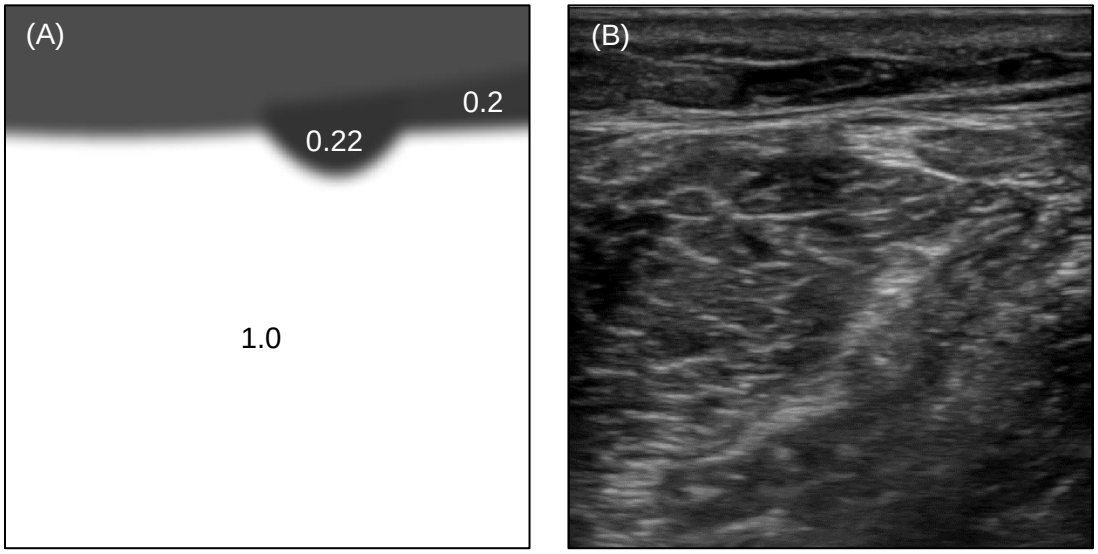

Figure 5-5 Material stiffness matrix (A) is visualized and shown next to its ultrasound image (B). Values shown in (A) are used to modify the simulation vector field. Values of 1.0 do not modify the vector field, while values between 1.0 and 0 cause a reduction in the vector field magnitude and resulting tissue movement.

Finally, the three vector field matrices for both the x and y direction are combined with the Gaussian matrix, *G*, and the stiffness factor matrix, *S*, as shown in Equations 5-13 and 5-14 to create two final vector field matrices, *U* for the x direction, and *V* for the y direction.

$$U = S * (U_1 + (U_2 + U_3) * G) \tag{5-13}$$

$$V = S * (V_1 + (V_2 + V_3) * G) \tag{5-14}$$

Figure 5-6 shows an example tissue deformation vector field created using the above methodology. This type of vector field is generated for each frame of the simulation, taking into account the updated needle position.

5.5.2 Inverse Mapping of the Ultrasound Image

Using the tissue deformation vector field, a transformed ultrasound image can now be created using inverse mapping and bilinear interpolation. Inverse mapping, or backwards mapping, is an image transformation technique where the color of each pixel in a new image is determined by referencing the color of pixels in an original image. If the location to be referenced in the original image lies between pixels, bilinear interpolation of the surrounding pixel color is used to approximate the pixel color value. Any references to pixels outside of the original image are referenced as black. The inverse transformation for each pixel is shown in Equation 5-15 where *p* is the pixel color referenced from location *(x, y)* in the original image. The transformation T^{-1} is the transformation matrix for each location *(x', y')* in the transformed image.

$$p(x,y) = T^{-1}(x',y') \tag{5-15}$$

The reference pixel locations are determined using the tissue deformation vector field matrices *U* and *V*. For example, given a pixel location *p'*(7, 8) in the transformed image, the reference location from the original image will be *p(7-U(7,8), 8-V(7,8))*. If the pixel location referenced lies between two pixels, then the bilinear interpolation Equation 5-16 is used to approximate the pixel value.

$$(x,y) \approx \frac{1}{(x_2-x_1)(y_2-y_1)}\big(f(Q_{11})(x_2-x)(y_2-y) + f(Q_{21})(x-x_1)(y_2-y) + f(Q_{12})(x_2-x)(y-y_1) + f(Q_{22})(x-x_1)(y-y_1)\big) \tag{5-16}$$

The pixel value to be determined is *f(x,y)*, while the following values of $f(Q_{ij})$ are known at pixels x_i and y_j with $Q_{11} = (x_1 , y_1)$, $Q_{12} = (x_1 , y_2)$, $Q_{21} = (x_2 , y_1)$, and $Q_{11} = (x_2 , y_2)$. Inverse mapping and bilinear interpolation is applied to an original reference ultrasound image, using each frame's unique tissue deformation vector field for each image frame in the ultrasound simulation. The reference image is not updated using the previous transformed image because continuous transforming of this image generates a blurring effect over time.

5.5.3 Simulation Performance

The performance of the simulation method was tested using a PC with an Intel (Santa Clara, CA) *Core i7-5930K* 3.50 GHz, six core central processing unit (CPU) and 32 GB of RAM. A test program was written using *MATLAB* 2018a. The ultrasound image and stiffness factor matrix from Figure 5-5 was used at a resolution of 580 px by 600 px. A mock needle insertion path was created for the simulation and the needle was simulated using a grey line. 100 image frames were simulated for 5 seconds of simulated ultrasound video. Parallel processing utilizing 6 CPU cores was used within the simulation loop to improve processing time.

The simulation was conducted 10 times and the average time to simulate 100 frames was 32.5 s. One of these frames with its vector field overlaid and a line indicating the needle position is show in Figure 5-6. Figure 5-7 shows the processing time of each ultrasound frame. The longest time to process a single frame was 0.48 s while the shortest time was 0.22 s. The major reason for the varying differences in frame processing time was the use of a matrix determinant when calculating the distance between the pixels in the image and the line segment representing the needle for matrix D_1. For pixels that are located in front of the needle path, using a determinant is not necessary when calculating the distance between the line segment representing the needle and the pixel since this distance equal to the Euclidean norm between the needle tip and the pixel coordinates. The result of this is that image frames that contain more needle will take longer to process than image frame that contain less needle. Ideally, for real time simulation a maximum frame processing time would be 0.033 s or 30 frames per second. While that was not achieved in this implementation of the ultrasound deformation simulation, it may be possible with the implementation of multithreading using a graphical processing unit which are better suited for complex image processing than a CPU.

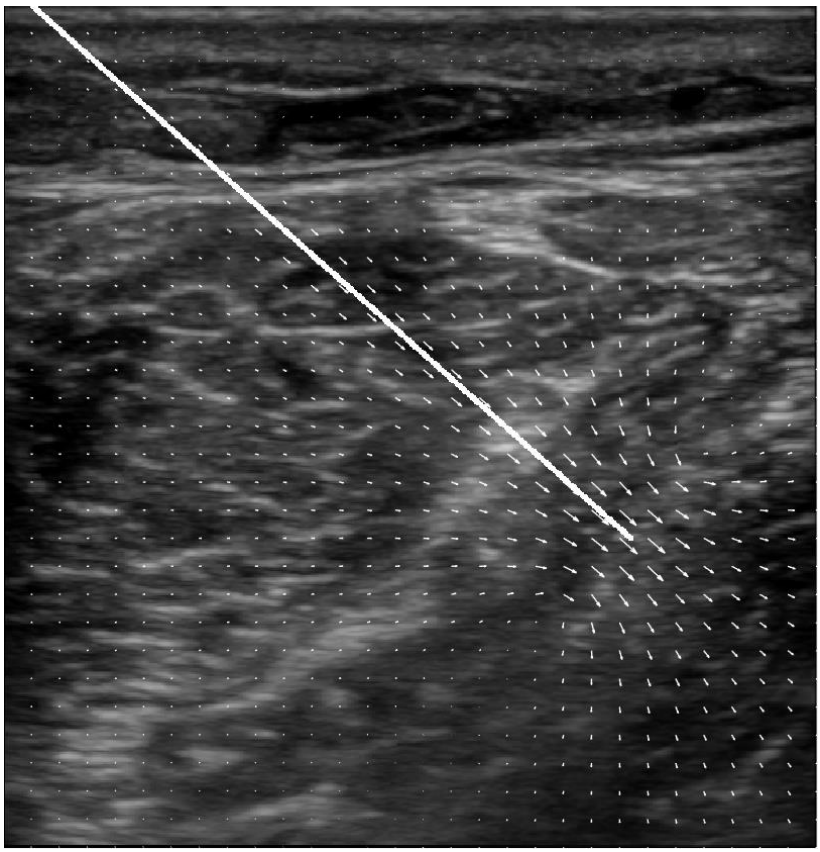

Figure 5-6 Simulated ultrasound frame. An average of the frame's vector field showing the simulated tissue movement is overlaid. Each arrow indicates the average direction for 20 px by 20 px. The white line indicates the simulated needle position.

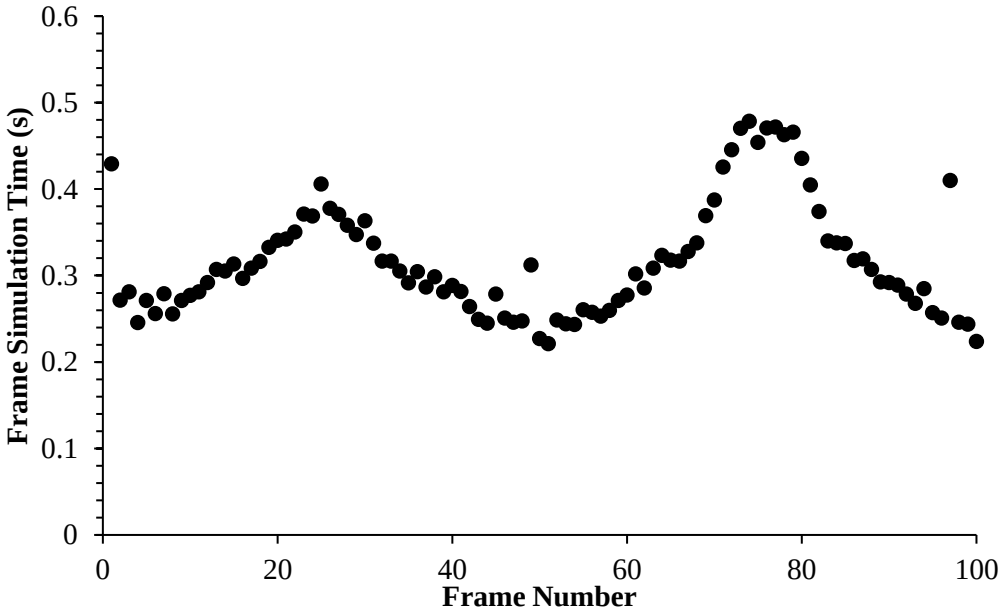

Figure 5-7 Processing time for each simulated ultrasound frame.

5.6 Conclusions

A new method of simulating ultrasound tissue-needle deformation was developed and tested. First, ultrasound video of a needle insertion was captured during a cadaver study to determine the characteristics tissue deformation seen during an ultrasound guided needle insertion. Using this image data, an optical flow analysis was performed and found that there were three distinct zones of tissue deflection: one zone where tissue near the needle being pulled in the direction of needle insertion, and a second and third zone above and below the needle where tissue rolls. Using this information, a method building a tissue deformation vector field to imitate these three zones of deformation was detailed. Finally, each frame of ultrasound deformation simulation was created using inverse mapping and bilinear interpolation to map the tissue deformation vector fields to an ultrasound image. While this simulation method is not fast enough to simulate real time ultrasound guided needle insertion using only a CPU, it may be possible to achieve 30 frames per second of simulation by implementing multithreading with a graphics processing unit.

Chapter 6
Creating Haptic Needle Forces Using Material Fracture

6.1 Introduction

The final stated intended contribution of this work is to develop a new method of generating haptic feedback that is both affordable and effective. Haptic feedback is most often controlled using a combination of software and physical hardware. For example, the haptic feedback conveying needle forces in the DHRT is controlled using a program to determine the amount of force to deliver and a robotic arm to deliver that force. Computers can provide precise control for haptic feedback, however this often comes at a significant monetary cost. This chapter presents a novel method of creating haptic needle force feedback through material fracture that is low cost and does not require computer control. The chapter will first discuss the importance of delicate hand motion control and haptic forces in needle insertion procedures such as peripheral nerve blocks (PNB). Next, a new device for creating haptic needle force using material fracture called the Low Cost Haptic Force Needle Insertion Simulator (LCNIS) is detailed. This is followed by a cadaver study where PNB needle forces were captured to use as a comparison to forces from the LCNIS. Finally, a series of experiments is conducted to create material fracture cartridges for the LCNIS that mimic the forces from the cadaver study.

The content of the chapter is based on the paper "Low Cost Haptic Simulation Using Material Fracture" currently under review.

6.2 Precise Needle Insertion

Delicate hand motion control is a necessary skill for completing invasive medical procedures such as peripheral nerve blocks (PNB), epidural anesthesia, CVC, and laparoscopic procedures. These procedures involve the precise insertion of needles and controlled cutting

punctures of tissue. For example, an ultrasound-guided PNB is a regional anesthesia procedure where an anesthetic drug is injected in close proximity to a peripheral nerve, such as the sciatic nerve using real-time image feedback from ultrasound [96]. PNB serves to interrupt pain signals allowing for effective pain relief or even completion of surgical procedures without the need for general anesthesia. It can also reduce the use of opioid based medications [97-99]. The effectiveness of the PNB depends on factors such as the precise placement of the local anesthetic around the target nerve without causing damage to the nerve or adjacent vital structures, and the amount of anesthetic injected. Failure to properly place the needle can result in a wide variety of adverse effects such as, neurological complications caused by nerve injury such as permanent neuropathy, transient neurapraxia hematoma due to vascular injury, ischemic injury caused by pressure and volume of the injected anesthetic, and in severe cases local anesthetic systemic toxicity can be caused by injection of anesthetic into the blood circulatory system [100-102]. Improved outcomes of ultrasound-guided PNB versus opioid based pain relief and general anesthesia have led to a significant increase in the use of ultrasound guided PNB over the past two decades, however there is currently no standard objective method for teaching ultrasound guided regional anesthesia procedures [103, 104].

As previously discussed, simulators offer an effective way to train a wide variety of competencies and often allow residents to focus their training on a specific task. One of the most important competencies for an anesthesiologist to obtain is the ability to accurately place a needle with ultrasound guidance while causing minimal harm to surrounding tissue and structures [105, 106]. Evaluation of needle skills has been conducted using both direct observation by a trained expert and quantitative methods using computer based motion tracking [107, 108]. Through the use of motion tracking, it has been found that one of the key differentiators in needle insertion skills is in the difference in needle motion between experts and novices [107, 109-112]. Experts have reduced movement, needle path length, and insertion time when compared to novices. Few anesthesia simulators for ultrasound guided procedures have been designed to address the training

of these fine motor skills despite this understood difference between experts and novices. One possible method of improving fine motor skills is through the use of haptic training. Research has shown that early exposure to haptic training can enhance performance in surgical simulator training suggesting that haptic training can improve surgical skills [113].

6.3 Design of the LCNIS

To address the needs for haptic training, the LCNIS was developed. This inexpensive device is able to provide diverse haptic training scenarios and use motion tracking to record and objectively evaluate user movement. The design of the LCNIS, shown in Figure 6-1, contains an innovative haptic cartridge to create a needle insertion force sensation for diverse patient scenarios. The LCNIS also contains an inertial measurement unit (IMU) and processor to measure movements and provide motion accuracy feedback. The syringe body of the LCNIS is 3D printed from acrylonitrile butadiene styrene (ABS) plastic and was designed to house the IMU, processor, and haptic cartridge. Precise guidance of the needle is achieved using a bronze bearing at the front of the syringe body. The needle used to puncture the haptic cartridge is a ground to a 30 degree round point and has a diameter of 1.60 mm.

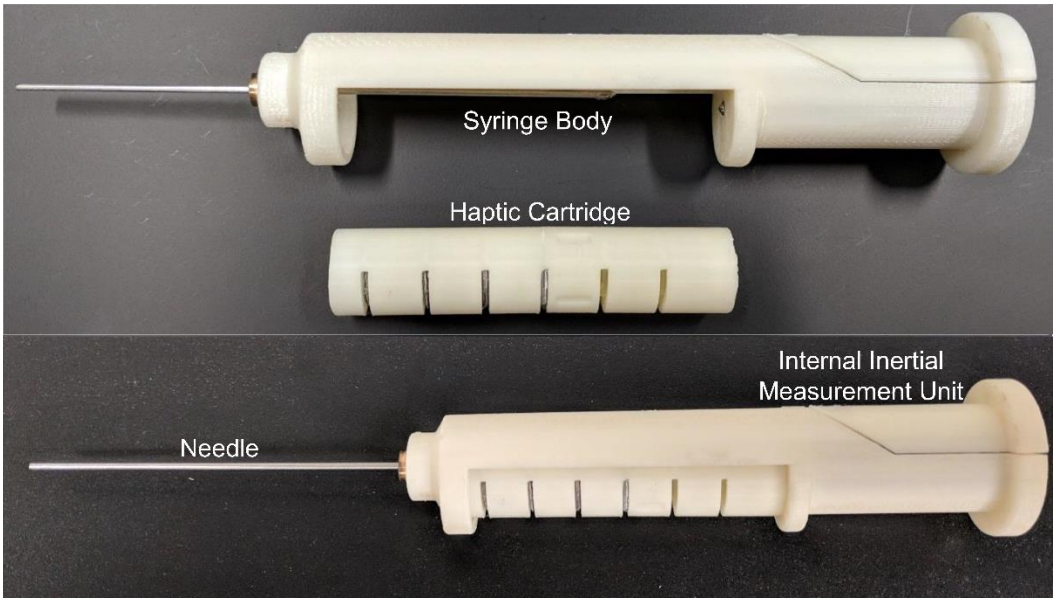

Figure 6-1 Pictured is the Low Cost Haptic Force Needle Insertion Simulator and one of the haptic cartridges used to provide force feedback.

The electronic processor and IMU component of the LCNIS are used for the real time measurement of the acceleration and angle of the device. The IMU contains an accelerometer to measure three dimensional acceleration and a gyroscope to measure changes in the angular velocity of the device. Equation 6-1 shows the complimentary filter used to calculate the real time angle of the device. Equation 6-2 is used to calculate the angle of the IMU from the measured 3-axis acceleration. φ and φ_0 are the current and previously measured angle respectively. v, dt, and φ_x are the angular velocity measured by the gyroscope, the time interval of the measurement, and the IMU angle calculated from gravitational acceleration. The variables a_x, a_y, and a_z are the measured accelerations from the IMU.

$$\varphi = 0.909 * (\varphi_0 + v * dt) + (1 - 0.909) * \varphi_x \tag{6-1}$$

$$\varphi_x = \left(\frac{180}{\pi}\right) * \tan^{-1} \frac{a_x}{\sqrt{{a_y}^2 + {a_z}^2}} \tag{6-2}$$

The complimentary filter constant of 0.909 was calculated using a time constant of 0.1s and a device sample rate of 100Hz. The complimentary filter is necessary to correct erroneous measurements due to natural drift in the gyroscope measurements and accelerometer

measurements which are vulnerable to vibrations. A complimentary filter is similar to a Kalman filter in that it is used to merge two different series of measurements into a single more accurate measurement. However, Kalman filters are computationally expensive, making a complimentary filter preferable during real-time calculations [114]. The calculated angles and acceleration are then transmitted to a connected PC using USB serial communication.

The haptic cartridge is a disposable cylinder filled with disks of material, as show in Figure 6-2, that provide the force sensation of inserting a needle into tissue. To operate the LCNIS, the user presses the blunt tip of the LCNIS needle into a hard surface which causes the needle to retract into the haptic cartridge as shown in Figure 6-2. As the needle slides into the cartridge, it punctures the various internal disks of material which provide the haptic sensation. Open slots along the body of the cartridge allow for disks of different haptic materials to be inserted at a variety of depths. Different disks of material provide varying levels of resisting force. For example, one disk may contain polycarbonate which provides very high needle puncture forces, whereas another disk may use polytetrafluoroethylene (PTFE) plastic film which provides low needle puncture forces. Additionally, materials such as a polyvinyl chloride (PVC) plastisol may be placed between the disks to provide a more gradual increase in force feedback. The advantages of this cartridge include the ability to provide haptic feedback without complex and expensive computer simulation and easy to design cartridges to match a wide variety of needle insertion force profiles. Additionally, the outer cylinder of each cartridge contains four channels that allow for a revolving mechanism to lock the cartridge into four distinct insertion positions, permitting for four insertions per cartridge. To create haptic cartridges with force feedback that accurately simulates human tissue, experiments were conducted as detailed in the haptic cartridge force experiment section.

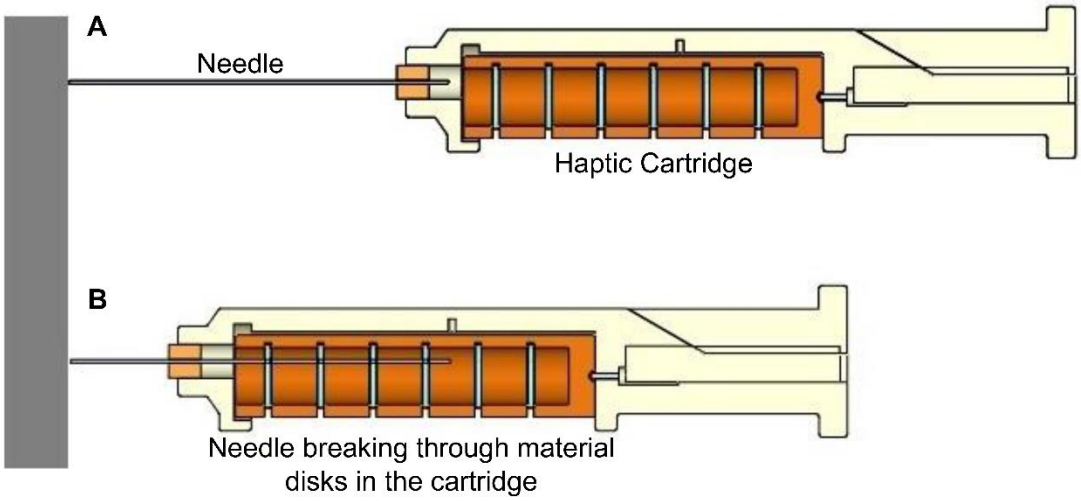

Figure 6-2 Cross-section view of the Low Cost Haptic Force Needle Insertion Simulator. (A) Needle Extended. (B) Insertion causes the needle to slide into the cartridge and break through disks of material

6.4 LCNIS Experimentation

Four experiments were performed to create haptic cartridges that provide realistic force feedback as seen in Table 6-1. Experiment 1 collected needle insertion forces from a cadaver. Experiment 2 determined the needle puncture forces of a variety of plastic materials for use in the haptic cartridge. Experiment 3 developed and validated an equation for predicting the force feedback from the haptic cartridges. Experiment 4 created a haptic cartridge to mimic needle forces measured during the cadaver experiment.

Table 6-1 Description of four experiments conducted, the materials used in each test, and each testing apparatus.

Experiment	Purpose	Materials	Insertion Force Measurement Apparatus
1	Measure needle insertion forces into a cadaver thigh	Cadaver thigh tissue	Hand-held force sensing syringe with 6-axis force transducer
2	Determine material properties for use in the LCNIS haptic cartridge	PTFE, Polycarbonate, PVC, UHMW, ABS, FEP	Linear actuator with six axis force transducer

3	Create and validate LCNIS haptic cartridge force prediction equation	LCNIS haptic cartridge containing PTFE, Polycarbonate, PVC, UHMW, ABS	Linear actuator with six axis force transducer
4	Create LCNIS haptic cartridge mimicking a cadaver	LCNIS haptic cartridge containing PTFE, PVC, ABS	Linear actuator with six axis force transducer

6.4.1 Cadaver Needle Force Experimental Methods

The cadaver insertions for Experiment 1 were conducted by an expert anesthesiologist with over 15 years of experience. Seven insertions were made into the thigh of a middle aged male cadaver using a Pajunk (Norcross, GA) *SonoPlex Stim* 21 Gauge 100 mm needle commonly used for PNB procedures. The thigh was chosen to simulate forces commonly associated with a sciatic PNB. Needle forces and position were captured using a previously developed force sensing needle [45]. The axial needle forces were measured by an ATI Industrial Automation (Apex, NC) *Nano17* 6-axis force transducer attached to the needle. Position was obtained using a Northern Digital Inc. (Waterloo, Ontario, Canada) *3D Guidance TrakSTAR Model 80* electromagnetic position tracker. The anesthesiologist was directed to insert the needle at a constant velocity to obtain the needle insertion force versus the needle depth.

6.4.2 Haptic Cartridge Force Experimental Methods

Experiment 2 measured the needle puncture forces of six different plastic materials to determine the materials that would provide the force feedback in the haptic cartridge. The 30 degree, 1.60 mm diameter needle used in LCNIS was mounted to a computer controlled Dunkermotoren (Bonndorf, Germany) linear actuator which advanced the needle at a constant velocity of 5 mm/s and measured needle position as shown in Figure 6-3. The needle cut through a variety of thin plastic materials, clamped between two disks, and attached to an ATI Industrial Automation (Apex, NC) *Gamma IP65* force transducer to measure needle forces versus the

needle position. The plastic materials tested were 0.08 mm thick ABS, 0.13 mm thick ABS, 0.01 mm thick fluorinated ethylene propylene (FEP), 0.05 mm thick PTFE, 0.13 mm thick Polycarbonate, 0.10 mm thick Ultra-high-molecular-weight polyethylene (UHMW), and 12.7 mm thick PVC plastisol. Four needle insertions were conducted for each material.

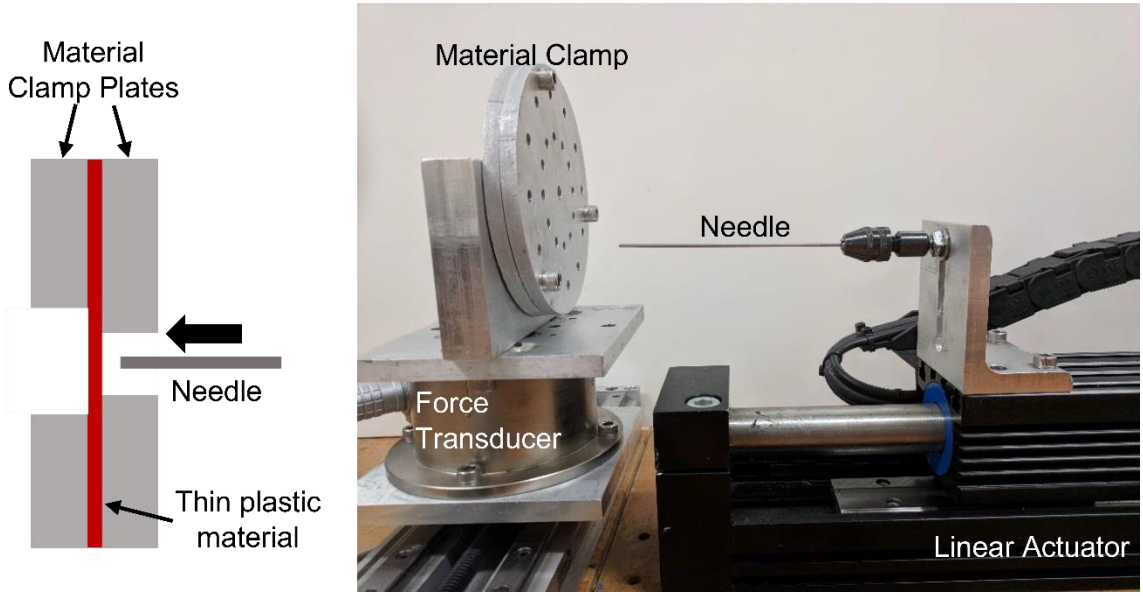

Figure 6-3 Experimental setup for needle insertions into thin plastic materials using computer controlled linear actuator.

Experiment 3 was conducted to validate an equation that would predict the needle forces measured from the haptic cartridge. The LCNIS was mounted to the previously used linear actuator with the needle pushing into a metal plate attached to the Gamma 65IP force transducer at a rate of 5 mm/s as shown in Figure 6-4. By pushing the blunt end of the needle into the metal plate, the 30 degree needle cutting tip is pressed through the haptic cartridge. This cutting force is then measured by the force transducer along with the position of the needle. Table 6-2 shows the materials used in the haptic cartridge, as well as the depths and thicknesses of each material in the cartridge. Between insertions, the cartridge was rotated 90 degrees to provide for a different entry point for each needle puncture. A total of four insertions were conducted into the cartridge. Experiment 4 used the same experimental procedure as Experiment 3 except the haptic cartridge used was designed to mimic the forces from the cadaver experiment. Eight insertions, four

insertions each into two identical cartridges, were performed using this custom cadaver haptic syringe.

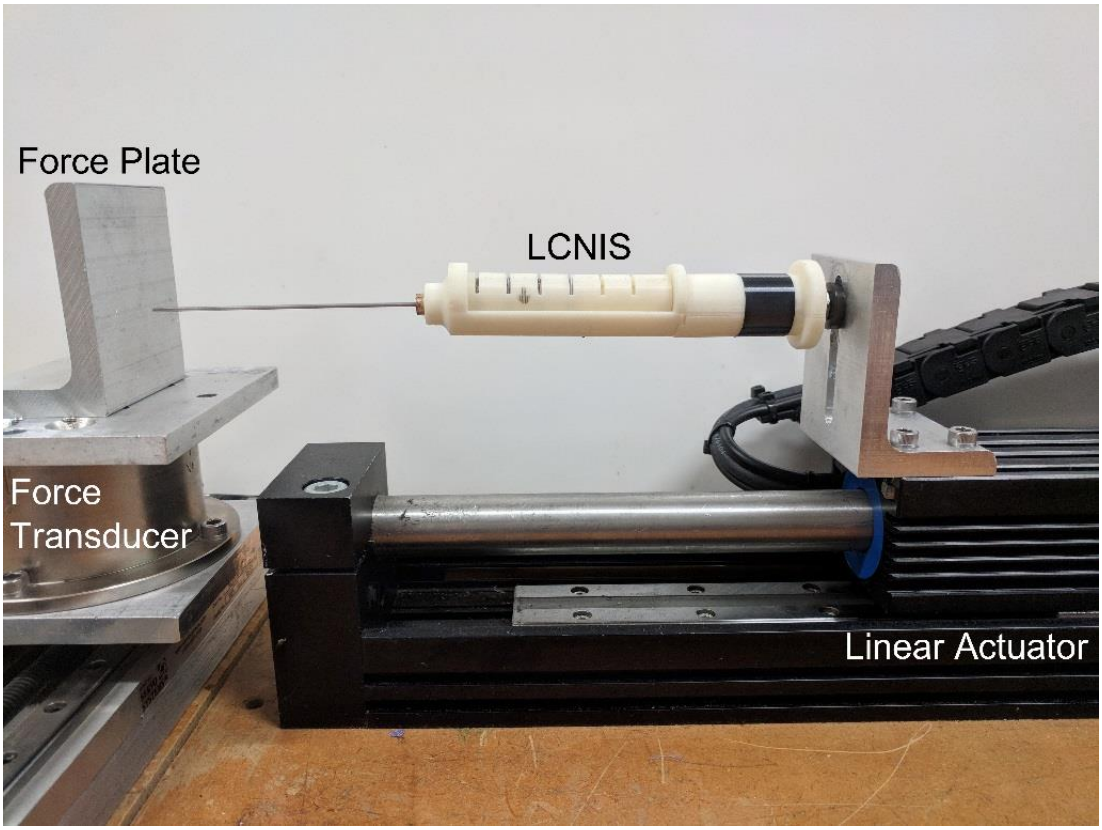

Figure 6-4 Experimental setup for measuring needle forces obtained from the Low Cost Haptic Needle Insertion Simulator (LCNIS).

Table 6-2 Thickness and cartridge depth of the materials used in the haptic cartridge in Experiment 3.

Material	Thickness (mm)	Depth (mm)
PTFE	0.05	0
PVC	11.40	0.05
Polycarbonate	0.13	11.4
ABS	0.08	45.7
ABS	0.13	22.9
UHMW	0.10	34.3

6.5 Results

6.5.1 Cadaver Results

The forces measured from one of the cadaver needle insertions in Experiment 1 are shown in Figure 6-5. The results of the insertions showed a wide variety of different needle force profiles. The force profile shown in Figure 6-5 was chosen to be mimicked by the LCNIS haptic cartridge because of its stable insertion velocity and minimal needle retraction. In the force profile, there is an early force peak of 8.56 N at a depth of 4.47 mm. This early peak occurs at the moment the needle breaks through the skin. The needle force then gradually increases over time to a maximum force of 15.5 N at a depth of 57.9 mm. While the force increases over time, there are a few sudden drops in force. This is typical of a needle insertion in biological tissue due to the lack of homogeneity of tissue and the periodic buildup and release of needle forces cutting into tissue [115].

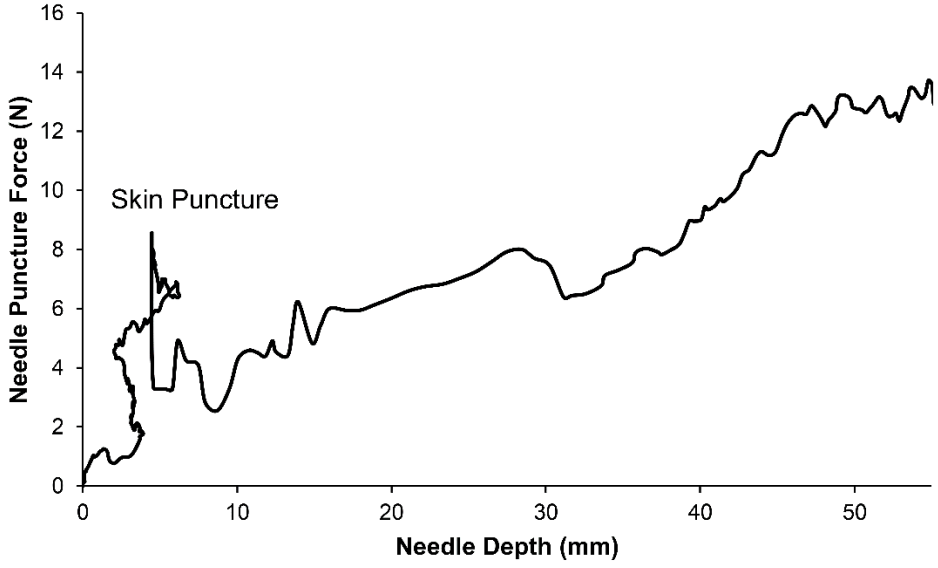

Figure 6-5 Measured needle forces versus needle depth during the insertion of a Pajunk *SonoPlex Stim* 21 Gauge 100 mm needle into the thigh of a cadaver.

6.5.2 Haptic Cartridge Experiments Results

For Experiment 2, the maximum needle forces and residual needle friction measured using the linear motor and thin plastic materials are shown in Table 6-3. Needle friction is defined as the average needle force measured after the needle tip has passed completely through the plastic material. The materials tested provide a wide variety of forces with the polycarbonate providing the strongest maximum puncture force at 9.85 N and the FEP providing the weakest maximum puncture force at 0.84 N. The different materials also had a low standard deviation of puncture force with the maximum standard deviation being 0.14 N in the polycarbonate and the lowest being 0.011 N in the 0.003" thick ABS. The PVC plastisol is a thicker and more flexible material than the other plastics tested. Because of this, the maximum insertion force occurs much deeper at 13.1 mm. The PVC plastisol was designed to be placed between thin disks of other materials in the cartridges. Using the experimental data, a linear equation, shown in Table 6-3, was fit to approximate the needle cutting force and friction force of the PVC plastisol based on the thickness of the material. Using the experimental data from Experiment 2, Equation 6-3 was developed to predict forces from the LCNIS haptic cartridge based on the placement of the different plastics in the syringe and the depth of the insertion. The variables used in Equation 6-3 are detailed in Table 6-4.

Table 6-3 Measured peak and friction forces for haptic cartridge materials from linear motor experiment.

Material	**Peak Force (N)**	**Depth of Max Force (mm)**	**Friction Force (N)**
PTFE	1.13	2.06	0.05
Polycarbonate	9.85	2.46	1.38
ABS 0.08 mm	3.70	2.24	0.44
ABS 0.13 mm	6.97	2.36	0.77
UHMW	6.00	2.61	0.67
FEP	0.84	2.19	0.11
PVC	= 0.2153 * Depth + .948	chosen	.948

$$F(x) = \begin{cases} \frac{F_{Pn}}{D_n - Z_n}(x - Z_n) + \sum_{i=1}^{n-1} f_i & for\ Z_n \le x \le D_n \\ \frac{f_n - F_{Pn}}{0.5}(x - D_n) + F_{Pn} + \sum_{i=1}^{n-1} f_i & for\ D_n < x \le D_n + 0.5 \\ \sum_{i=0}^{n} f_i & for\ D_n + 0.5 < x < Z_{n+1} \\ \vdots & \end{cases} \quad (6\text{-}3)$$

Table 6-4 Constants used in haptic cartridge needle force prediction Equation 6-3.

x	Needle Depth
n	Number integer label for material, first material n = 1, second n = 2, …
Z_n	Depth of material n (mm)
D_n	Depth of maximum force for material n
F_{Pn}	Peak force of material n
f_n	Friction force of material n

The results of Experiment 3, in Figure 6-6, show the predicted forces using Equation 6-3 for a haptic cartridge plotted against the actual forces recorded from insertions haptic cartridge Experiment 2. The five major peaks occur where the needle breaks through each of the 5 disks of material in the cartridge. A gradual increase in force also occurs between the first and second forces peaks due to the needle puncturing through the PVC plastisol. The error between the predicted force measurement and the average of the measured forces for each of the five force peaks were 0.27 N, -1.76 N, 0.13 N, -0.33 N, and -0.50 N. The standard deviation of each of the five force peaks were 0.04 N, 0.70 N, 0.47 N, 0.56 N, and 0.97 N showing consistency between insertions.

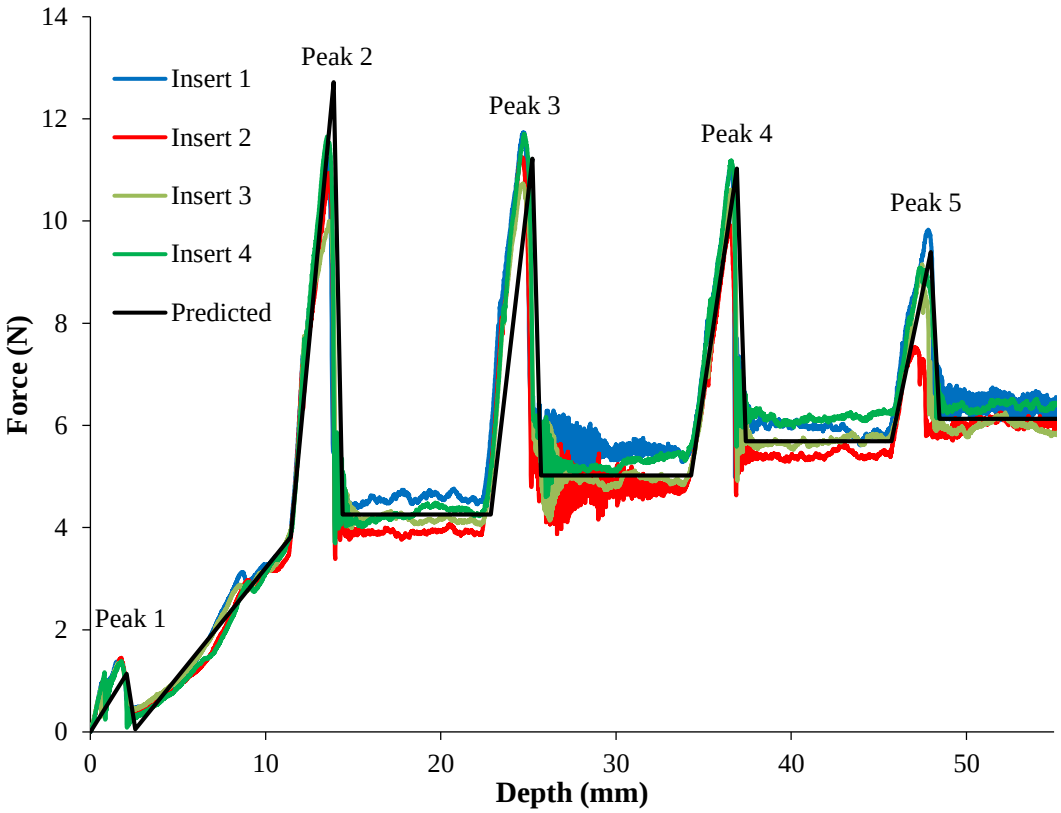

Figure 6-6 Needle forces from a haptic cartridge in the Low Cost Haptic Needle Insertion Simulator containing a variety of thin plastic materials, and the predicted needle forces.

Experiment 4 used the data from the cadaver and plastic needle puncture experiments to create a custom cadaver haptic cartridge to mimic the forces of a PNB into the thigh of a cadaver. Table 6-5 shows the details of the materials used in the custom cadaver haptic cartridge. Figure 6-7 shows the results of Experiment 4. The predicted needle insertion force is shown with the force measured from the cadaver mimicking haptic cartridge and the cadaver needle insertion experiment. Only one of the haptic cartridge insertions is shown in Figure 6-7 for clarity. The error between the cadaver cartridge and the three main peaks was 0.01 N, 1.00 N, and 1.54 N. The error between the maximum force of the cartridge and the cadaver was 0.40 N. Again, there was consistency with the cartridge force peaks with the standard deviation of the three peaks being 0.60 N, 0.55 N, and 0.41 N. The standard deviation of the maximum force was 1.50 N.

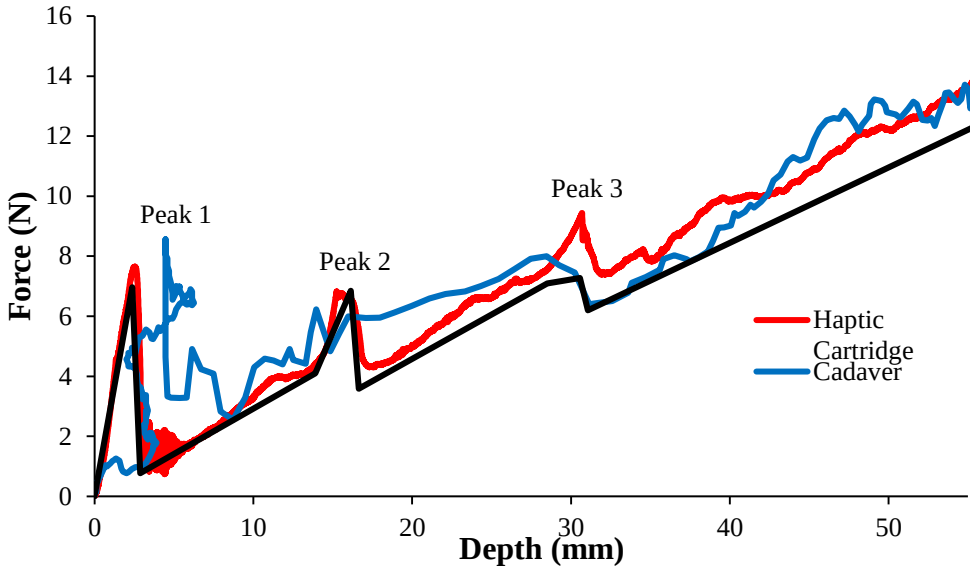

Figure 6-7 Needle forces from the custom cadaver cartridge in the Low Cost Haptic Needle Insertion Simulator and the predicted needle forces.

Table 6-5 Materials and depth of the material used in the LCNIS custom cadaver haptic cartridge.

Material	Thickness (mm)	Depth (mm)
ABS	0.127	0
PVC	13.8	0.127
ABS	0.0762	13.9
PVC	14.5	14.0
PTFE	0.0508	28.5
PVC	29.3	28.6

6.6 Discussion

The results of the cadaver experiment show that the initial puncture of the skin around the thigh provides a large amount of resisting force compared to the puncture of subcutaneous tissue. The skin puncture occurred at a depth of 4.47 mm, and the force transducer did not measure a force of this magnitude again until the needle reached a depth of 39 mm. This large skin puncture force is typical of needle punctures and poses one of the greatest challenges in accurately positioning a PNB needle [45]. Additional peaks in force occur throughout the insertion. During a

needle insertion, an anesthesiologist should insert the needle at a controlled rate to prevent overshooting the target position or unintentionally harming nearby anatomical structures.

The results from the thin plastic material testing, Experiment 2, show a wide variety of needle puncture forces depending on the material. This variety makes these materials ideal for use in the LCNIS haptic cartridge as it allows for diverse haptic cartridges to be developed. Testing showed that using Equation 6-3 in conjunction with the thin plastic material puncture data enables the accurate prediction of forces obtained from the haptic cartridges. The cartridge was also shown to be consistent for all four insertions into the material with insertion forces remaining within 1 N of each other between insertions. This consistency aided by the precision bearing placed at the front of the syringe accurately guiding the needle through 4 distinct puncture locations on the disks of materials as seen in Figure 6-8. Through various testing, it was found that it is important for the plastic films in the disks to resist tearing between puncture holes. If tearing between holes occurs, the puncture force will not be accurately predicted.

Figure 6-8 ABS plastic film disk used in the LCNIS haptic cartridge. Four distinct puncture holes are shown from four insertions into the cartridge.

The final validation testing, Experiment 4, showed that the custom cadaver haptic cartridge was able to successfully emulate the forces experienced during a needle insertion into a cadaver thigh. By using two identical cartridges for this experiment, it was shown that the cartridges can provide repeatable force feedback. The PVC plastisol placed between disks of other plastic materials enabled the cartridge to effectively emulate the gradual, continuous increase in force during a needle insertion. The third force peak in the custom cadaver cartridge

was slightly larger than predicted. This is possibly due to the PVC plastisol pressing tightly into the PTFE disk. This may have negated the decrease in force that would be normally expected to occur when the needle tip exits the PVC since the tip immediately began pressing into the PTFE.

The LCNIS also achieved its goal of being low cost. The total cost of the electronic components is $47. Currently, the 3D printing cost of the syringe bodies and haptic cartridge cylinders is $58 and $14 respectively. Production for the LCNIS would use injection molding to reduce this cost compared to 3D printing. The LCNIS provides an inexpensive alternative to robotic haptic training systems based on devices such as the 3D Systems (Rock Hill, SC) *Geomagic Touch*, which cost over $1000 before being integrated into a haptic training system.

6.7 Conclusions

The LCNIS is able to successfully emulate the forces experienced during a needle insertion at a fraction of the cost of traditional haptic training devices. The design of the LCNIS allows for easy exchange of its haptic cartridge and measurement of syringe movements. Equations have also been developed that allow for the creation of custom haptic cartridges for use in the LCNIS. These cartridges are then able to recreate the forces experienced during a needle insertion into a variety of materials including needle insertions into cadaver tissue. Future work should include the creation of a graphical user interface for the LCNIS, and the development of a trainee performance assessment method utilizing the LCNIS's IMU capabilities to provide training of motor skills during needle insertion.

Chapter 7
Conclusions and Future Work

7.1 Conclusions

Patient simulation has become an instrumental part of surgical training. Hospitals today face a wide variety of training challenges such as restrictions on resident work hours and overstressed facilities. This has forced residency programs to find more efficient methods of training that do not sacrifice the quality of education. Furthermore, for many standard procedures such as CVC, complication rates need to be reduced. To reduce these complications, new more effective training methods need to be developed. New technologies and simulation techniques are necessary to achieve these goals. This dissertation contributes to the simulation of needle insertion procedures by exploring improved methods of simulating patients and human tissue.

The major findings and accomplishments of this dissertation are:

A new material that mimics both human tissue needle insertion force properties and echogenicity was developed. By using a mixture of PVC plastisol, mineral oil, and chalk powder, a new low cost method of producing ultrasound training manikins was created. To assess the PVC plastisol-based mixture, the needle insertion forces and the ultrasound image quality were examined. The needle insertion forces were found to be similar to that of cadaver tissue and commercially available manikins. At a depth of 16.6 mm, PVC plastisol needle insertion forces were found to be 1.68 N, 0.87 N, and 0.82 N depending on the ratio of PVC plastisol, PVC softener and mineral oil, compared to 1.41 N in a cadaver. The ability to alter this force using different ratios of the mixture allows the material to mimic a variety of tissue types. The results of the ultrasound image comparison survey given to experts in CVC found that the ultrasound images of the PVC plastisol mixture highly resembled those of real neck tissue, and were more realistic than both commercially available and commonly used homemade manikins. Of all the materials surveyed, the two PVC plastisol mixture images were the only material images with a

positive Bradley-Terry maximum likelihood value (0.288 and 0.772) relative to images of living neck tissue, meaning that they were perceived as the most realistic materials by the experts surveyed. Creating manikins using this PVC plastisol mixture was also found to be highly affordable, costing approximately $15 for a manikin tissue insert, compared to over $1000 for commercial manikins [42]. This makes it a great option for training programs without significant funding.

The Dynamic Haptic Robotic Trainer (DHRT) for central venous catheterization shows that haptic computer simulation allows for diverse patient training and is proven to be as effective as manikin training. By providing effective training using a variety of scenarios, CVC complication rates can be reduced, resident training can be more efficient, and residents can be better exposed to a wide variety of patient types. Early DHRT testing with third year medical students found that successful simulated CVC insertion using the DHRT increased at a rate of 4.2% per practice attempt. Students who were first exposed to CVC manikin training, were 22% more likely to have a successful first insertion using the DHRT than those with no manikin exposure prior to DHRT training implying that manikin simulation skills transfer to the DHRT. Using these results and new cadaver needle force models, the DHRT was upgraded and a user interface was added to the system. This newly upgraded system was integrated into a surgical residency intern training program to validate the effectiveness of the system. It was found that user scores increased from 52% to 96% of the maximum possible score between the first training session and the final session. This performance approached the recorded performance of an expert and trained surgical resident who had scores of 98% and 96% respectively. High expert performance and poor novice performance imply that the DHRT may be able to accurately distinguish between expert and novice CVC skills. It was also found that by changing training scenario factors such as simulated vessel size and depth, the difficulty of the scenario could be altered.

Ultrasound guided needle insertion tissue motion was characterized into three distinct zones of motion: tissue pulled parallel to insertion direction due to friction, and tissue rotating above and below the needle. By recognizing these three zones of motion, a new method of simulating tissue deflection during an ultrasound guided procedure was developed. For this experiment, a method known as optical flow was used to track tissue movement in an ultrasound video of a peripheral nerve block. For these experiments, the center of tissue rotation above and below the needle was found to 1.34 mm above and below the needle, and 4.53 mm behind the needle tip. The magnitude of the tissue movement fit well to a Gaussian distribution, with the needle forces decreasing in a direction perpendicular to the needle. Using these findings, a method of generating vector fields to mimic the three zones of motion was developed. Using inverse image mapping, and these vector fields as the mapping reference, ultrasound guided needle insertion imaging was effectively simulated.

A novel method of simulating haptic feedback using material fracture was developed which provides a low cost but highly accurate haptic simulation. A device known as the Low Cost Haptic Needle Insertion Simulator was developed to test the method of creating haptic feedback using material fracture. The device uses material filled cartridges that are punctured by a retracting needle to simulate needle force. First cadaver experiments were performed to capture needle insertion forces from a peripheral nerve block. Next, experiments were conducted to determine the needle puncture forces and needle friction forces of a variety of materials such as 0.08 mm thick ABS plastic and 0.13 mm thick PTFE plastic which had average puncture forces of 6.97 N and 1.13 N respectively. Cartridges for the LCNIS were designed to contain disks of these thin materials, and an equation was developed to predict the force of a needle puncturing through this cartridge. The maximum average error of the prediction was found to be 1.76 N with a standard deviation of 0.70 N during puncture into polycarbonate. The minimum average error of the prediction was found to be 0.13 N with a standard deviation of 0.47 N during puncture into 0.08 mm thick ABS plastic. Finally, using the prediction equation, a

cartridge was designed to mimic the forces of the cadaver needle insertion. The error between the three peak forces of the cartridge insertion and the cadaver insertion were 0.01 N, 1.00 N, and 1.54 N with standard deviations of 0.60 N, 0.55 N, and 0.41 N. By using material fracture to simulate haptic feedback, the cost of haptics was significantly reduced. A haptic robot such as the *Geomagic Touch* costs over $1000, while a 3D printed haptic cartridge for the LCNIS costs only $14. This cost could be reduced through more large scale production techniques such as injection molding.

The original contributions of this work are as follows:

(1) A new material the mimics both the human tissue needle insertion force properties and echogenicity was developed.
(2) It was shown that varied computer haptic training using a device such as the Dynamic Haptic Robotic Trainer for central venous catheterization is an effective method for training percutaneous procedures.
(3) Tissue movement during ultrasound guided needle insertion was characterized and a new method of simulating this movement was developed from this characterization.
(4) A novel method of simulating haptic needle forces using material fracture was presented and experimentally validated.

7.2 Recommendations for Future Work

This dissertation contributed to the field of needle insertion simulation in a variety of ways including low cost manikin simulation, advanced computer haptic simulation, and novel methods of generating haptic needle forces. There are many areas in which the work presented here could be expanded upon. The following are recommendations for future work:

- Expand the DHRT to simulate a wider variety of ultrasound guided needle insertion procedures such as peripheral nerve blocks. The DHRT's full six degrees of freedom ultrasound simulation and three degrees of freedom force feedback give the device strong potential to simulate many procedures outside of jugular CVC. Ultrasound simulations of other parts of the body such as the thigh for federal central lines or peripheral nerve blocks could be designed. This work could involve improved needle insertion force characterizations that account for the puncture of tissues such as nerves. By expanding the DHRT to other procedures, the device can become a diverse training platform as opposed to a singular training device.
- Expand the training of the DHRT to dynamically create practice scenarios to cater to individual training needs. Currently, the DHRT uses a set training progression during residency training. However, as more resident training data is acquired, it may be possible to analyze this data and produce dynamic or individualized training progression. For example, a trainee who struggles with obese patients would receive different practice scenarios than a trainee who finds thin patients to be most difficult. Furthermore, patients could be procedurally generated as opposed to predesigned. More DHRT practice data would be required to conduct this type of analysis. Research could include the development of an algorithm akin to a control system where the inputs are previous user performance and outputs are results of the current practice. This algorithm could then generate new practice scenarios to better train the user.
- Expand the method of using inverse image mapping for ultrasound simulation to 3D. The method of using inverse mapping to simulation tissue movement discussed in Chapter 5 is currently limited to 2D simulation. This is useful for certain applications, but this should be expanded to be useful in 3D applications. This would make the simulation technique more useful to complex simulators such as the DHRT. It would also expand the understanding of needle tissue interaction.

- Expand the LCNIS to include a graphical user interface and determine methods to evaluate trainee performance. The LCNIS has great potential considering its realistic force feedback at a low cost. However, currently the device only contains an IMU. This limits its measurement readings to accelerations and angular velocities. A study should be performed to measure the motions of experts and novices using the LCNIS. This will allow for the determination of differences in movement between experts and novices and lead to the development of a performance evaluation. This evaluation could then be implemented into an effective user interface for the device.

References

[1] Walter, A. J., 2006, "Surgical education for the twenty-first century: Beyond the apprentice model," Obstetrics and Gynecology Clinics of North America, 33(2), pp. 233-+.

[2] Carter, B. N., "The fruition of Halsted's concept of surgical training," Surgery, 32(3), pp. 518-527.

[3] Osborne, M. P., 2007, "William Stewart Halsted: his life and contributions to surgery," The Lancet Oncology, 8(3), pp. 256-265.

[4] Kerr, B., and O'Leary, J. P., 1999, "The training of the surgeon: Dr. Halsted's greatest legacy," American Surgeon, 65(11), pp. 1101-1102.

[5] Franzese, C. B., and Stringer, S. P., 2007, "The evolution of surgical training: Perspectives on educational models from the past to the future," Otolaryngologic Clinics of North America, 40(6), pp. 1227-+.

[6] Jamal, M. H., Wong, S., and Whalen, T. V., 2014, "Effects of the reduction of surgical residents' work hours and implications for surgical residency programs: a narrative review," Bmc Medical Education, 14.

[7] Bhananker, S. M., and Cullen, B. F., 2003, "Resident work hours," Current Opinion in Anesthesiology, 16(6), pp. 603-609.

[8] Gopal, R., Glasheen, J. J., Miyoshi, T. J., and Prochazka, A. V., 2005, "Burnout and internal medicine resident work-hour restrictions," Archives of Internal Medicine, 165(22), pp. 2595-2600.

[9] Connors, R. C., Doty, J. R., Bull, D. A., May, H. T., Fullerton, D. A., and Robbins, R. C., 2009, "Effect of work-hour restriction on operative experience in cardiothoracic surgical residency training," The Journal of Thoracic and Cardiovascular Surgery, 137(3), pp. 710-713.

[10] Frank, J. R., Snell, L. S., Cate, O. T., Holmboe, E. S., Carraccio, C., Swing, S. R., Harris, P., Glasgow, N. J., Campbell, C., Dath, D., Harden, R. M., Iobst, W., Long, D. M., Mungroo, R., Richardson, D. L., Sherbino, J., Silver, I., Taber, S., Talbot, M., and Harris, K. A., 2010, "Competency-based medical education: theory to practice," Med Teach, 32(8), pp. 638-645.

[11] Long, D. M., 2000, "Competency-based residency training: The next advance in graduate medical education," Academic Medicine, 75(12), pp. 1178-1183.

[12] Sonnadara, R. R., Mui, C., McQueen, S., Mironova, P., Nousiainen, M., Safir, O., Kraemer, W., Ferguson, P., Alman, B., and Reznick, R., 2014, "Reflections on Competency-Based Education and Training for Surgical Residents," Journal of Surgical Education, 71(1), pp. 151-158.

[13] Touchie, C., and ten Cate, O., 2016, "The promise, perils, problems and progress of competency-based medical education," Medical Education, 50(1), pp. 93-100.

[14] Gordon, J. A., Wilkerson, W. M., Shaffer, D. W., and Armstrong, E. G., 2001, "“Practicing” Medicine without Risk: Students' and Educators' Responses to High-fidelity Patient Simulation," Academic Medicine, 76(5), pp. 469-472.

[15] Maran, N. J., and Glavin, R. J., 2003, "Low- to high-fidelity simulation – a continuum of medical education?," Medical Education, 37, pp. 22-28.

[16] Samia, H., Khan, S., Lawrence, J., and Delaney, C. P., 2013, "Simulation and Its Role in Training," Clinics in Colon and Rectal Surgery, 26(1), pp. 47-55.

[17] Okuda, Y., Bryson, E. O., DeMaria, S., Jacobson, L., Quinones, J., Shen, B., and Levine, A. I., 2009, "The Utility of Simulation in Medical Education: What is the Evidence?," Mount Sinai Journal of Medicine, 76(4), pp. 330-343.

[18] Cooper, J. B., and Taqueti, V. R., 2004, "A brief history of the development of mannequin simulators for clinical education and training," Quality and Safety in Health Care, 13(suppl 1), p. i11.
[19] "Laparoscopic Endo Trainer," JBS Mediitech India Ltd, http://jbsmediitec.co.in/?products=laparoscopic-endo-trainer.
[20] Medicine, P., "Square Knot," Training Program Medical Students, Penn Surgery, http://www.uphs.upenn.edu/surgery/Education/medical_students/graphics/knots/alt_square8.gif.
[21] Barry Issenberg, S., McGaghie, W. C., Petrusa, E. R., Lee Gordon, D., and Scalese, R. J., 2005, "Features and uses of high-fidelity medical simulations that lead to effective learning: a BEME systematic review," Medical Teacher, 27(1), pp. 10-28.
[22] Scalese, R. J., Obeso, V. T., and Issenberg, S. B., 2008, "Simulation Technology for Skills Training and Competency Assessment in Medical Education," Journal of General Internal Medicine, 23(1), pp. 46-49.
[23] 2018, "CAE iSTAN," https://caehealthcare.com/patient-simulation/istan/.
[24] Frost, D. W., Cavalcanti, R. B., and Toubassi, D., 2011, "Instruction Using a High-Fidelity Cardiopulmonary Simulator Improves Examination Skills and Resource Allocation in Family Medicine Trainees," Simulation in Healthcare, 6(5), pp. 278-283.
[25] G., T., N., P., G., M., F., G., A., P., and F, M., 2011, "New techniques for computer-based simulation in surgical training," Int J of Biomedical Engineering and Technology, 5(4), pp. 303 - 316.
[26] Gorman, P. J., Meier, A. H., Rawn, C., and Krummel, T. M., 2000, "The future of medical education is no longer blood and guts, it is bits and bytes," The American Journal of Surgery, 180(5), pp. 353-356.
[27] Duffy, A. J., Hogle, N. J., McCarthy, H., Lew, J. I., Egan, A., Christos, P., and Fowler, D. L., 2005, "Construct validity for the LAPSIM laparoscopic surgical simulator," Surgical Endoscopy and Other Interventional Techniques, 19(3), pp. 401-405.
[28] 2018, "CAE Veimdix," https://caehealthcare.com/ultrasound-simulation/vimedix/.
[29] 2018, "LAPSIM," https://surgicalscience.com/systems/lapsim/.
[30] Evans, L. V., Dodge, K. L., Shah, T. D., Kaplan, L. J., Siegel, M. D., Moore, C. L., Hamann, C. J., Lin, Z. Q., and D'Onofrio, G., 2010, "Simulation Training in Central Venous Catheter Insertion: Improved Performance in Clinical Practice," Academic Medicine, 85(9), pp. 1462-1469.
[31] Ma, I. W. Y., Brindle, M. E., Ronksley, P. E., Lorenzetti, D. L., Sauve, R. S., and Ghali, W. A., 2011, "Use of Simulation-Based Education to Improve Outcomes of Central Venous Catheterization: A Systematic Review and Meta-Analysis," Academic Medicine, 86(9), pp. 1137-1147.
[32] Earle, M., De Portu, G., and De Vos, E., 2016, "Agar ultrasound phantoms or low-cost training without refrigeration," African Journal of Emergency Medicine, 6(1), pp. 18-23.
[33] Shah, S., Bellows, B. A., Adedipe, A. A., Totten, J. E., Backlund, B. H., and Sajed, D., 2015, "Perceived barriers in the use of ultrasound in developing countries," Critical Ultrasound Journal, 7(1), p. 11.
[34] Bude, R. O., and Adler, R. S., 1995, "An Easily Made, Low-Cost, Tissue-Like Ultrasound Phantom Material," Journal of Clinical Ultrasound, 23(4), pp. 271-273.
[35] Nachshon, A., Mitchell, J. D., Mueller, A., Banner-Goodspeed, V. M., and McSparron, J. I., 2017, "Expert Evaluation of a Chicken Tissue-based Model for Teaching Ultrasound-guided Central Venous Catheter Insertion," J Educ Perioper Med, 19(1), p. E503.
[36] Pepley, D. F., Sonntag, C. C., Prabhu, R. S., Yovanoff, M. A., Han, D. C., Miller, S. R., and Moore, J. Z., 2018, "Building Ultrasound Phantoms With Modified Polyvinyl Chloride: A Comparison of Needle Insertion Forces and Sonographic Appearance With Commercial and Traditional Simulation Materials," Simul Healthc.

[37] Sultan, S. F., Shorten, G., and Iohom, G., 2013, "Simulators for training in ultrasound guided procedures," Medical Ultrasonography, 15(2), pp. 125-131.
[38] Burlew, M. M., Madsen, E. L., Zagzebski, J. A., Banjavic, R. A., and Sum, S. W., 1980, "A new ultrasound tissue-equivalent material," Radiology, 134(2), pp. 517-520.
[39] Madsen, E. L., Zagzebski, J. A., Banjavie, R. A., and Jutila, R. E., 1978, "Tissue mimicking materials for ultrasound phantoms," Medical Physics, 5(5), pp. 391-394.
[40] Culjat, M. O., Goldenberg, D., Tewari, P., and Singh, R. S., 2010, "A Review of Tissue Substitutes for Ultrasound Imaging," Ultrasound in Medicine and Biology, 36(6), pp. 861-873.
[41] Morrow, D. S., and Broder, J., 2015, "Cost-effective, Reusable, Leak-resistant Ultrasound-guided Vascular Access Trainer," The Journal of Emergency Medicine, 49(3), pp. 313-317.
[42] Amini, R., Kartchner, J. Z., Stolz, L. A., Biffar, D., Hamilton, A. J., and Adhikari, S., 2015, "A novel and inexpensive ballistic gel phantom for ultrasound training," World Journal of Emergency Medicine, 6(3), pp. 225-228.
[43] Li, W., Belmont, B., and Shih, A., 2015, "Design and Manufacture of Polyvinyl Chloride (PVC) Tissue Mimicking Material for Needle Insertion," Procedia Manufacturing, 1, pp. 866-878.
[44] Li, W., Belmont, B., Greve, J. M., Manders, A. B., Downey, B. C., Zhang, X., Xu, Z., Guo, D., and Shih, A., 2016, "Polyvinyl chloride as a multimodal tissue-mimicking material with tuned mechanical and medical imaging properties," Medical Physics, 43(10), pp. 5577-5592.
[45] Pepley, D., Yovanoff, M., Mirkin, K., Miller, S., Han, D., and Moore, J., "Measurement of Syringe Needle Forces for a Haptic Robotic Training Device," Proc. Design of Medical Devices Conference, ASME.
[46] Tsotsolis, N., Tsirgogianni, K., Kioumis, I., Pitsiou, G., Baka, S., Papaiwannou, A., Karavergou, A., Rapti, A., Trakada, G., Katsikogiannis, N., Tsakiridis, K., Karapantzos, I., Karapantzou, C., Barbetakis, N., Zissimopoulos, A., Kuhajda, I., Andjelkovic, D., Zarogoulidis, K., and Zarogoulidis, P., 2015, "Pneumothorax as a complication of central venous catheter insertion," Annals of Translational Medicine, 3(3), p. 40.
[47] Bernard, R. W., Stahl, W. M., and Chase, R. M., 1971, "Subclavian Vein Catheterizations - Prospective Study .2. Infectious Complications," Annals of Surgery, 173(2), pp. 191-&.
[48] Turner, H., and Firth, D., 2012, "Bradley-Terry Models in R: The BradleyTerry2 Package," 2012, 48(9), p. 21.
[49] Pepley, D., Yovanoff, M., Mirkin, K., Miller, S., Han, D., and Moore, J. Z., 2016, "Design Of A Virtual Reality Haptic Robotic Central Venous Catheterization Training Simulator," ASME 2016 International Design Engineering Technical Conferences and Computers and Information in Engineering ConferenceCharlotte, North Carolina.
[50] Pepley, D., Yovanoff, M., Mirkin, K., Miller, S., Han, D., and Moore, J., 2016, "A Virtual Reality Haptic Robotic Simulator for Central Venous Catheterization Training," J Med Device, 10(3), pp. 030937-030937-030932.
[51] Gordon, A. C., Saliken, J. C., Johns, D., Owen, R., and Gray, R. R., 1998, "US-guided puncture of the internal jugular vein: Complications and anatomic considerations," Journal of Vascular and Interventional Radiology, 9(2), pp. 333-338.
[52] Ishizuka, M., Nagata, H., Takagi, K., and Kubota, K., 2010, "Right Internal Jugular Vein Is Recommended for Central Venous Catheterization," Journal of Investigative Surgery, 23(2), pp. 110-114.
[53] Graham, A. S., Ozment, C., Tegtmeyer, K., Lai, S., and Braner, D. A. V., 2007, "Central Venous Catheterization," New England Journal of Medicine, 356(21), p. e21.
[54] Sznajder, J., Zveibil, F. R., Bitterman, H., Weiner, P., and Bursztein, S., 1986, "Central vein catheterization: Failure and complication rates by three percutaneous approaches," Archives of Internal Medicine, 146(2), pp. 259-261.

[55] Kunkler, K., 2006, "The role of medical simulation: an overview," The International Journal of Medical Robotics and Computer Assisted Surgery, 2(3), pp. 203-210.
[56] Smith, C. C., Huang, G. C., Newman, L. R., Clardy, P. F., Feller-Kopman, D., Cho, M., Ennacheril, T., and Schwartzstein, R. M., 2010, "Simulation Training and Its Effect on Long-Term Resident Performance in Central Venous Catheterization," Simulation in Healthcare, 5(3), pp. 146-151.
[57] Wanzel, K. R., Ward, M., and Reznick, R. K., 2002, "Teaching the surgical craft from selection to certification," Current Problems in Surgery, 39(6), pp. 577-659.
[58] Coles, T. R., Meglan, D., and John, N. W., 2011, "The Role of Haptics in Medical Training Simulators: A Survey of the State of the Art," Ieee Transactions on Haptics, 4(1), pp. 51-66.
[59] Morris, D., Tan, H., Barbagli, F., Chang, T., and Salisbury, K., 2007, "Haptic feedback enhances force skill learning," World Haptics 2007: Second Joint EuroHaptics Conference and Symposium on Haptic Interfaces for Virtual Environment and Teleoperator Systems, Proceedings, pp. 21-26.
[60] Mohamadipanah, H., Parthiban, C., Nathwani, J., Rutherford, D., DiMarco, S., and Pugh, C., 2016, "Can a virtual reality assessment of fine motor skill predict successful central line insertion?," American Journal of Surgery, 212(4), pp. 573-+.
[61] Coles, T. R., John, N. W., Gould, D., and Caldwell, D. G. C., 2011, "Integrating Haptics with Augmented Reality in a Femoral Palpation and Needle Insertion Training Simulation," Ieee Transactions on Haptics, 4(3), pp. 199-209.
[62] Silva, J. P., Plescia, T., Molina, N., Tonelli, A. C. d. O., Langdorf, M., and Fox, J. C., 2016, "Randomized study of effectiveness of computerized ultrasound simulators for an introductory course for residents in Brazil," JEEHP, 13, p. 16.
[63] Vaughan, N., Dubey, V. N., Wee, M. Y. K., and Isaacs, R., 2013, "A review of epidural simulators: Where are we today?," Medical Engineering & Physics, 35(9), pp. 1235-1250.
[64] Lee, R. A., van Zundert, T. C. R. V., van Koesveld, J. J. M., van Zundert, A. A. J., Stolker, R. J., Wieringa, P. A., and Gatt, S. P., 2012, "Evaluation of the Mediseus (R) Epidural Simulator," Anaesthesia and Intensive Care, 40(2), pp. 311-318.
[65] "Geomagic Touch."
[66] Gordon, A., Kim, I., Barnett, A. C., and Moore, J. Z., 2015, "Needle Insertion Force Model for Haptic Simulation," (56833), p. V002T003A003.
[67] Pepley, D., Yovanoff, M., Mirkin, K., Miller, S., Han, D., and Moore, J., 2017, "Measurement of Syringe Needle Forces for a Haptic Robotic Training Device," Journal of Medical Devices.
[68] Pepley, D. F., A., G., Yovanoff, M., Mirkin, K., Han, D., Miller, S., and Moore, J., 2017, "Training Surgical Residents with a Haptic Robotic Central Venous Catheterization Simulator," Journal of Surgical Education, 74/(6)(November/December).
[69] Gordon, A., Kim, I., A, B., and J, M., "Needle Insertion Force Model for Haptic Simulation," Proc. Proceedings of the ASME International Manufacturing Science and Engineering Conference.
[70] "Geomagic Touch X."
[71] Yovanoff, M., Pepley, D., Mirkin, K., Moore, J., Han, D., and Miller, S., 2017, "Personalized Learning in Medical Education: Designing a User Interface for a Dynamic Haptic Robotic Trainer for Central Venous Catheterization," Proceedings of the Human Factors and Ergonomics Society Annual Meeting, 61(1), pp. 615-619.
[72] Lin, B. S., Kong, C. W., Tarng, D. C., Huang, T. P., and Tang, G. J., 1998, "Anatomical variation of the internal jugular vein and its impact on temporary haemodialysis vascular access: an ultrasonographic survey in uraemic patients," Nephrology Dialysis Transplantation, 13(1), pp. 134-138.
[73] Bannon, M. P., Heller, S. F., and Rivera, M., 2011, "Anatomic considerations for central venous cannulation," Risk Management and Healthcare Policy, 4, pp. 27-39.

[74] Parmar, S., Parikh, S., and Mehta, H., 2013, "Anatomical variations of the internal jugular vein in relation to carotid artery : an ultrasound study," Int J Med Sci Public Health, 2(2), pp. 223-228.
[75] DENYS, B. G., and URETSKY, B. F., 1991, "Anatomical variations of internal jugular vein location: Impact on central venous access," Critical Care Medicine, 19(12), pp. 1516-1519.
[76] Barrington, M. J., and Kluger, R., 2013, "Ultrasound Guidance Reduces the Risk of Local Anesthetic Systemic Toxicity Following Peripheral Nerve Blockade," Regional Anesthesia and Pain Medicine, 38(4), pp. 289-297.
[77] Piacherski, V., Marochkov, A., Brukhnou, A., and Kokhan, Z., 2012, "Comparison of Three Methods of Regional Anesthesia of Peripheral Nerves and Plexuses," Open Journal of Anesthesiology, Vol.02No.05, p. 7.
[78] Marhofer, P., Greher, M., and Kapral, S., 2005, "Ultrasound guidance in regional anaesthesia," British Journal of Anesthesia, 94(1), pp. 7-17.
[79] Abrahams, M. S., Aziz, M. F., Fu, R. F., and Horn, J. L., 2009, "Ultrasound guidance compared with electrical neurostimulation for peripheral nerve block: a systematic review and meta-analysis of randomized controlled trials," British Journal of Anesthesia, 102(3), pp. 408-417.
[80] Randolph, A. G., Cook, D. J., Gonzales, C. A., and Pribble, C. G., 1996, "Ultrasound guidance for placement of central venous catheters: A meta-analysis of the literature," Critical Care Medicine, 24(12), pp. 2053-2058.
[81] Froehlich, C. D., Rigby, M. R., Rosenberg, E. S., Li, R. S., Roerig, P. L. J., Easley, K. A., and Stockwell, J. A., 2009, "Ultrasound-guided central venous catheter placement decreases complications and decreases placement attempts compared with the landmark technique in patients in a pediatric intensive care unit," Critical Care Medicine, 37(3), pp. 1090-1096.
[82] Karakitsos, D., Labropoulos, N., De Groot, E., Patrianakos, A. P., Kouraklis, G., Poularas, J., Samonis, G., Tsoutsos, D. A., Konstadoulakis, M. M., and Karabinis, A., 2006, "Real-time ultrasound-guided catheterisation of the internal jugular vein: a prospective comparison with the landmark technique in critical care patients," Critical Care, 10(6), p. R162.
[83] Mercaldi, C. J., and Lanes, S. F., 2013, "Ultrasound Guidance Decreases Complications and Improves the Cost of Care Among Patients Undergoing Thoracentesis and Paracentesis," Chest, 143(2), pp. 532-538.
[84] Mahmood, F., Matyal, R., Skubas, N., Montealegre-Gallegos, M., Swaminathan, M., Denault, A., Sniecinski, R., Mitchell, J. D., Taylor, M., Haskins, S., Shahul, S., Oren-Grinberg, A., Wouters, P., Shook, D., and Reeves, S. T., 2016, "Perioperative Ultrasound Training in Anesthesiology: A Call to Action," Anesthesia and Analgesia, 122(6), pp. 1794-1804.
[85] Gogalniceanu, P., Sheena, Y., Kashef, E., Purkayastha, S., Darzi, A., and Paraskeva, P., 2010, "Is Basic Emergency Ultrasound Training Feasible as Part of Standard Undergraduate Medical Education?," Journal of Surgical Education, 67(3), pp. 152-156.
[86] Rao, S., van Holsbeeck, L., Musial, J. L., Parker, A., Bouffard, J. A., Bridge, P., Jackson, M., and Dulchavsky, S. A., 2008, "A pilot study of comprehensive ultrasound education at the Wayne state university school of medicine - A pioneer year review," Journal of Ultrasound in Medicine, 27(5), pp. 745-749.
[87] Feller-Kopman, D., 2007, "Ultrasound-guided internal jugular access - A proposed standardized approach and implications for training and practice," Chest, 132(1), pp. 302-309.
[88] Tsui, B., Dillane, D., Pillay, J., and Walji, A., 2008, "Ultrasound imaging in cadavers: training in imaging for regional blockade at the trunk," Canadian Journal of Anesthesia, 55(2), p. 105.

[89] Petrinec, K., 2013, "Patient-Specific Interactive Ultrasound Image Simulation with Soft-Tissue Deformation," Doctor of Philosophy, University of Califorinia Los Angeles, Los Angeles California.
[90] Solberg, O. V., Lindseth, F., Torp, H., Blake, R. E., and Hernes, T. A. N., 2007, "Freehand 3D ultrasound reconstruction algorithms - A review," Ultrasound in Medicine and Biology, 33(7), pp. 991-1009.
[91] Reichl, T., Passenger, J., Acosta, O., and Salvado, O., "Ultrasound goes GPU: real-time simulation using CUDA," Proc. SPIE Medical Imaging, SPIE, p. 10.
[92] Gjerald, S. U., Brekken, R., Hergum, T., and D'hooge, J., 2012, "Real-Time Ultrasound Simulation Using the GPU," Ieee Transactions on Ultrasonics Ferroelectrics and Frequency Control, 59(5), pp. 885-892.
[93] Zhu, Y. N., Magee, D., Ratnalingam, R., and Kessel, D., 2007, "A training system for ultrasound-guided needle insertion procedures," Medical Image Computing and Computer-Assisted Intervention - Miccai 2007, Pt 1, Proceedings, 4791, pp. 566-+.
[94] Delingette, H., 1998, "Toward realistic soft-tissue modeling in medical simulation," Proceedings of the Ieee, 86(3), pp. 512-523.
[95] Farneback, G., 2003, "Two-frame motion estimation based on polynomial expansion," Image Analysis, Proceedings, 2749, pp. 363-370.
[96] Wright, I., 2011, "Peripheral Nerve Blocks in the Outpatient Surgery Setting," AORN Journal, 94(1), pp. 59-77.
[97] Hadzic, A., Arliss, J., Kerimoglu, B., Karaca, P. E., Yufa, M., Claudio, R. E., Vloka, J. D., Rosenquist, R., Santos, A. C., and Thys, D. M., 2004, "A comparison of infraclavicular nerve block versus general anesthesia for hand and wrist day-case surgeries," Anesthesiology, 101(1), pp. 127-132.
[98] Beaudoin, F. L., Haran, J. P., and Liebmann, O., 2013, "A Comparison of Ultrasound-guided Three-in-one Femoral Nerve Block Versus Parenteral Opioids Alone for Analgesia in Emergency Department Patients With Hip Fractures: A Randomized Controlled Trial," Academic Emergency Medicine, 20(6), pp. 584-591.
[99] Richman, J. M., Liu, S. S., Courpas, G., Wong, R., Rowlingson, A. J., McGready, J., Cohen, S. R., and Wu, C. L., 2006, "Does continuous peripheral nerve block provide superior pain control to opioids? A meta-analysis," Anesthesia and Analgesia, 102(1), pp. 248-257.
[100] Liguori, G. A., 2004, "Complications of regional anesthesia - Nerve injury and peripheral neural blockade," Journal of Neurosurgical Anesthesiology, 16(1), pp. 84-86.
[101] Jeng, C. L., Torrillo, T. M., and Rosenblatt, M. A., 2010, "Complications of peripheral nerve blocks," Br J Anaesth, 105, pp. I97-I107.
[102] Brull, R., McCartney, C. J. L., Chan, V. W. S., and El-Beheiry, H., 2007, "Neurological complications after regional anesthesia: Contemporary estimates of risk," Anesthesia and Analgesia, 104(4), pp. 965-974.
[103] Memtsoudis, S. G., Kuo, C., Ma, Y., Edwards, A., Mazumdar, M., and Liguori, G., 2011, "Changes in Anesthesia-Related Factors in Ambulatory Knee and Shoulder Surgery United States 1996-2006," Regional Anesthesia and Pain Medicine, 36(4), pp. 327-331.
[104] Sites, B. D., Spence, B. C., Gallagher, J. D., Wiley, C. W., Bertrand, M. L., and Blike, G. T., 2007, "Characterizing novice behavior associated with learning ultrasound-guided peripheral regional anesthesia," Regional Anesthesia and Pain Medicine, 32(2), pp. 107-115.
[105] Naik, V. N., Perlas, A., Chandra, D. B., Chung, D. Y., and Chan, V. W. S., 2007, "An assessment tool for brachial plexus regional anesthesia performance: Establishing construct validity and reliability," Regional Anesthesia and Pain Medicine, 32(1), pp. 41-45.
[106] Friedman, Z., Katznelson, R., Devito, I., Siddiqui, M., and Chan, V., 2006, "Objective assessment of manual skills and proficiency in performing epidural anesthesia - Video-assisted validation," Regional Anesthesia and Pain Medicine, 31(4), pp. 304-310.

[107] Chin, K. J., Tse, C., Chan, V., Tan, J. S., Lupu, C. M., and Hayter, M., 2011, "Hand Motion Analysis Using the Imperial College Surgical Assessment Device Validation of a Novel and Objective Performance Measure in Ultrasound-Guided Peripheral Nerve Blockade," Regional Anesthesia and Pain Medicine, 36(3), pp. 213-219.
[108] Slater, R. J., Castanelli, D. J., and Barrington, M. J., 2014, "Learning and Teaching Motor Skills in Regional Anesthesia A Different Perspective," Regional Anesthesia and Pain Medicine, 39(3), pp. 230-239.
[109] Datta, V., Mackay, S., Mandalia, M., and Darzi, A., 2001, "The use of electromagnetic motion tracking analysis to objectively measure open surgical skill in the laboratory-based model," Journal of the American College of Surgeons, 193(5), pp. 479-485.
[110] Moorthy, K., Munz, Y., Sarker, S. K., and Darzi, A., 2003, "Objective assessment of technical skills in surgery," British Medical Journal, 327(7422), pp. 1032-1037.
[111] Howells, N. R., Brinsden, M. D., Gill, R. S., Carr, A. J., and Rees, J. L., 2008, "Motion analysis: A validated method for showing skill levels in arthroscopy," Arthroscopy-the Journal of Arthroscopic and Related Surgery, 24(3), pp. 335-342.
[112] Corvetto, M. A., Fuentes, C., Araneda, A., Achurra, P., Miranda, P., Viviani, P., and Altermatt, F. R., 2017, "Validation of the imperial college surgical assessment device for spinal anesthesia," Bmc Anesthesiology, 17.
[113] Strom, P., Hedman, L., Sarna, L., Kjellin, A., Wredmark, T., and Fellander-Tsai, L., 2006, "Early exposure to haptic feedback enhances performance in surgical simulator training: a prospective randomized crossover study in surgical residents," Surgical Endoscopy and Other Interventional Techniques, 20(9), pp. 1383-1388.
[114] Higgins, W. T., 1975, "A Comparison of Complementary and Kalman Filtering," IEEE Transactions on Aerospace and Electronic Systems, AES-11(3), pp. 321-325.
[115] Okamura, A. M., Simone, C., and O'Leary, M. D., 2004, "Force modeling for needle insertion into soft tissue," Ieee Transactions on Biomedical Engineering, 51(10), pp. 1707-1716.

VITA

David F. Pepley
dpep56@gmail.com

Education

The Pennsylvania State University, University Park, PA
Ph.D. Mechanical Engineering — May 2019
M.S. Mechanical Engineering — Dec 2017

Grove City College, Grove City, PA
B.S. Mechanical Engineering — May 2015

Patent and Invention Disclosures

J. Z. Moore, Miller, S. R., Han, D., Kim, I., **Pepley, D**., Yovanoff, M., Patent pending, "Dynamic Haptic Robotic Trainer." (Submitted Application: August 2016). Serial number: 62/377,149

Peer Reviewed Journal Publications

Pepley D. F., Sonntag C. C., Prabhu R. S., Yovanoff M. A. Yovanoff, Han D. C., Miller S. R., Jason Z. Moore, "Building ultrasound phantoms with modified polyvinyl chloride: a comparison of needle insertion forces and sonographic appearance with commercial and traditional simulation materials." Simulation in Healthcare, In Print, Available online April 3, 2018.

Pepley D. F. , Yovanoff M. A., Mirkin K. A., Miller S. R., Han D. C., Moore J. Z., "Integrating Cadaver Needle Forces Into a Haptic Robotic Simulator." ASME. *Journal of Medical Devices*. vol. 12/(1), 2017.

Pepley D. F., Gordon A. B., Yovanoff M. A., Mirkin K. A., Miller S. R., Han D. C., Moore J. Z., "Training Surgical Residents with a Haptic Robotic Central Venous Catheterization Simulator.", *Journal of Surgical Education*, vol 74/(6), pp. 1066-1076, 2017.

Pepley D., Yovanoff M., Mirkin K., Miller S., Han D., and Moore J., "A Virtual Reality Haptic Robotic Simulator for Central Venous Catheterization Training." ASME. *Journal of Medical Devices*, vol. 10, pp. 030937-1 to 030937-2, 2016.

Yovanoff M. A., Chen H., **Pepley D. F.,** Mirkin A., Han D. C., Moore J. Z., Miller S. R., "Investigating the Effect of Simulator Functional Fidelity and Personalized Feedback on Central Venous Catheterization Training." *Journal of Surgical Education,* In Print, Available online March 21, 2018.